MODELING TIME DEPENDENT BEHAVIORS OF POLYMERIC SANDWICH COMPOSITES AT VARIOUS ENVIRONMENTAL CONDITIONS

A Dissertation

by

BENTOLHODA DAVOODI

Submitted to the Office of Graduate and Professional Studies of
Texas A&M University
in partial fulfillment of the requirements for the degree of

DOCTOR OF PHILOSOPHY

Chair of Committee,	Anastasia Muliana
Committee Members,	Terry S. Creasy
	Harry A. Hogan
	Maryam S. Sakhaeifar
Head of Department,	Andreas A. Polycarpou

December 2017

Major Subject: Mechanical Engineering

ABSTRACT

Polymeric sandwich composites are appealing for lightweight structures that require high strength and stiffness such as parts of aircraft, marine vessels, civil infrastructures and wind turbine blades. In wind turbine blades, sandwich composites with polymeric foam or honeycomb core and fiber-reinforced polymer (FRP) skins are a promising solution to obtain sufficiently lightweight blades with high bending stiffness and strength. In naval structures, sandwich composites with foam core and fiber-reinforced composite skins are used to create a light, corrosion resistant and stiff structure. However, there are many challenging and unresolved scientific issues that engineers face in using sandwich composites in the above applications. Polymeric sandwich composites undergo complex loading histories in addition to constant exposure to hostile environments, i.e., temperature and humidity changes. Moreover, one of the characteristics of polymers is their prominent viscoelastic response when subjected to mechanical loading. The viscoelastic response of polymers becomes more pronounced at elevated temperatures and high humidity. Coupled mechanical loading and hostile environments cause the constituents of the sandwich structures to experience different time-dependent behavior and degradation, leading to complex failure mechanisms in sandwich composites. The aim of this study is to describe the performance of sandwich composites subjected to mechanical loading histories and various environmental conditions, by incorporating knowledge of the behavior in each constituent (skin, core, fiber-matrix constituents).

ACKNOWLEDGEMENTS

I would like to thank my committee chair, Dr. Muliana, and my committee members, Dr. Creasy, Dr. Hogan and Dr. Sakhaeifar, for their guidance and support throughout the course of this research.

Thanks also go to my friends and colleagues and the department faculty and staff for making my time at Texas A&M University a great experience.

Finally, thanks to my wonderful husband for his encouragement, patience and love.

This study is supported by the National Science Foundation (NSF) under grant CMMI-1266037 and Office of Naval Research (ONR) under grant N00014-13-1-0604.

CONTRIBUTORS AND FUNDING SOURCES

Contributors

This work was supported by a dissertation committee consisting of Professors Anastasia Muliana, Terry S. Creasy and Harry A. Hogan of the Department of Mechanical Engineering and Professor Maryam S. Sakhaeifar of the Department of Civil Engineering.

Funding Sources

This study is supported by the National Science Foundation (NSF) under grant CMMI-1266037 and Office of Naval Research (ONR) under grant N00014-13-1-0604.

NOMENCLATURE

1D	One dimensional
3D	Three dimensional
ASTM	American Society for Testing and Materials
B	Material parameter
C3D20	nonlinear three dimensional continuum elements
$\boldsymbol{C}$	fourth-order elastic stiffness tensor
CFRP	carbon fiber-reinforced polymer
E_o	Relaxation modulus
E	Elastic modulus
E_∞	relaxed modulus
Eq	equation
F	strain measure
f	yield function
FE	Finite element
FRP	fiber reinforced polymer
G	shear modulus
GFRP	Glass fiber reinforced polymer
I	second moment of an area
K_B	bulk modulus
L	length

mm	millimeter
MPa	Megapascal
NSF	National Science Foundation
N	Newton
NaCl	Sodium chloride
ONR	Office of Naval Research
P	Piola stress
PU	polyurethane
PVC	polyvinylchloride
PZT	Lead Zirconate Titanate
QLV	Quasi linear viscoelastic
RT	Room temperature
t	time
UMAT	User material
v	Stretch tensor
W	load
wt	weight

Greek symbols

τ_{Rn}	characteristics of relaxation time
δ_{ij}	Kronecker delta
σ_{ij}	stress
$\boldsymbol{\sigma}$	Stress tensor

$\bar{\sigma}$	Von Mises equivalent stress
ν_0	Poisson's ratio
ε	strain
$\boldsymbol{\varepsilon}$	Strain tensor
$\dot{\boldsymbol{\varepsilon}}$	Strain rate tensor
$\dot{\boldsymbol{\varepsilon}}^{\boldsymbol{el}}$	Elastic strain rate tensor
$\dot{\boldsymbol{\varepsilon}}^{\boldsymbol{pl}}$	Plastic strain rate tensor
$\mathbf{S}$	Deviatoric stress
δ	deflection
θ	temperature
λ	Material parameter

Subscripts

f	foam
s	skin

Superscripts

pl	plastic
el	elastic

TABLE OF CONTENTS

Page

LIST OF FIGURES

Page

LIST OF TABLES

Page

1. INTRODUCTION AND LITERATURE REVIEW

1.1. Polymeric Sandwich Composites and Their Applications

Sandwich structures consist of two thin face sheets (skins) with high stiffness and strength which are bonded with an adhesive to both sides of a relatively thick core. This sandwich system forms a lightweight structure with high strength and stiffness, and predominantly loaded under bending and/or twisting. The face sheets are usually made of metals or fiber composite laminates and the core is typically made of wood, and foams or honeycombs of polymeric or metallic materials. The skins carry the tensile and compressive loads and the core sustains the shear loads and holds the skins in positions away from the neutral axis of the structures, which maximizes the flexural stiffness of the structure [1]. When fiber composite laminates are used for skins, several materials that are used as fiber are glass, Aramid or Kevlar, because of their light weight, carbon and Boron for their high strength, and Silicon carbide for high temperature resistance. The common matrix materials include polymers, minerals and metals. Polymeric matrix includes thermoplastic resins such as polypropylene, polyphenylene sulfone, polyamide, polyetheretherketone, etc. and thermoset resins such as polyesters, phenolics, melamines, silicones, polyurethanes, epoxies. Mineral matrix includes silicon carbide and carbon that are often used in high temperature applications, and aluminum alloys, titanium alloys and oriented eutectics are some examples of metallic matrix [2]. For applications which having light weight is important, foams are the most efficient core materials and because of its simplicity of changing the core and skin materials in

manufacturing, sandwich construction are flexible in designing for different shape and deflection requirements [3].

The significant characteristics of sandwich composites are light weight, [2] superior bending stiffness, good acoustic damping, ease of machining and forming [4]. Sandwich composites also have an improved stiffness to weight ratio and it is also possible to optimize the performance by changing the core and skin materials and their thickness [5]. This flexibility in design is another advantage of using sandwich composites in structural applications.

In Airbus A310, sandwich composites are used in several components, i.e., vertical and horizontal stabilizer, front landing gear hatch, motor mast reinforcement, and in Airbus A320 they are used in motor case, vertical and horizontal stabilizer. Also using sandwich composites in fighter aircrafts improved the maneuverability of the aircraft. Examples of fighter aircrafts that have structures made of sandwich composites are European airplane Alphajet or Airplane Mirage 2000 A.M.D-B.A. Some characteristics of composite components in aircraft industry are:

1. Light weight that leads to save in fuel and improves performances.
2. Saving in long-term cost of product by good fatigue resistance that enhances the life.
3. Good corrosion resistance that leads to less frequent of inspection needed which saves the maintenance cost.

Another application of sandwich composites is in parts of helicopters, such as blades, vertical and horizontal stabilizer and rotor shaft [2]. Compared to metallic construction, using the composite in the secondary structures allows for 15% mass reduction and this saving is even more when using them in working pieces such as the elements of transmission of power and control parts that the mass reduction is up to 50%.

In recent years there have been interests in sandwich composite bridge decks because of their inherent strength and stiffness per unit weight advantages compared to the traditional steel reinforced concrete [6]. Composite bridge decks are exposed to the loads due to actions of wheel, chemical attack, and changing in temperature and moisture including freeze and thaw shrinkage and humidity and these situations made them the weakest element in the bridge system. Vinylester polymer and E-glass fibers are typical materials used in bridge deck structures [7]. Also sandwich composites with polyurethane foam core and metallic (steel) skins are used to create stiff structures, without the need for secondary stiffening in lightweight decks. In the rehabilitation projects, weigh reduction of replacement decks leads to decreasing in dead load and consequently raises the live load rating of the structure [6].

Sandwich composites also have many applications in ship structures including the current and potential use in hulls and superstructures, bulkheads, decks, propellers, advanced mast systems and other equipment [8]. Polymeric sandwich composites are used in different boats and small ships, such as yachts, power boats, naval patrol boats, landing craft and mine hunting ships. Current sandwich composites used in marine

applications are usually made with thin face skins of fiber reinforced polymer laminate and a thick core of a very light material. A wide range of fibers such as glass, carbon and Kevlar fibers and resins like polyesters, vinylester and epoxy are being used in composite skins. A variety of core materials has been used in marine sandwich composites, and the most common materials are polyvinylchloride (PVC) foam, polyurethane foam and balsa wood [9]. The benefits of using composites are decreasing the weight, flatness for stealth requirements, and increased corrosion resistance. There has been a number of ships entirely made of sandwich composites consisting of foam cores and fiber reinforced skins. These structures have high strength and rigidity combined with light weight, low radar and magnetic signatures and good resistance to shock. [10] Hall et al. [11] investigated the performance of sandwich construction used in Navy minehunter by determining the physical properties of core materials and testing composite structures for their mechanical strength and resistance to underwater shocks. These tests provide information on failure modes and loading in various core materials for ship's designers. They reported that in both static and cyclic loadings, failure is due to shear and initiates in the foam core.

Another important application of sandwich composites is for wind turbine blades. In wind turbine blades, sandwich composites with polymeric foam or honeycomb core and fiber reinforced polymer (FRP) skins are a good solution to obtain sufficiently lightweight blades with high bending stiffness and strength. The blades of a wind turbine rotor are the most critical part of the wind turbine system [12]. The important

requirements for wind turbine blades are high stiffness, low density and long fatigue life and sandwich composites are the preferable choice because of their properties [13].

1.2. The Effect of Environments (Temperature and Moisture) On the Mechanical Properties of Sandwich Composites

Foam core sandwich composite structures which are used in naval structures have many advantages, such as high stiffness to weight ratio and corrosion resistance and leads to weight saving in marine structural applications; however, they are exposed to harsh environment. Xiaoming et al. [14] investigated long-term exposure of sea-water on foam core sandwich composite structures. They focused on understanding damages caused by sea water in foam materials, increases in weight and volumetric expansion of strains and degradation. In addition, the influences of sea water on the fracture behavior of foam materials and on interfacial debonding fracture, are studied experimentally and modeled using computational fracture mechanics. They showed that most of sea-water effects on the foams was limited to the exterior area. They also conducted experiments to investigate the effect of sea-water on the toughness of PVC foam. It was shown that the sea-water absorption in the crack tip area causes the increase in foam toughness. Similarly, they showed that the effect of exposure to external temperatures is limited to the outer facings because of the high thermal insulation properties of foam and both temperature and sea water reduce the elastic moduli of the foam.

Siriruk et al. [15] studied the degradation and its effect on the mechanical behavior in sandwich composite structures comprising of PVC foam core and carbon fiber

reinforced vinyl ester skins due to exposure to sea water. They presented both experimental and analytical results concerning the properties and response of PVC foams and sandwich composites. Siriruk et al. [16] also studied sandwich structures in naval structures that are exposed to sea water and temperature fluctuations in long period of time. They investigated the influences of sea water on the interfacial mechanical response between foam and skins. Their testing results indicate that in the specimen that was affected by sea water, the delamination crack propagates at the interface region while in the dry sandwich composite specimen the crack stays within the foam. They also showed that fracture toughness decreases after sea water exposure and it should be considered in the design of ship structures.

Kolat et al. [17] investigated the influence of core material selection and environmental conditions on the fracture toughness of sandwich structures. The study shows that fracture toughness of sandwich composite systems with polyurethane and coremat core increases under effect of sea water while with using wood and plywood the fracture toughness decreases after conditioning in sea water. The obtained data in this work, directly used by boat designers. Joshi et al. [18] analyzed the influence of moisture diffusion on viscoelastic sandwich composites deformation, and assumed the elastic and time-dependent properties of the foam core depend on the moisture concentration and conducted coupled analyses of moisture diffusion and deformation to predict the viscoelastic sandwich systems performance. They showed that the simulated results are capable in capturing the accelerated time-dependent responses at higher moisture concentration.

1.3. Time Dependent Studies on Polymeric Sandwich Composites

Creep deformations in the polymeric constituents in the sandwich composites can influence the overall life performance of the polymeric sandwich structures. Also composite sandwich structures are often subjected to static and repetitive loadings such as the repetitive loading on the ship hull because of sea water waves, repeated loading due to motor vehicle over the bridge deck and aeroacoustics excitation of a turbine engine housing influenced by rotating turbine blades [1]. These repeated loadings can lead to fatigue failure in structures.

Du et al. [19] investigated the creep response in sandwich composites with honeycomb core for a period of 30 days. Their result showed linear viscoelastic response in ambient conditions and loading equal to 30% of failure loading. Higher relative humidity lead to significant acceleration of creep strain. Shenoi et al. [20] studied creep and creep–fatigue in a sandwich structure including fiber-reinforced polymeric faces and a PVC foam core. They used both Burger and power law models for describing the creep behavior, which was compared with experimental results. They showed that creep is mainly due to the core for the sandwich composites and the creep response of the foam core material depends on the stress levels. Garrido et al. [21] conducted experimental and analytical studies on the creep behavior of sandwich composite consist of glass-fiber reinforced polymer faces and rigid polyurethane foam core. They proposed a creep model to simulate the long-term deformations in sandwich composites by considering the viscoelastic contributions from the core material under shear and the glass-fiber reinforced polymer faces under tension/compression.

In this study the viscoelastic behavior of the PU foam core under shear stresses was described using Findley's power law model and it was found that the linear viscoelastic behavior of material depends on stress level. The time exponents were assumed to be relatively unaltered. Using Findley's power law that replaces the hyperbolic sine dependency of stress by a linear dependency, it was possible to determine a time-dependent shear modulus and finally provide predictions that are stress independent. Chen et al. [22] carried out several three point bending creep tests on the sandwich composite samples made of various core and skin materials with different core and skin thicknesses and their result showed that the flexural creep behavior of the sandwich composite sample is influenced by the shape of honeycomb core, core and skin thickness, and skin material type. Kim et al. [23] developed a multi-scale model to integrate different constitutive models of the constituents in the sandwich structures and in this study the quasi-static and creep tests were conducted for bulk epoxy, GFRP, polyurethane foam, and sandwich specimens under uniaxial tension and bending at room temperature and at 80^{o}C.

Scudamore and Cantwell [24] studied the moisture effect on the mechanical behavior of sandwich structures. They used sandwich composite structures consisting of E-glass/epoxy as skins and an aluminum honeycomb core and showed that exposure to sea-water in long term leads to degradation of the bond between the epoxy matrix and the aluminum core and causes cracks along the skin-core interface. Li and Weitsman [14] also investigated the sensitivity of the material properties of sandwich structures exposed to seawater in a long time period. They measured the fracture toughness of the foam core

material and the face/core debonding fracture toughness in the case of sandwich specimens and characterized the fracture toughness of wet and dry foams. They showed that sea water absorption, increases the foam toughness. This may be due to the mechanical softening and the ductility of the wet foam when the glass transition temperature was decreased. Also, to study the influences of seawater on the skin and core debonding, the pre-crack sandwich composites were immersed in seawater, and it was concluded that the fracture toughness at the core and skin interfaces showed degradation because of the presence of seawater.

Ishai et al. [25] investigated the long-term temperature and moisture effects on damage tolerance of sandwich composites made of carbon fiber-reinforced plastic (CFRP) and glass fiber-reinforced plastic (GFRP) skins and a syntactic foam core. Tests were done on immersed sandwich panels at temperatures 25 ^{o}C and 50^{o}C. During the exposure to moisture and high temperature, moisture absorption versus time was recorded by weight measurements and then an impact test was conducted and it was concluded that there is a remarkable strength reduction due to moisture content of syntactic foam specimens. Ishiaku et al. [26] also defined that a degradation happens in mechanical properties of sandwich composites due to moisture absorption. Belingardi et al. [27] characterized the sandwich composite properties with skins made of glass fiber epoxy and a polymeric foam core using a series of static and quasi-static tests. They showed the dependency of the structural response of the sandwich to the foam core strength properties. The viscoelastic creep behavior of sandwich composite beams and the effect of temperature changes are analytically investigated by Ramezani et al. [28]. Their results show that

creep of the core leads to remarkable differences in the internal forces and stress concentrations, which can have an important effect on the performance of sandwich beams under sustained loads. Also Hamed et al. [29] presented a theoretical modeling of creep response of sandwich composite beams which considers the influences of different boundary conditions and the viscoelastic properties of the core material. The theoretical approach combines the concept of the linear Boltzman's principle of superposition as discussed by Findley [30] with the concepts of the high-order sandwich theory by Frostig [31]. Hamed et al. carried out a parametric study to investigate the capability of the model and the effect of boundary conditions on the creep behavior of sandwich composite and showed the concentration of shear and transverse normal stresses near the edges and their variation in time and the effect of boundary conditions in the creep response of sandwich composite beams. The change in deflection, internal forces and stresses with time shows different trends that depend on the boundary conditions of the beam. Figueroa et al. [32] investigated creep to failure and cyclic creep in foam core sandwich composites in seawater. The deflection was about 15% higher and lifetime reduction of over 50% were observed in specimens subjected to seawater compared to baseline condition. In cyclic creep, significantly reduced life and considerable damage were observed compared to creep to failure specimens.

Coupled mechanical loading and hostile environments cause the constituents of the sandwich structures to experience different time-dependent behavior and degradation. Hostile environments could accelerate aging and change the life performance of the sandwich structures. Jeon [33] investigated a multi-scale experimental and modeling

approaches on time dependent response of different constituents of sandwich composite (polymeric matrix, skin, and foam core) and their interaction on the overall creep performance of smart polymer sandwich constructions. Kim et al. [34] studied the time-dependent response of smart sandwich composites consist of glass fiber reinforced polymer (GFRP) skins, polyurethane foam core, and PZT crystals embedded in the GFRP skins. They developed a multi-scale model to integrate different constitutive models of the constituents in the sandwich composite structures. They conducted quasi-static and creep tests for bulk epoxy, polyurethane foam, GFRP and sandwich composite specimens under uniaxial tension and bending, at room temperature and at 80^{o}C and characterization of material and model verification are done using experimental data.

Several studies have been done on investigating the time-dependent response of sandwich composites and the effects of using different materials as core and skin on the overall performance of composites under mechanical loadings. However, a comprehensive study on investigating the effect of environmental conditions (moisture and high temperature) and nonlinear mechanical response of the constituents on the time-dependent response of sandwich composite behaviors is currently lacking. In this study, two systems of polymeric sandwich composites are investigated under quasi-static, creep and stress relaxation tests at different environmental conditions. The influences of different constituents on the overall performance of sandwich composites are also studied.

2. RESEARCH OBJECTIVES

The objectives of this study are:

2.1. Determination of Mechanical Responses of Polymeric Sandwich Composites and Their Constituent Behaviors under Different Mechanical Loading and Environmental Conditions

Two systems of polymeric sandwich composites are studied. The first system consists of glass fiber reinforced polymeric (GFRP) composites with epoxy matrix for skins and polyurethane foam core. The second system consists of carbon fiber reinforced polymeric (CFRP) composites with vinylester matrix and PVC foam core. The first sandwich composites are typically used for aircraft and wind turbine blades while the second systems are often used in naval structures. Experimental data on the sandwich composites and their constituents are obtained from UC Davis (Dr. La Saponara's group). The following mechanical tests are considered: quasi-static, creep and relaxation tests at different environmental conditions. The baseline tests (dry and ambient temperature) are considered for both sandwich systems. The first sandwich systems are also tested after immersion in deionized water at room temperature and high temperature (50°C), while the second sandwich systems are also tested after immersion in sea water at room temperature and 50°C. A nonlinear viscoelastic constitutive model, for small deformation gradient problems, is formulated and implemented in finite element (FE). The model is used to understand the nonlinear time-dependent responses of the constituents at various environmental conditions. The multi-scale FE framework that consists of FRP skins and foam core is used for predicting the overall performance of

sandwich composites under different loading conditions such as quasi static and creep. The nonlinear mechanical response of sandwich composites obtained from the FE simulation will be compared with experimental data.

2.2. Determination of Life Performance of Polymeric Sandwich Composites under Mechanical Loadings and Environmental Conditions

After calibrating the material parameters in the model for each constituent in the sandwich composites, the FE framework will be used to understand life performance of sandwich structures and predict failure initiation in sandwich composites under various loading histories and environmental conditions. The presented modeling and simulation of sandwich composites that incorporate different mechanical responses of the constituents will be useful in designing polymeric sandwich structures.

The organization of this study is as follows. Section 3 discusses a quasi linear viscoelastic constitutive material model in order to describe nonlinear mechanical responses of polymers undergoing moderate deformations. In section 4, experimental procedures for testing the sandwich composites and their constituents are explained. Section 5 includes the results and discussion of the response of foam, CFRP and GFRP skins and sandwich composites under uniaxial and bending tests in different environmental condition such as dry at ambient temperature, immersed in liquid at ambient temperature and immersed in liquid at 50°C. To investigate the time dependent material properties, creep, stress relaxation and cyclic relaxation tests were done on foam and sandwich composites. Section 6 is the conclusion of this study.

3. CONSTITUTIVE MATERIAL MODELS FOR THE CONSTITUENTS

In this chapter the constitutive materials models are described. The sandwich composites consist of polymeric foam core with viscoelastic behavior and fiber reinforced polymeric skin with elastic or elastic plastic behavior.

3.1. Nonlinear Viscoelastic Constitutive Model for Polymeric Constituents

The nonlinear viscoelastic model that is used in this study is based on the quasi-linear viscoelastic (QLV) model of Muliana et al. [35]. The model is used in order to describe responses of polymers undergoing moderate deformations. The QLV constitutive model is originally proposed by Fung [36] for modeling biological materials. The polymers are assumed to be isotropic and homogeneous and the material moduli changes with the extent of exposure to temperatures and/or moisture changes. The one-dimensional (1D) QLV model is written as:

$$P(t) = \int_{0^-}^{t} E(t-s)\frac{dF}{d\varepsilon}\frac{d\varepsilon}{ds}ds \tag{3.1}$$

where E is the relaxation modulus, F is the strain measure, and P is the first Piola-Kirchhoff stress (force divided by the undeformed cross-sectional area). The extensional strain is defined as

$$\varepsilon(t) = \frac{L(t)}{L(0^-)} - 1 \tag{3.2}$$

where L(t) is the length at current time t. In this study, the following form of the strain measure is used

$$F\big(\varepsilon(t)\big) = A\big[e^{B\varepsilon(t)} - 1\big] \tag{3.3}$$

where A and B are the material constants and can be calibrated by fitting experimental data. It is assumed that we can separate the time-dependent function from the deformation dependent part in predicting the nonlinear stress relaxation:

$$P(t) = K(t)P^{el}(\varepsilon) \tag{3.4}$$

where $K(\mathrm{t}) = \frac{E(t)}{E(0)}$ is the normalized time-dependent function in which $K(0) = 1.0$ and $P^{el}(\varepsilon)$ is the nonlinear elastic stress response. The QLV model in Eq. (3 – 1) can be rewritten as:

$$P(t) = \int_{0^-}^{t} K(t-s)\frac{dP^{el}}{d\varepsilon}\frac{d\varepsilon(s)}{ds}ds \tag{3.5}$$

where

$$\frac{dP^{el}}{d\varepsilon} = E(0)ABe^{B\varepsilon} = E_0 e^{B\varepsilon} \tag{3.6}$$

In the uniaxial case, there are two material parameters that should be characterized from experiments, E_o and B, which are related to the instantaneous elastic response. Also the time-dependent function K(t) can be characterized from experiment and the parameter E_o corresponds to the elastic (Young's) modulus in a linearized elastic response. With the relaxation modulus, the QLV constitutive model for viscoelastic polymer is:

$$P(t) = \int_{0^-}^{t} E(t-s)\frac{dF}{d\varepsilon}\frac{d\varepsilon}{ds}ds \tag{3.7}$$

where $E(t)$ is the relaxation modulus of polymer and can be written as

$$E(t) = E_\infty + \sum_{n=1}^{N} E_n\, e^{\frac{-t}{\tau_{Rn}}} \tag{3.8}$$

where τ_{Rn} is the characteristics of relaxation time, E_n is the coefficient in the time-dependent part, N is the number of term in the Prony series, and E_∞ is the relaxed modulus. The variable F in Eq. (3.7) is the nonlinear strain measure.

Three-dimensional (3D) quasi-linear viscoelastic (QLV) model for isotropic materials, considering a generalization of the one-dimensional quasi-linear viscoelastic model, is:

$$\sigma_{\mathrm{ij}}(\mathrm{t}) = \int_{0^-}^{\mathrm{t}} 2G(t-s)\frac{\mathrm{d}F_{\mathrm{ij}}}{\mathrm{d}s}\mathrm{d}s + \delta_{\mathrm{ij}}\int_{0^-}^{\mathrm{t}} \lambda(t-s)\frac{\mathrm{d}F_{\mathrm{kk}}}{\mathrm{d}s}\mathrm{d}s \tag{3.9}$$

where δ_{ij} is the Kronecker delta and λ is the material parameter, which is one of the two Lame's constants and defined as:

$$\lambda = K_{\mathrm{B}} - (2/3)G \tag{3.10}$$

G is the shear modulus and K_{B} is bulk modulus which both are material parameters that have the same time-dependent behavior as the extensional relaxation modulus. The corresponding Poisson's ratio assumed to be constant,ν_0 which leads to:

$$G(t) = \frac{E(t)}{2(1+\nu_0)} \tag{3.11}$$

$$K_B(t) = \frac{E(t)}{3(1-2\nu_0)} \tag{3.12}$$

The strain measure in a generalized 3D quasi-linear viscoelastic model is defined as:

$$F\big(\bar{\varepsilon}(t)\big) = A\big[e^{B\bar{\varepsilon}(t)} - 1\big] \tag{3.13}$$

$$\bar{\varepsilon}(t) = \sqrt{\varepsilon_{ij}\varepsilon_{ij}} \tag{3.14}$$

$$\frac{dF_{ij}}{ds} = ABe^{B\bar{\varepsilon}(t)}\frac{d\varepsilon_{ij}}{ds} \tag{3.15}$$

$$\frac{dF_{kk}}{ds} = ABe^{B\bar{\varepsilon}(t)}\frac{d\varepsilon_{kk}}{ds} \tag{3.16}$$

and the 3D quasi-linear viscoelastic model becomes

$$\sigma_{ij}(t) = 2C_1\int_{0^-}^{t} K(t-s)\,\frac{dP^{el}}{d\bar{\varepsilon}}\frac{d\varepsilon_{ij}}{ds}ds \;+\; \delta_{ij}C_2 \times \int_{0^-}^{t} K(t-s)\frac{dP^{el}}{d\bar{\varepsilon}}\frac{d\varepsilon_{kk}}{ds}ds \tag{3.17}$$

where

$$C_1 = \frac{1}{2(1+\nu_0)} \tag{3.18}$$

$$C_2 = \frac{1}{3(1+2\nu_0)} - \frac{1}{3(1+\nu_0)} \tag{3.19}$$

$$\frac{dP^{el}}{d\bar{\varepsilon}} = E_0 e^{B\bar{\varepsilon}} \tag{3.20}$$

The normalized time dependent function is

$$K(t) = K_\infty + \sum_{n=1}^{N} K_n \, e^{\frac{-1}{\tau_{Rn}}} \tag{3.21}$$

$$K(0) = K_\infty + \sum_{n=1}^{N} K_n = 1.0 \tag{3.22}$$

and the QLV model becomes:

$$\sigma_{ij}(d,t) = 2C_1 \int_{0^-}^{t} K(t-s) E_0 e^{B\bar{\varepsilon}} \frac{d\varepsilon_{ij}}{ds} ds + \delta_{ij} C_2 \int_{0^-}^{t} K(t-s) E_0 e^{B\bar{\varepsilon}} \frac{d\varepsilon_{kk}}{ds} ds \tag{3.23}$$

The above model is implemented in user material subroutine (UMAT) of ABAQUS FE analyses. The numerical algorithm was formulated by Muliana et al. [35] and is summarized in the Appendix. The two nonlinear material parameters E_0 and B are determined from quasi-static tests, while the time-dependent parameters are determined from creep or relaxation tests. For isotropic polymers, the Poisson's ratio is characterized from experiments.

In this study we do not consider any degradation in the material model, but the model that is used is capable of taking degradation in account as a function of concentration of water, temperature and nonlinear strain.

3.1. Elastic-Plastic Model for Skins

The elastic-plastic material model [37], [38] is used to simulate the behavior of FRP skins in the sandwich composite. Some of the FRP skins show an elastic-plastic response

under mechanical loading, which will be shown later in this study. A rate-independent plasticity model is considered in order to capture the elastic-plastic response of the FRP skins. From the experimental observation for mechanical deformation of the FRP skins, the strains are relatively small, which allow for additive decompositions of the elastic and plastic deformations. Thus, the total strain rate is given as:

$$\dot{\boldsymbol{\varepsilon}} = \dot{\boldsymbol{\varepsilon}}^{\boldsymbol{el}} + \dot{\boldsymbol{\varepsilon}}^{\boldsymbol{pl}} \tag{3.24}$$

where $\dot{\boldsymbol{\varepsilon}}$ is the total (mechanical) strain rate, $\dot{\boldsymbol{\varepsilon}}^{el}$ is the elastic strain rate, and $\dot{\boldsymbol{\varepsilon}}^{pl}$ is the plastic strain rate. Equation (3.24) is an approximation when the elastic strains are infinitesimal. The rate of deformation tensor is work-conjugate to the Cauchy stress tensor and is used to define the strain rate:

$$\dot{\boldsymbol{\varepsilon}} = \frac{1}{2}\left(\frac{\partial v}{\partial x} + \left(\frac{\partial v}{\partial x}\right)^{T}\right) \tag{3.25}$$

The linear elastic isotropic constitutive equation can be written as

$$\boldsymbol{\sigma} = \boldsymbol{C}: \boldsymbol{\varepsilon}^{\boldsymbol{el}} \tag{3.26}$$

which $\boldsymbol{C}$ denotes the fourth-order elastic stiffness tensor. For notational convenience we can write the above stress-strain relationship in vector notation in (3.26).

$$\begin{Bmatrix}\sigma_{11}\\ \sigma_{22}\\ \sigma_{33}\\ \sigma_{12}\\ \sigma_{13}\\ \sigma_{23}\end{Bmatrix} = \frac{E}{(1+\nu_0)(1-2\nu_0)}\begin{Bmatrix} 1-\nu_0 & \nu_0 & \nu_0 & 0 & 0 & 0 \\ & 1-\nu_0 & \nu_0 & 0 & 0 & 0 \\ & & 1-\nu_0 & 0 & 0 & 0 \\ & & & 1-2\nu_0 & 0 & 0 \\ & sym. & & & 1-2\nu_0 & 0 \\ & & & & & 1-2\nu_0 \end{Bmatrix}\begin{Bmatrix}\varepsilon_{11}^{el}\\ \varepsilon_{22}^{el}\\ \varepsilon_{33}^{el}\\ \varepsilon_{12}^{el}\\ \varepsilon_{13}^{el}\\ \varepsilon_{23}^{el}\end{Bmatrix} \quad (3.27)$$

where E is Young modulus and ν_0 is the Poison ratio. The yield function is often expressed in terms of an equivalent stress, i.e. a scalar measure of the magnitude of the Cauchy stress tensor. Von Mises equivalent stress is:

$$\bar{\sigma} = \bar{\sigma}[\boldsymbol{\sigma}] = \sqrt{\frac{3}{2}\boldsymbol{S}:\boldsymbol{S}} \quad (3.28)$$

which deviatoric tensor is

$$\boldsymbol{S} = dev[\boldsymbol{\sigma}] = \boldsymbol{\sigma} - \frac{tr[\boldsymbol{\sigma}]}{3}\boldsymbol{I} \quad (3.29)$$

Using Von Mises equivalent stress definition, the yield function is written as:

$$f[\boldsymbol{\sigma}, \bar{\varepsilon}^{pl}] = \bar{\sigma}[\boldsymbol{\sigma}] - k[\bar{\varepsilon}^{pl}] \quad (3.30)$$

The yield surface is

$$f[\boldsymbol{\sigma}, \bar{\varepsilon}^{pl}] = 0 \quad (3.31)$$

$k\left[\bar{\varepsilon}_{pl}\right]$ shows the isotropic hardening. The hardening parameters are state variables that are introduced to allow the model to describe some of the complexity of the inelastic response of real materials. In perfect plasticity which is the simplest plasticity model, the yield surface acts as a limit surface and there are no hardening parameters. In this study, from observed experimental tests of FRP skins, discussed in Chapter 4, an elastic-perfectly plastic deformation model is adopted.

4. EXPERIMENTS

The experimental part of this study was done in UC Davis (Dr. Valeria La Saponara's group). Two sandwich composite systems were manufactured using out-of-autoclave Vacuum Assisted Resin Transfer Molding. The first system is glass fiber reinforced polymer (GFRP) having E-glass fibers (quasi-unidirectional Vectorply E-LR 0908, with layup $[90]_4$ per skin) and epoxy (Pro-set LAM 125/LAM237, with an infusion ratio of 100:28 resin:hardener by weight ratio for the skins and polyurethane (PU) foam,(General Plastics FR-3704, nominal thickness 19.1 mm) for the core. We refer to this system as "GFRP/PU". The resin cure cycle consisted of 14 hours at room temperature, followed by 8 hours at 82 °C in a convection oven. The GFRP/PU sandwich and its constituents (GFRP and PU) are immersed in distilled water at 25^{o}C and 50^{o}C. The second system is a sandwich with skins made of carbon fibers (quasi unidirectional Torayca T700S, with layup $[90]_4$ per skin) and vinylester (Hetron FR 992, with additives cobalt naphthenate and methyl ethyl ketone peroxide with an infusion ratio of 100:0.15:1.25 by volume), and a polyvinylchloride foam core (DIAB Divinycell H100, nominal thickness 25.5 mm). We refer to this system herein as "CFRP/PVC". The vinylester had a cure cycle of 45 minutes at room temperature and four hours at 82 °C. The CFRP/PVC sandwich and its constituents (CFRP and PVC) are immersed in artificial sea water at 25^{o}C and 50^{o}C.

These composite systems and their constituents (pure resins, FRP skins, foam cores) are subjected to gravimetric tests, prior to mechanical loading. Table 4-1 provides the immersion testing conditions for the samples, with different durations dictated by

experimental constraints[1]. The expression "artificial sea water" stands for a solution of deionized water and 3.5 % wt. content of NaCl.

Table 4-1: Immersion testing conditions

Temperature	**Immersion fluid**	**Sample**	**Duration (days)**
50°C	Deionized water	GFRP skins, PU foam	150
50°C	Artificial sea water	CFRP skins, PVC foam	107
50°C	Deionized water	GFRP/PU	188
50°C	Artificial sea water	CFRP/PVC	53
RT	Deionized water	pure epoxy, GFRP skins, PU foam	345
RT	Artificial sea water	pure vinylester, CFRP skins, PVC foam	210

Baseline and conditioned sandwich composites and their constituents were subjected to several types of mechanical tests on a hydraulic axial machine (MTS 810). Typically, bending tests (quasi-static, creep and stress relaxation) were conducted on foam and sandwich samples, while quasi-static axial tests were run for monolithic FRP samples, following the requirements of the appropriate ASTM standard. The bending test setups are shown in Figure 4-1. The picture on the left is the test setup for three point bending test on PU foam, and the right picture is four point bending test on a PVC foam sample.

[1] The immersion tests were planned until saturation was reached or up to 6 months. Immersion heaters were used in all tests. The evaporation rate of the room temperature water was slow enough not to require periodic refilling of the tank.

Figure 4-1 : Three and four point bending tests

In addition, polymeric resin, fiber reinforced polymer skin and sandwich composites were manufactured and tested at different loading and environmental condition. Table 4-2 and Table 4-3 show a list of experimental tests conducted at UC Davis. Two sandwich composite systems are considered. The first system is made of polyurethane foam core and GFRP skins with epoxy matrix. The second system is made of PVC foam core and CFRP skin with vinylester matrix. Testing is first done for the constituents within sandwich composites which are used to support the development of the

constitutive model and calibrate the material parameters. Testing on sandwich composites is considered for validation of the model.

Table 4-2: Summary of experimental tests in system 1

Specimen	**Testing mode**	**loading condition**
pure epoxy	Uniaxial tension	ramp
Polyurethane foam	bending	ramp/creep
GFRP skin	Uniaxial tension	ramp
Sandwich beam	bending	ramp/creep

Table 4-3: Summary of experimental tests in system 2

Specimen	**Testing mode**	**loading condition**
pure Vinylester	Uniaxial tension	ramp
PVC foam	bending	ramp/creep
CFRP skin	Uniaxial tension	ramp
Sandwich beam	bending	ramp/creep

The tests mentioned in Table 4-2 and Table 4-3 are conducted in three different environmental conditions, which are baseline (dry and room temperature), after immersion in fluid at room (25°C) and elevated temperature (50°C). The specimens for System 1 are immersed in deionized water, while the specimens in System 2 are immersed in sea water. All the tests as shown in the tables above are done for two different projects, System 1 (GFRP/PU) is for National Science Foundation (NSF) project and System 2 (CFRP/PVC) is for Office of Naval Research (ONR).

5. RESULTS AND DISCUSSION

In this chapter, the results are discussed for uniaxial, quasi static bending and time dependent tests and models for foams, skins and sandwich composites.

5.1. Response of Uniaxial Tension Tests

To characterize the skin behavior and obtain material parameters for the instantaneous elastic responses, the uniaxial test is performed on coupons of epoxy, vinylester, GFRP and CFRP. In FE analyses, one element is used to simulate loading under uniaxial tension due to a uniform stress and strain distributions (see Fig. 5.1). The dimensions of the coupons that are used in different uniaxial tests are shown in Table 5-1.

Table 5-1: Coupon dimension

Specimen	**width (mm)**	**thickness (mm)**
epoxy coupon	25.78	1.66
vinylester coupon	26.61	1.14
GFRP	25.7	1.6
CFRP	26.5	1.3

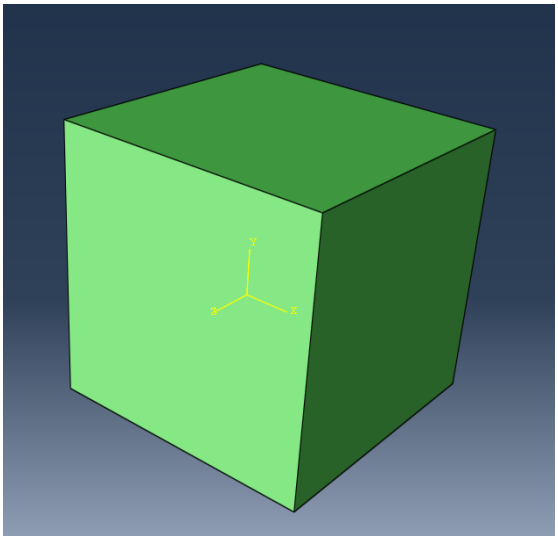

Figure 5-1 : One element model for uniaxial test

The uniaxial tests are conducted on various specimens in different environmental conditions. Table 5-2 shows the uniaxial tests on pure resins and FRPs.

Table 5-2: Uniaxial tension tests on pure resins and FRP

Material	**Condition**
Pure Epoxy	Baseline
	Immersion in deionized water at 25°C
	Immersion in deionized water at 50°C
GFRP	Baseline
	Immersion in deionized water at 25°C
	Immersion in deionized water at 50°C
Pure Vinylester	Baseline
	Immersion in sea water at 25°C
	Immersion in sea water at 50°C
CFRP	Baseline
	Immersion in sea water at 25°C
	Immersion in sea water at 50°C

The uniaxial tests are done on pure epoxy and experimental results and predictions are shown in Figure 5-2 to Figure 5-18. The calibrated material parameters are given in Table 5-3 and Table 5-4. The Poisson ratio for epoxy is measured as 0.34 and for vinylester is 0.25.

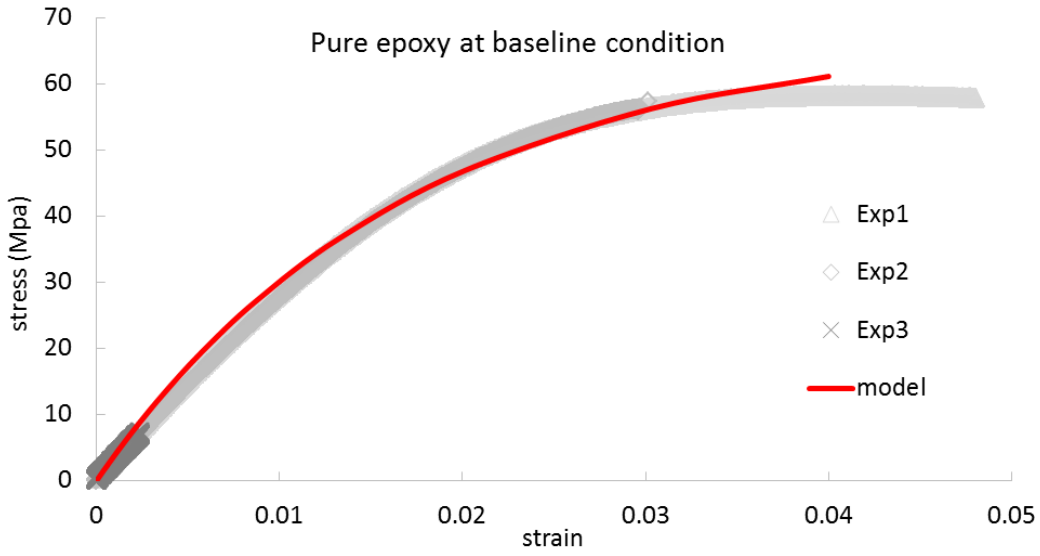

Figure 5-2 : Pure Epoxy in baseline condition; model and experiment

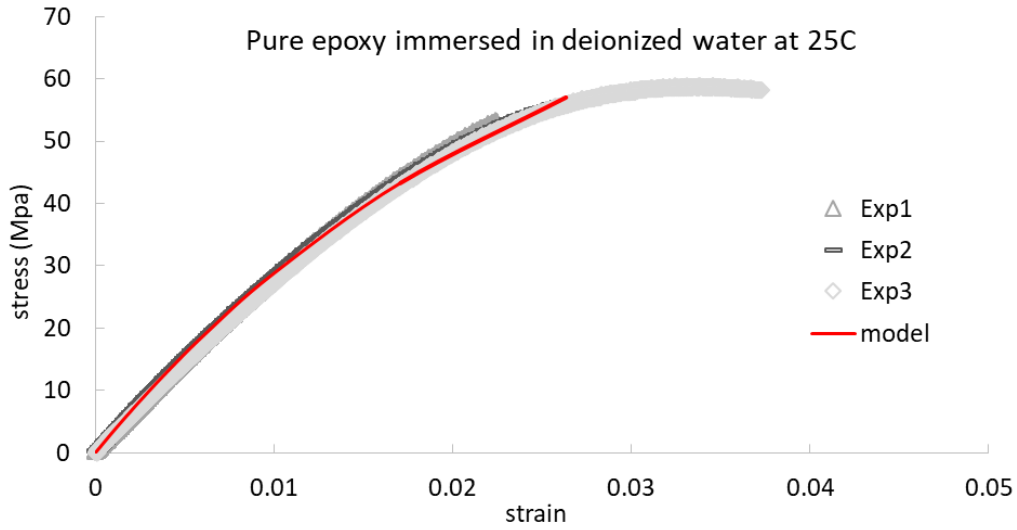

Figure 5-3: Pure epoxy immersed in deionized water at 25°C; model and experiment

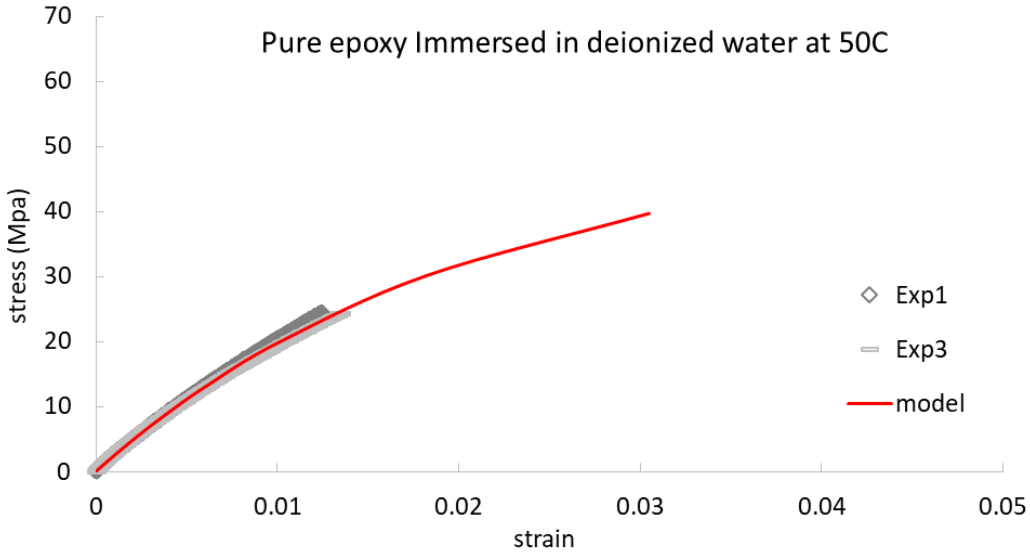

Figure 5-4: Pure epoxy conditioned at 50°C; model and experiment

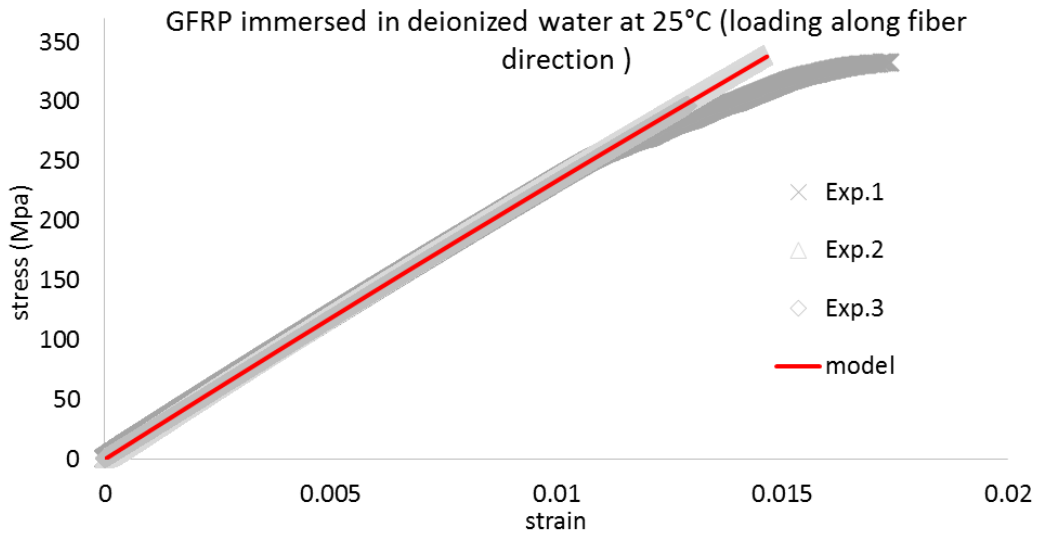

Figure 5-5: GFRP immersed in deionized water at 25°C (loading along fiber direction)

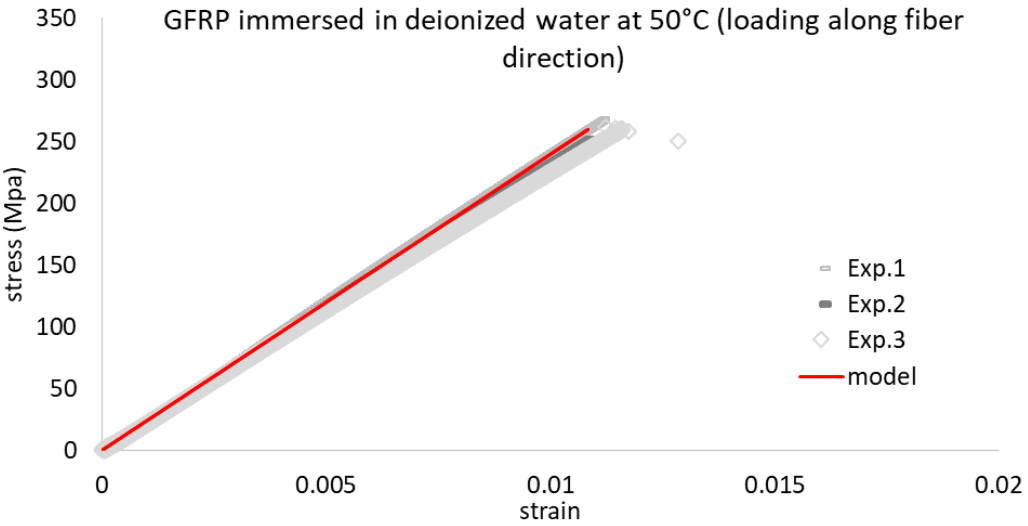

Figure 5-6: GFRP immersed in deionized water at 50°C (loading along fiber direction); model and experiment

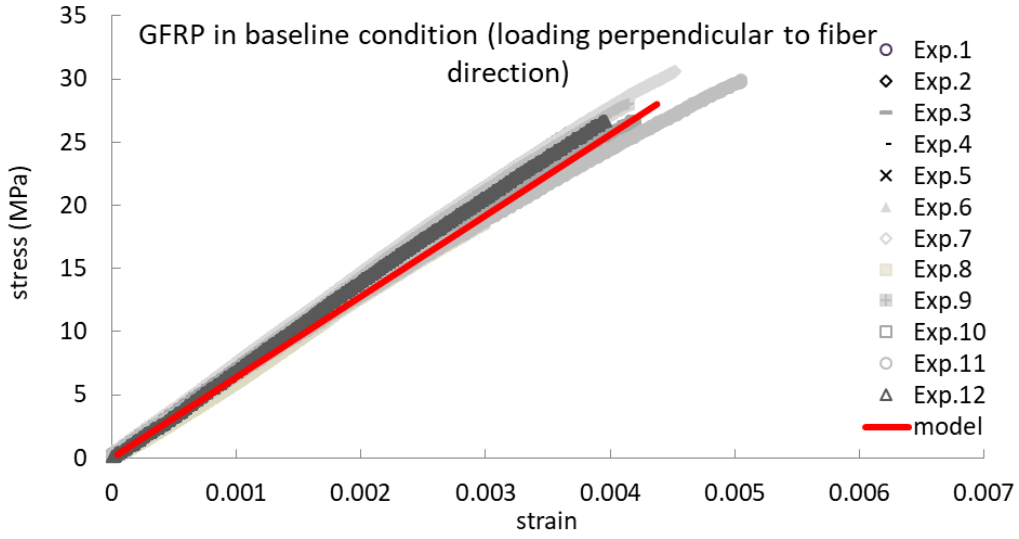

Figure 5-7: GFRP in baseline condition (loading perpendicular to fiber direction); model and experiment

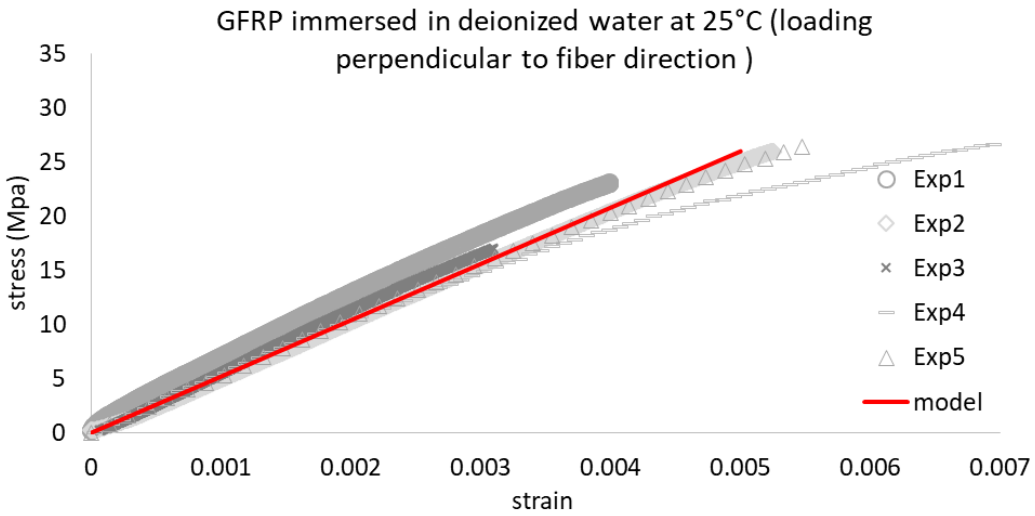

Figure 5-8: GFRP immersed in deionized water at 25°C (loading perpendicular to fiber direction); model and experiment

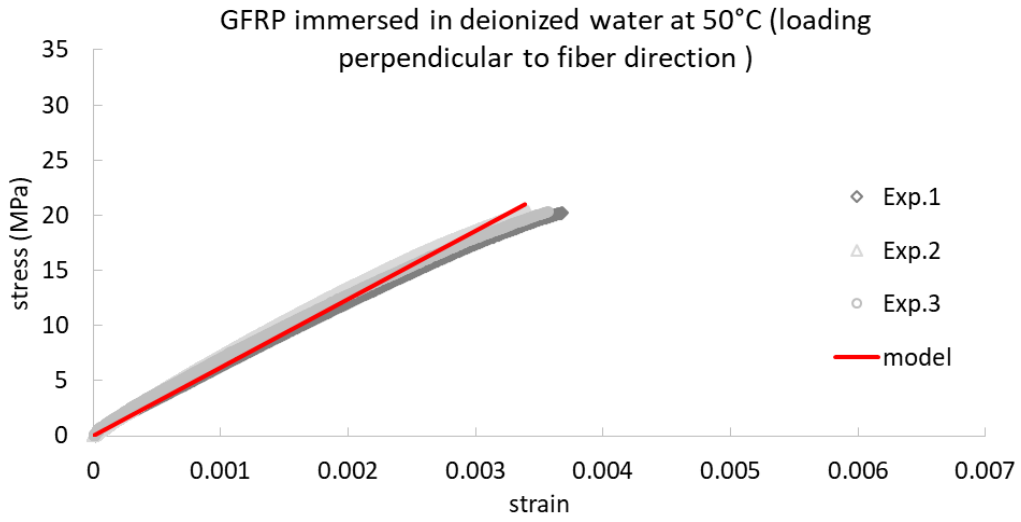

Figure 5-9: GFRP immersed in deionized water at 50°C (loading perpendicular to fiber direction); model and experiment

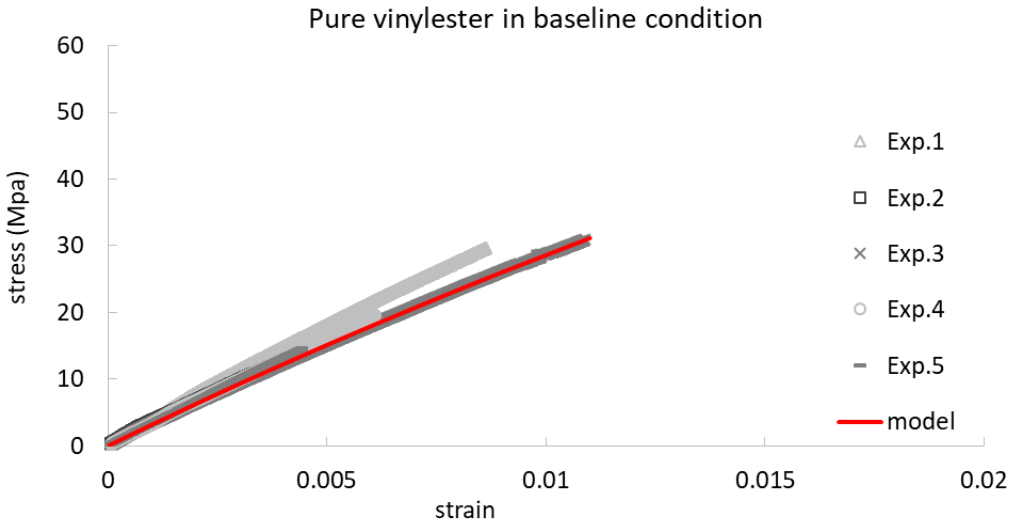

Figure 5-10: Pure vinylester in baseline condition; model and experiment

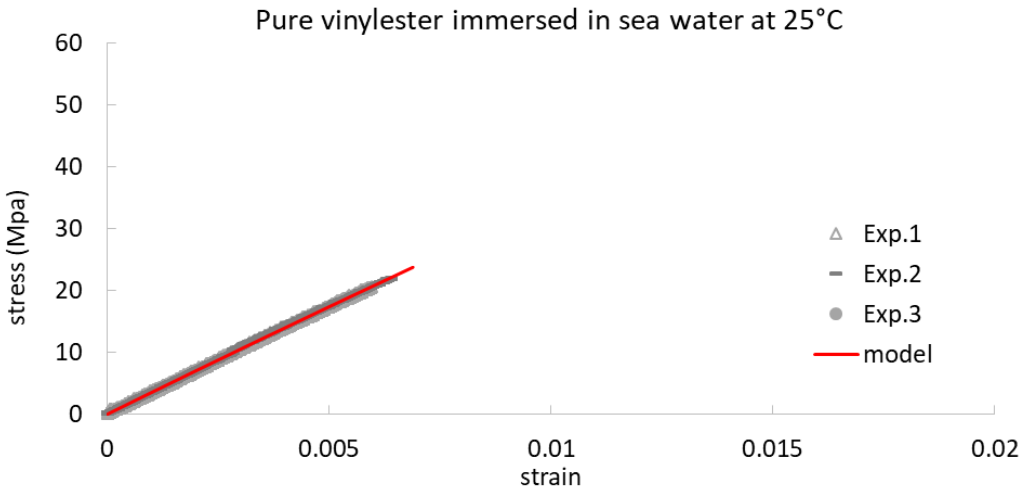

Figure 5-11: Pure vinylester immersed in sea water at 25°C; model and experiment

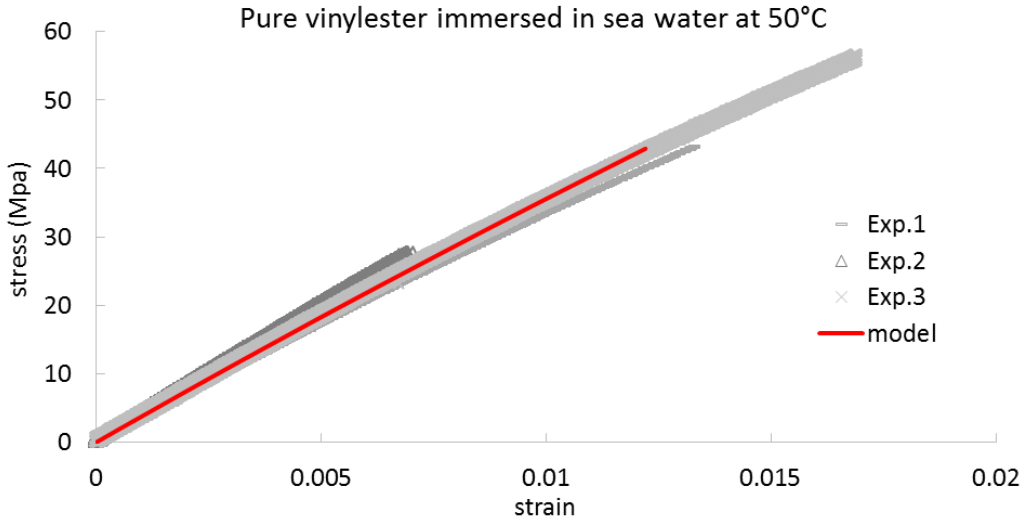

Figure 5-12: Pure vinylester immersed in sea water at 50°C; model and experiment

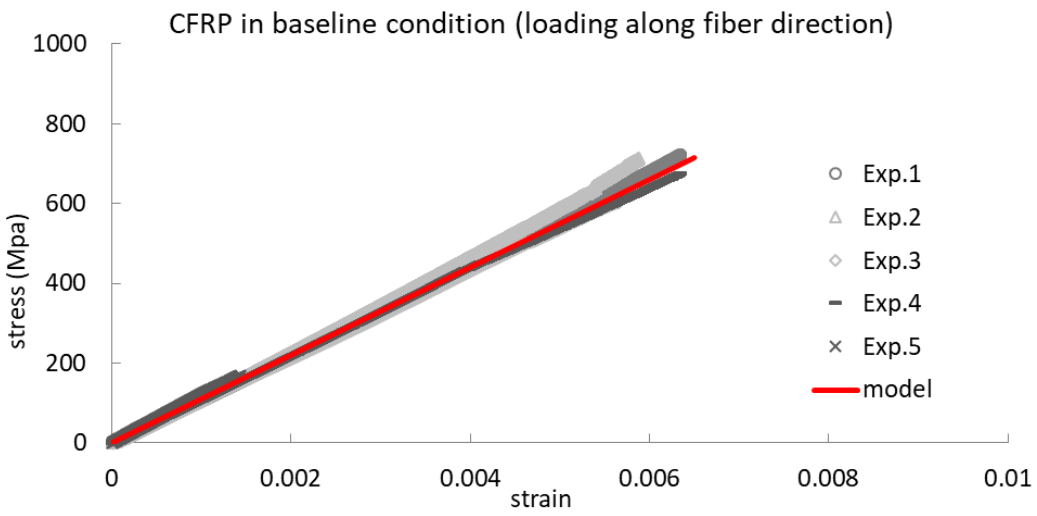

Figure 5-13: CFRP in baseline condition (loading along the fiber direction); model and experiment

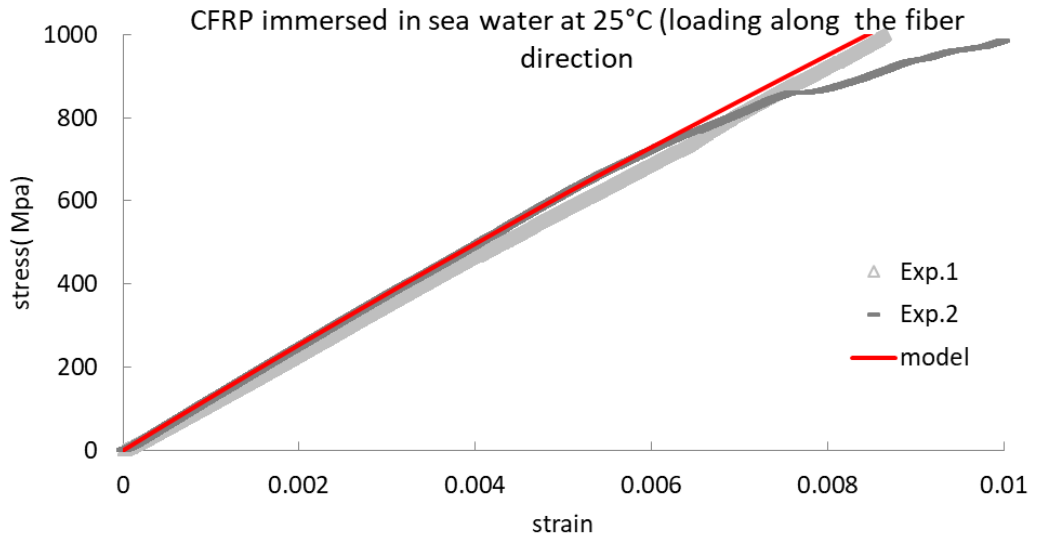

Figure 5-14: CFRP immersed in sea water at 25°C (loading along the fiber direction; model and experiment

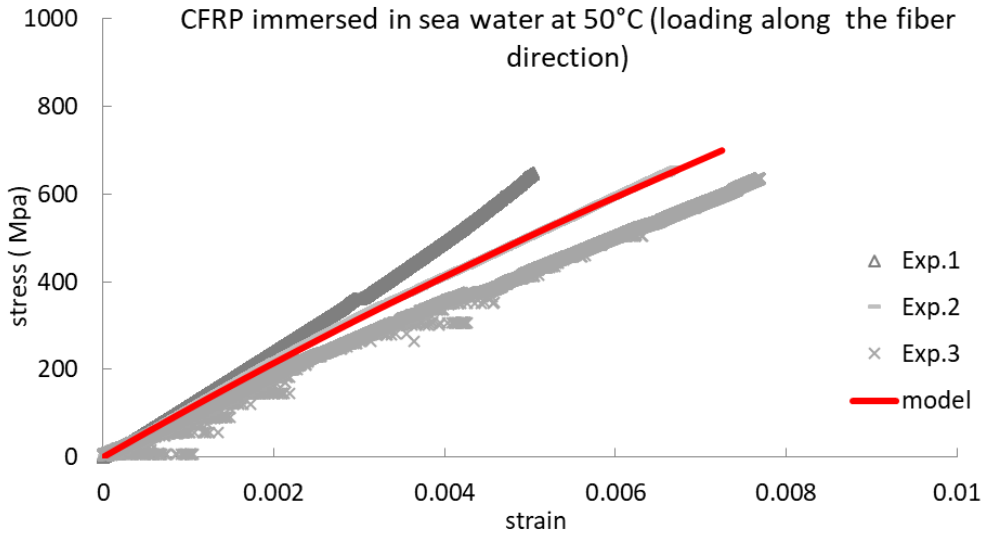

Figure 5-15: CFRP immersed in sea water at 50°C (loading along the fiber direction); model and experiment

In CFRP specimens with loading along the off-axis fiber direction of 90°, the elastic-plastic material model is used for describing their mechanical response. Figure 5-16 to Figure 5-18 show the responses of CFRP in the 90° off axis angle at different environmental conditions. Table 5-3 and Table 5-4 summarize the calibrated material parameters for epoxy and vinylester matrix, and GFRP and CFRP skins under different environmental conditions.

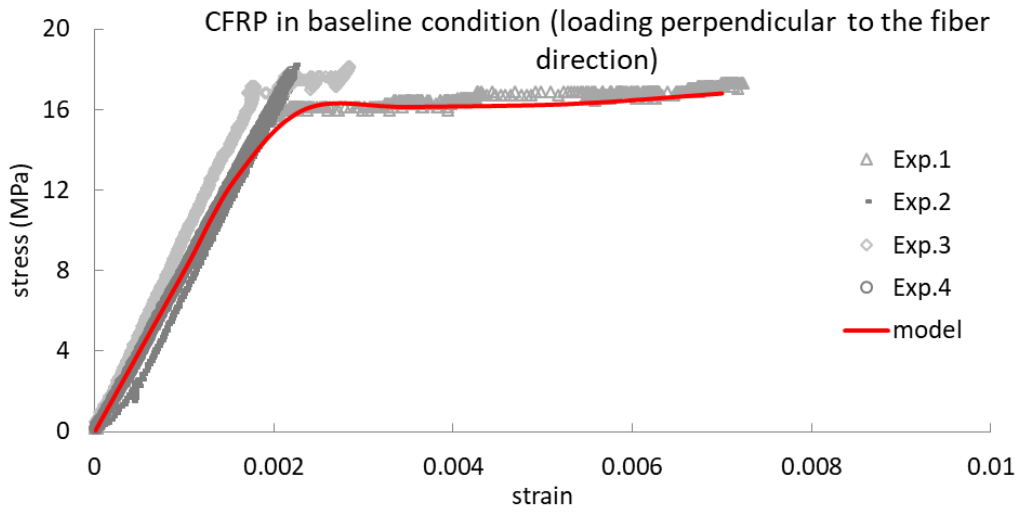

Figure 5-16: CFRP in baseline condition (loading perpendicular to the fiber direction); model and experiment

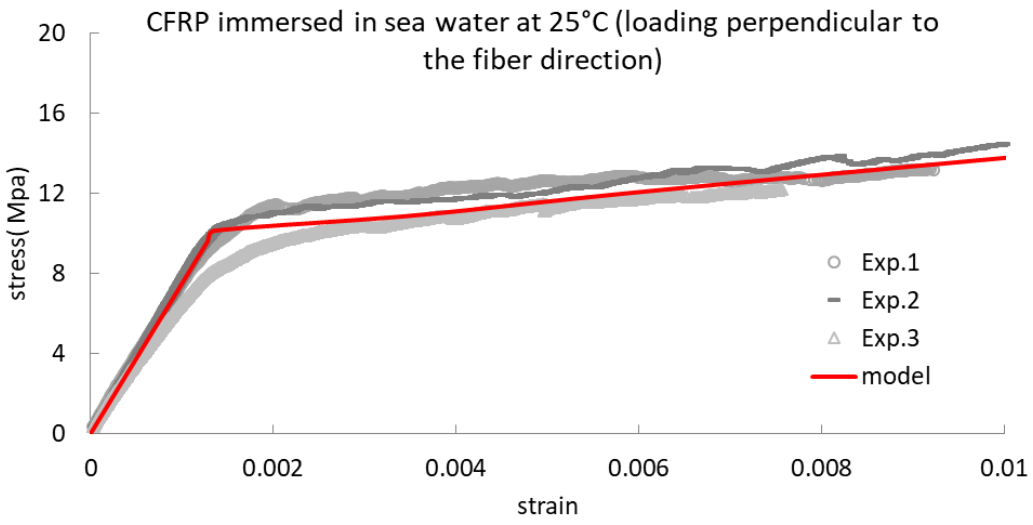

Figure 5-17: CFRP immersed in sea water at 25°C (loading perpendicular to the fiber direction); model and experiment

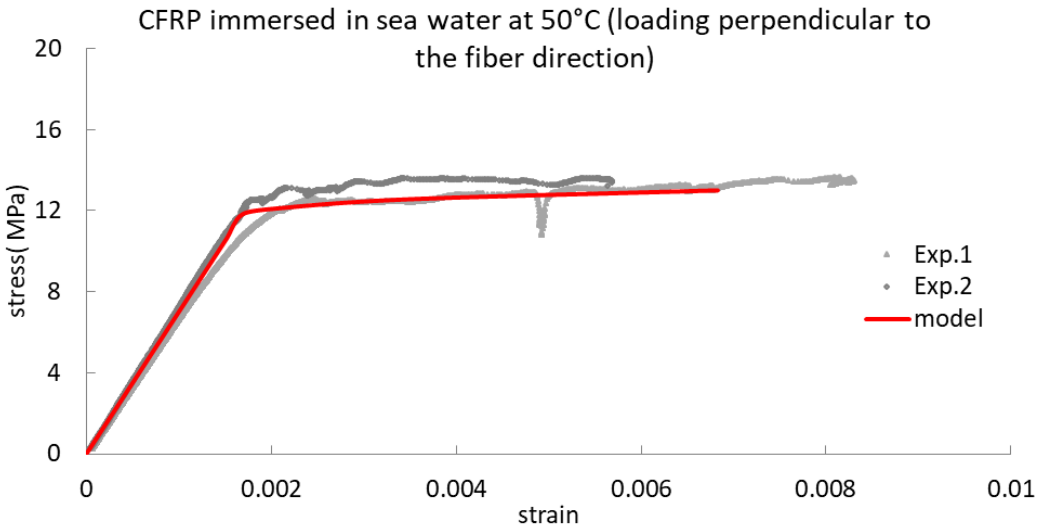

Figure 5-18: CFRP immersed in sea water at 50°C (loading perpendicular to the fiber direction); model and experiment

Table 5-3: Mechanical properties of pure epoxy and vinylester

Material	condition	E(MPa)	B	standard deviation for experiments
pure epoxy	baseline	4000	53	0
	Immersion in deionized water at 25C	3500	36	0
	Immersion in deionized water at 50C	2500	43	0
pure vinylester	baseline	3200	20	89
	Immersion in sea water at 25C	3540	7	0
	Immersion in sea water at 50C	3670	10	278

Table 5-4: Mechanical properties of GFRP and CFRP matrix

Material		E (MPa)	B	standard deviation for experiments	E (MPa)	yield stress (MPa)	standard deviation for experiments
		loading along fiber direction			loading perpendicular to fiber direction		
GFRP	baseline	–	–		6800	–	192
	Immersion in deionized water at 25C	24000	5	0	5200	–	164
	Immersion in deionized water at 50C	24000	0	500	6200	–	150
CFRP	baseline	110000	0	2302	8000	16	541
	Immersion in sea water at 25C	160000	50	0	7500	10.4	288
	Immersion in sea water at 50C	112000	37	10816	7000	12	282

Also from the experiments that we have done on foams and fiber reinforced polymeric skins, the observed ultimate stresses and strains are given in Table 5-5 for pure resins, CFRP and GFRP and Table 5-6 shows the load and deflection at the point of failure. We should consider that these stresses and strains are not exact and in some experiments show some variations.

Table 5-5: Ultimate (failure) stress and strain for resins and FRP skins

Material	**baseline**		**Conditioned at 25°C**		**Conditioned at 50°C**	
	Stress (MPa)	strain	Stress (MPa)	strain	Stress (MPa)	strain
Pure Epoxy	60	0.03	60	0.02	25	0.015
Pure Vinylester	30	0.009	20	0.0065	45	0.013
GFRP (loading along fiber direction)	–	–	320	0.015	250	0.011
GFRP (loading perpendicular to fiber direction)	25	0.004	25	0.005	20	0.0035
CFRP (loading along fiber direction)	700	0.006	1500	0.011	500	0.006
CFRP (loading perpendicular to fiber direction)	17	0.007	15	0.011	13	0.006

Table 5-6: Ultimate (failure) Load and deflection for foams

Material	**baseline**		**Conditioned at 25°C**		**Conditioned at 50°C**	
	Load (N)	Deflection (mm)	Load(N)	Deflection (mm)	Load (N)	Deflection (mm)
Polyurethane foam	80	12	75	12	80	12
PVC foam	430	14	400	19	1300[2]	16

[2] From four point bending test

5.2. Quasi Static Bending Model and Tests

In This part the three point and four point bending models for foam and sandwich composite are discussed.

5.2.1. Three Point Bending Model for Foam

The FE analysis is now used for describing bending in polymeric foams. The dimensions of the foam specimens are given in Table 5-7. It is a simply supported beam with loading in the middle of the beam.

Table 5-7: Foam dimensions

Specimen	**thickness (mm)**	**width (mm)**	**length (mm)**	**span length (mm)**
Polyurethane beam	19	57.3	165	150
PVC beam	25.5	57.2	165	150

The diagram of three point bending is shown in Figure 5-19. Figure 5-20 shows the experimental test setup. The simply supported mechanical boundary conditions are assumed for FE model. In order to model a simply supported beam, one side of the beam is constrained to prevent displacement in y direction and on the other side of the beam, the displacements in y and x direction are restricted. Figure 5-21 shows the boundary conditions and the loading in mid-section of the beam. Also, two point are considered to have constraint to prevent displacement in the z direction. The FE mesh of the beam is generated using the nonlinear three dimensional continuum elements (C3D20) and a convergence study has performed in order to determine the number of elements required for the analyses. The convergence study is performed by comparing the result from the

FE analysis, within a linear elastic range, with the analytical solution of a linear elastic beam.

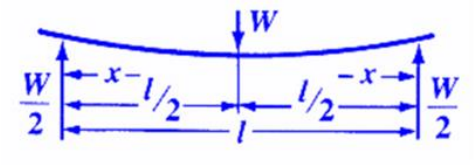

Figure 5-19 Three point bending diagram

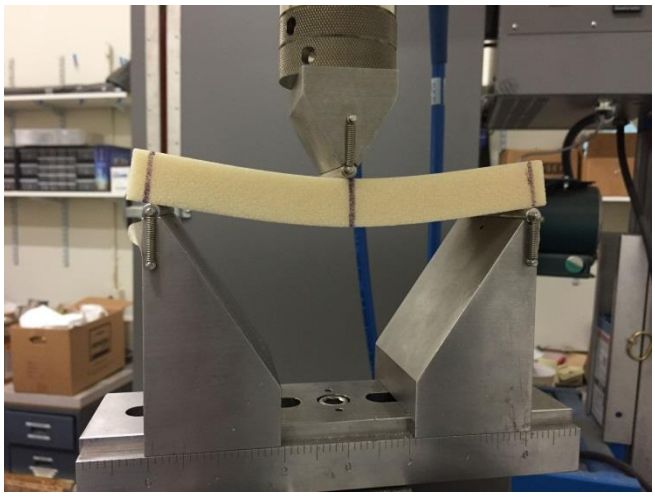

Figure 5-20 Three point bending test set up

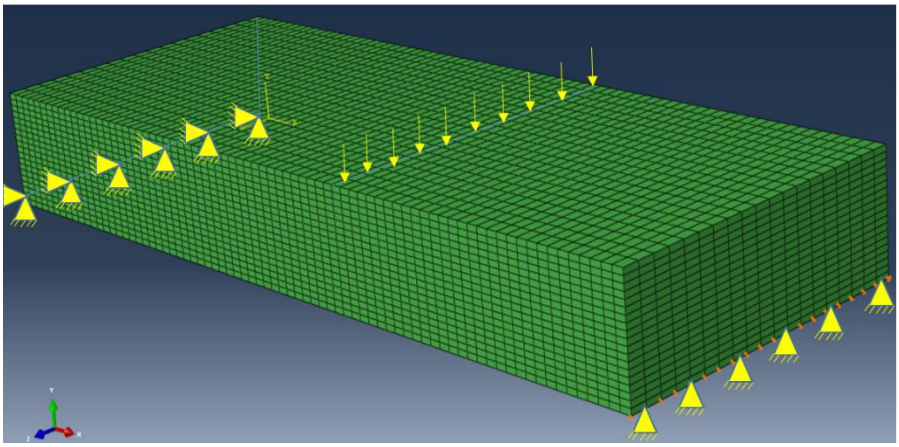

Figure 5-21: Boundary conditions of three point bending model

For the analytical calculation of the deflection in quasi static three point bending test we have

$$\delta = w\left(\frac{L^3}{48EI} + \frac{1.2L}{4AG}\right) \qquad (5-1)$$

where δ is the deflection at the mid-section of the beam, W is the load at mid-section, L is beam length and E is elastic modulus. I is the second moment of an area for rectangular cross section of the beam, A is cross section area and G is shear modulus. These dimensions and properties are shown in Table 5-8 for PVC foam. The shear modulus for isotropic material is:

$$G = \frac{E}{2(1+\nu)} \qquad (5-2)$$

Table 5-8: PVC foam properties and dimensions

PVC foam (ONR)							
ν	Max load (N)	Length (mm)	E (MPa)	G (MPa)	I	Thickness (mm)	Width (mm)
0.25	420	150	65	26	79037.89	25.5	57.2

The load-displacement plot for PVC foam in baseline condition is shown in Figure 5-22. Quasi static test was done five times to get repeatable results. By assuming the Young modulus equal to 65 MPa in Eq. 5-27, the analytical result captures the linear part of plot well. The overall response of foam under bending is nonlinear, as shown in Figure 5-22. The nonlinear material parameters were calibrated from the QLV model using FE model and are shown in Figure 5-23. The material properties that is obtained from calibration, assuming Poisson ratio equal to 0.25, are E= 75 MPa and B=7.2. Comparing the elastic modulus from calibration with analytical calculation we can see that they are almost in agreement. In analytical calculation a linear elastic behavior is assumed and the difference between the elastic modulus in analytical and model is because of the nonlinearity of material behavior.

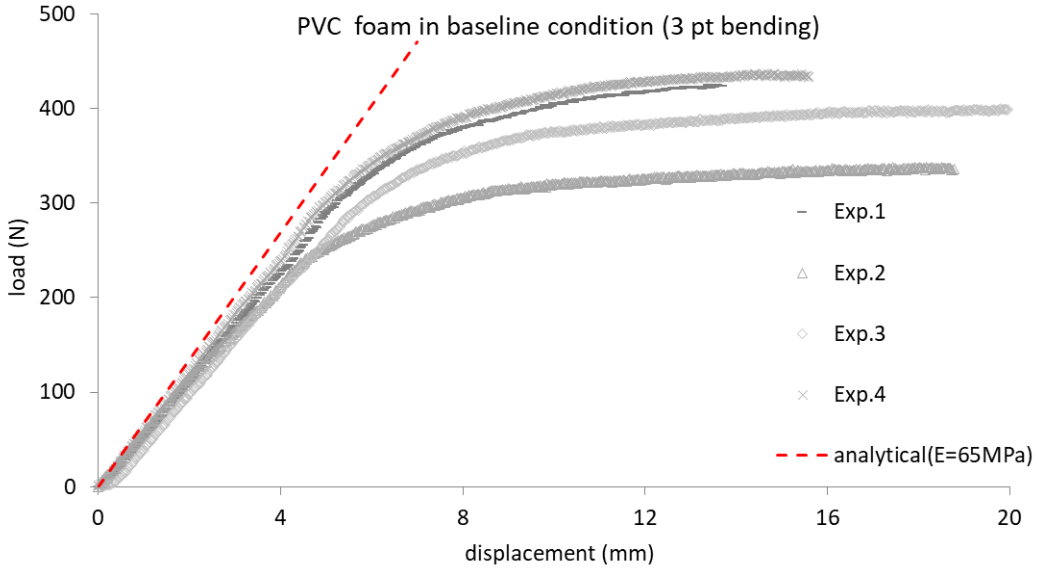

Figure 5-22 : Experimental and analytical result for 3 point bending in PVC baseline foam

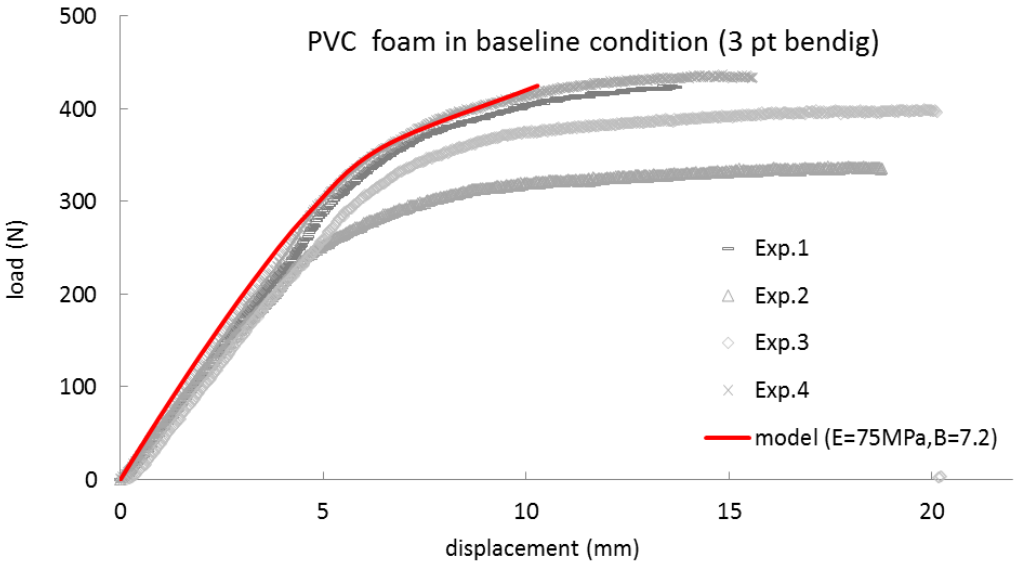

Figure 5-23: FE result of PVC foam in baseline condition under quasi static test and comparison with experiment

In addition, three point bending tests are conducted for conditioned PVC foam after immersion in sea water at ambient temperature. The nonlinear material parameters calibration is shown in Figure 5-24.

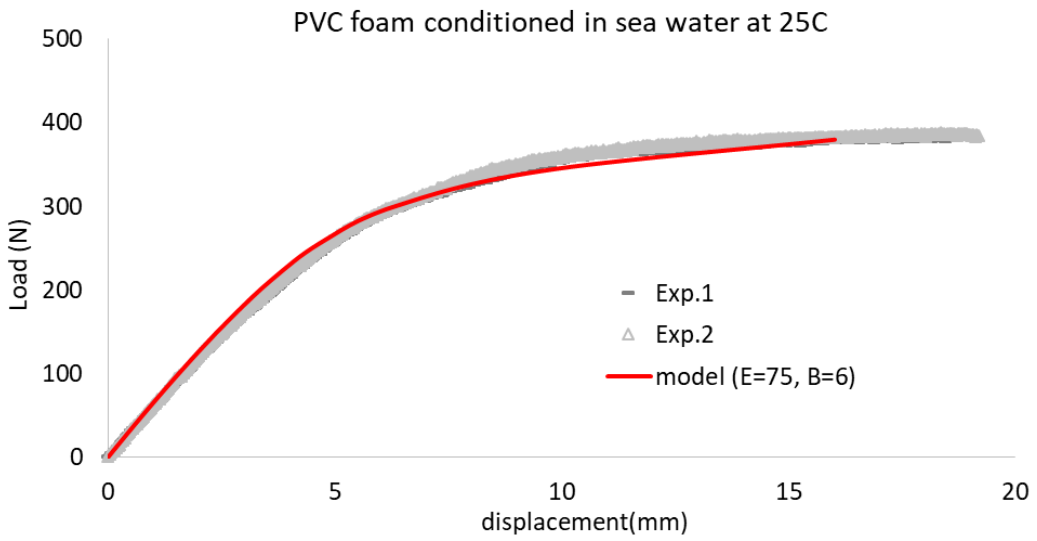

Figure 5-24: PVC foam conditioned in sea water at room temperature; model and experiment

Also three point bending tests are conducted on Polyurethane foam in three different environmental conditions such as baseline, immersed in deionized water at ambient temperature and immersed in deionized water at 50°C. By assuming the Young modulus equal to 24 MPa and using properties in Table 5-9 and Eq. 5-27, the analytical result captures the linear part of the plot well. It is shown in Figure 5-25. The overall responses of foam under bending are nonlinear and the nonlinear model result for different environmental conditions are shown Figure 5-26 to Figure 5-28.

Table 5-9: Polyurethane foam properties and dimensions

Polyurethane foam (NSF)							
ν	Max load(N)	Length (mm)	E (MPa)	G (MPa)	I	Thickness (mm)	Width (mm)
0.34	80	150	24	9.23	29150.75	19	51

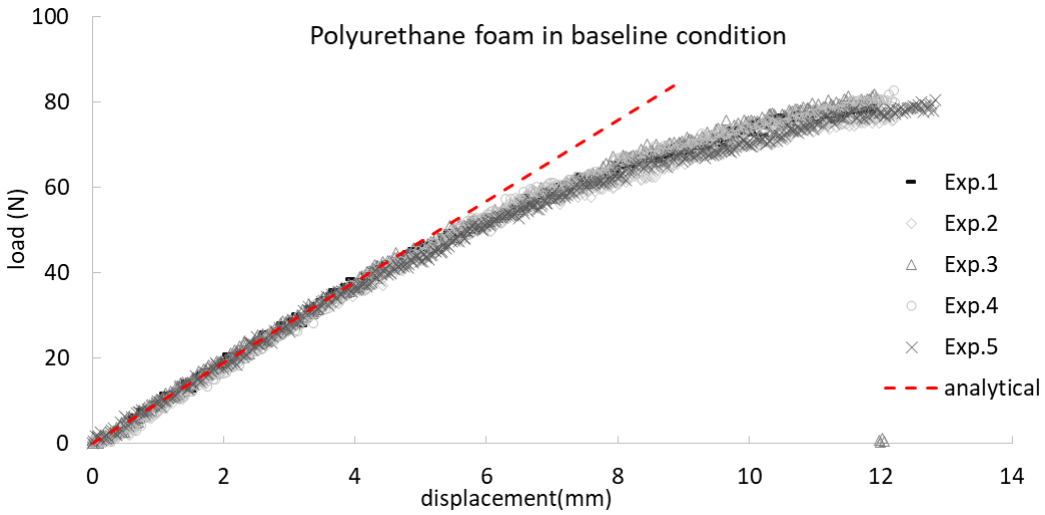

Figure 5-25: Polyurethane foam at baseline condition; analytical result and experiment

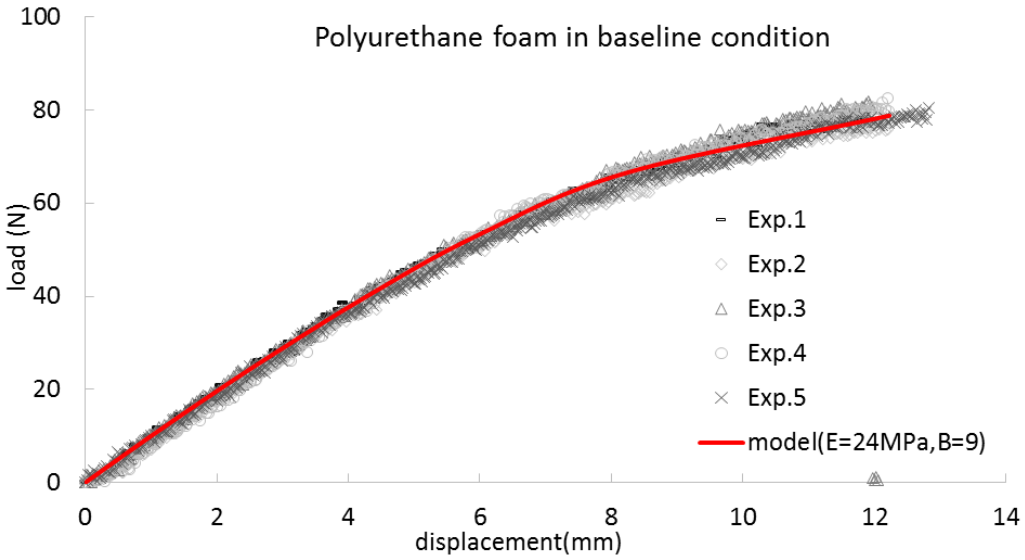

Figure 5-26: Polyurethane foam in baseline condition; model and experiment

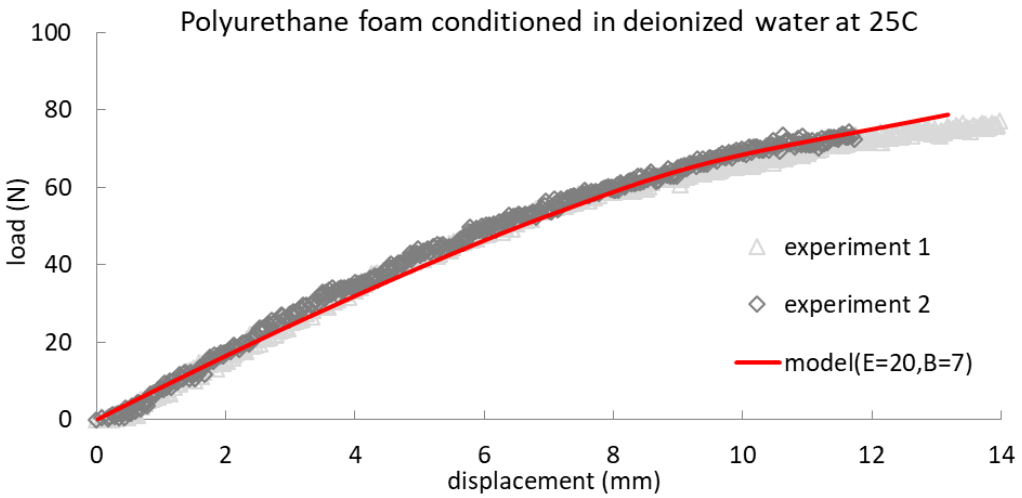

Figure 5-27: Polyurethane foam conditioned in deionized water at ambient temperature; model and experiment

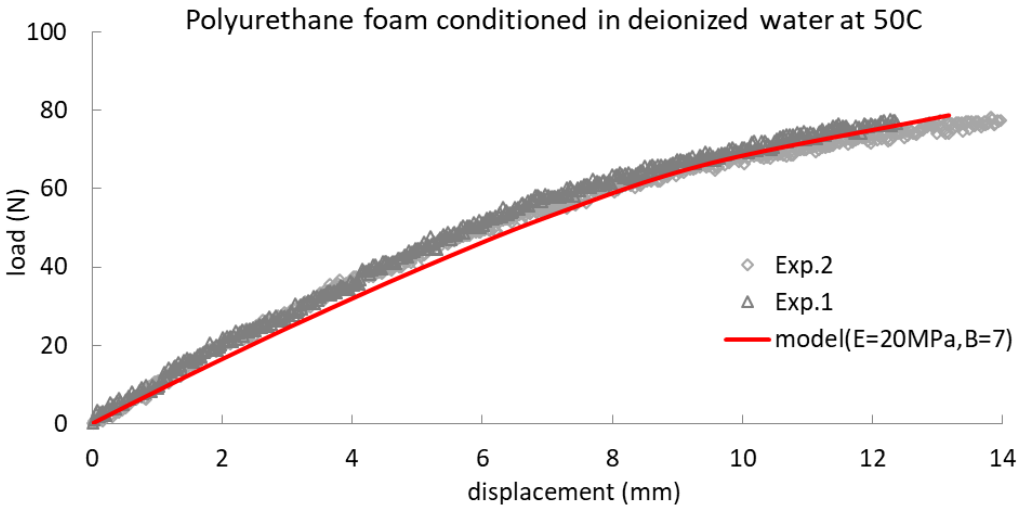

Figure 5-28: Polyurethane foam conditioned at 50 C; model and experiment

The material properties obtained from three point bending tests for foams are shown in Table 5-10.

Table 5-10: Material properties for foam in three point bending

material	condition	3 points bending result		standard deviation for experiments
		E(Mpa)	B	
PVC foam	baseline	75	7.2	2.7
	conditioned in sea water at 25C	75	6	0
Polyurethane	baseline	24	9	0
	conditioned in deionized water at 25C	20	7	0
	conditioned in deionized water at 50C	20	7	0

5.2.2. Four Point Bending Model for Foam

This model is used for simulating the bending in foam and sandwich composites. In this study both three point bending and four point bending tests are done on the specimens with the same material to check the accuracy and reliability of the result. In some cases, only four point bending test is done. The dimensions of foam specimens are the same as the ones used in three point bending and the prescribed loads are shown in Figure 5-29 and the boundary conditions are shown in Figure 5-30. The distance between two loads is about 90 mm and each load line is located at about 30 mm from the beam end. The four point bending test set up and foam under bending are shown in Figure 5-31.

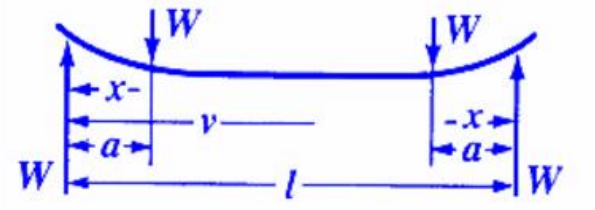

Figure 5-29 Four point bending diagram

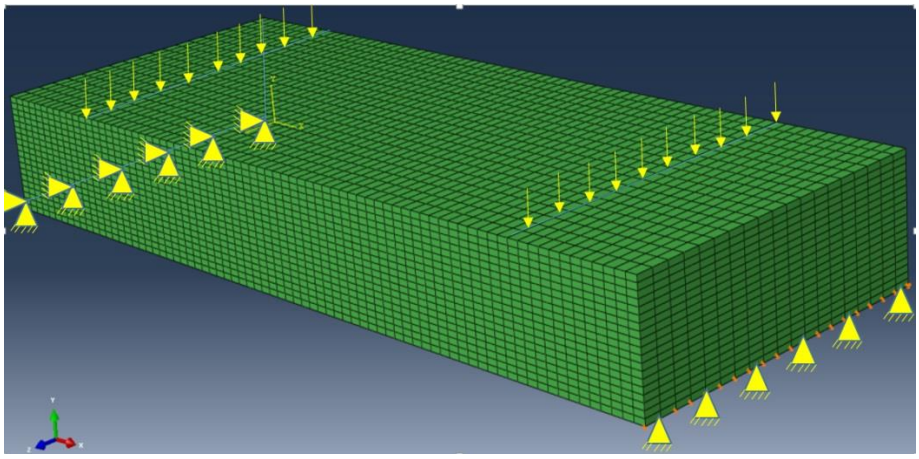

Figure 5-30: Boundary condition in four point bending

Figure 5-31: Four point bending test on PVC foam

For the beam under four point bending the deflection is

$$\delta = \frac{wa^2}{6EI}(3l - 4a) + \frac{wa}{2AG} \qquad (5-3)$$

where W is the load, δ is the deflection at the loads, a is distance between support and loading, L is the beam length and E is elastic modulus. I is the second moment of area for rectangular cross section of the beam, A is cross section area and G is shear modulus. These dimensions and properties are shown in Table 5-11.

Table 5-11: PVC foam properties and dimensions in four point bending

PVC foam							
ν	Max load(N)	Length (mm)	*E* (MPa)	*G* (MPa)	*I*	Thickness (mm)	Width (mm)
0.25	1300	150	65	26	78761.53	25.5	57

The load-displacement plot is shown in Figure 5-32. The quasi static tests were repeated 3 times. By assuming the Young modulus equal to 65 MPa the analytical result for linear elastic material capture the linear part of plot well. Next, the FE analysis is performed for capturing the nonlinear responses of PVC foams, as shown in Figure 5-33.

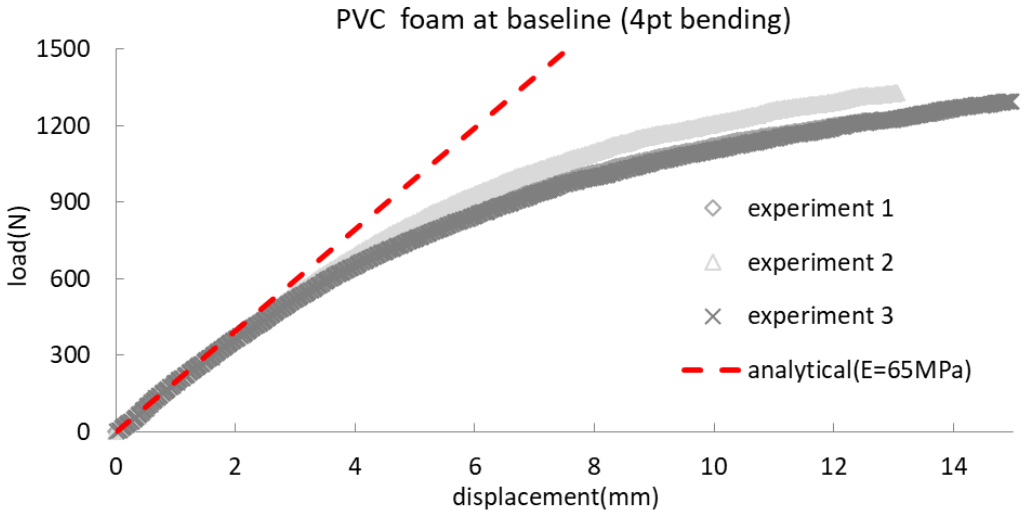

Figure 5-32 : Experimental and analytical result for 4 point bending in PVC baseline foam

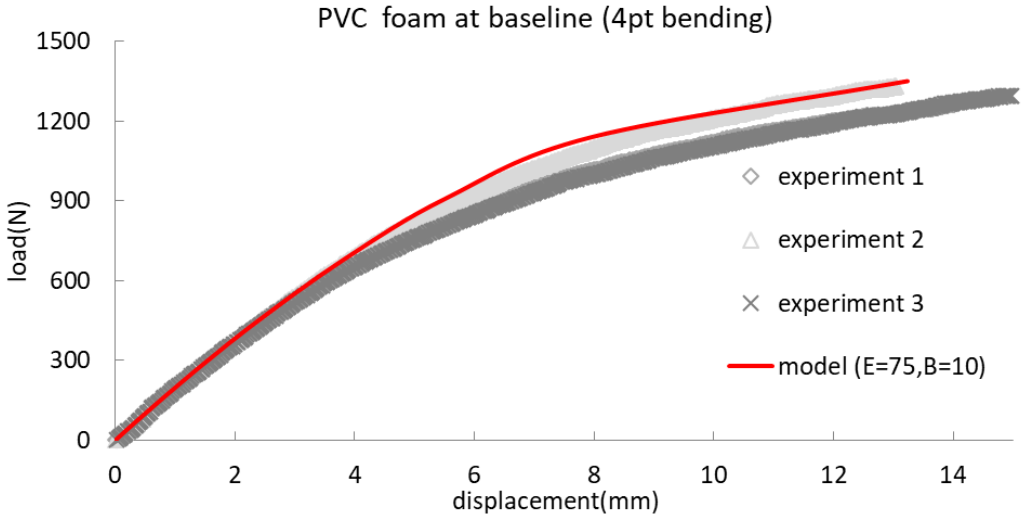

Figure 5-33 : Experimental and FE result for 4 point bending in PVC baseline foam

From the calibration we obtain material properties as follow: E=75 MPa, B=10. The comparison between results of four point bending and 3 point bending are shown in

Figure 5-34 .In this plot the 4 point bending result is compared with the 4 point bending model when the material properties from 3 point bending is used.

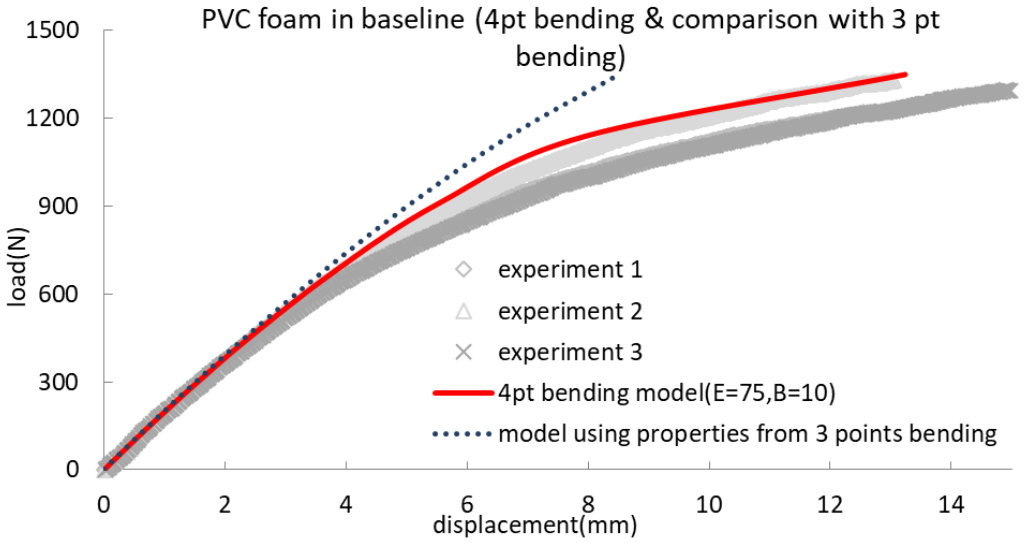

Figure 5-34: Comparison between four point and three point bending for PVC in baseline condition

Figure 5-34 shows that there is an agreement, especially in elastic region, between the result for three point bending test and four point bending test. Also the moment-curvature diagram is shown in Figure 5-35 for 3 point bending and 4 point bending, which indicates similar behavior. Deviation starts at highly nonlinear response, but they are relatively small.

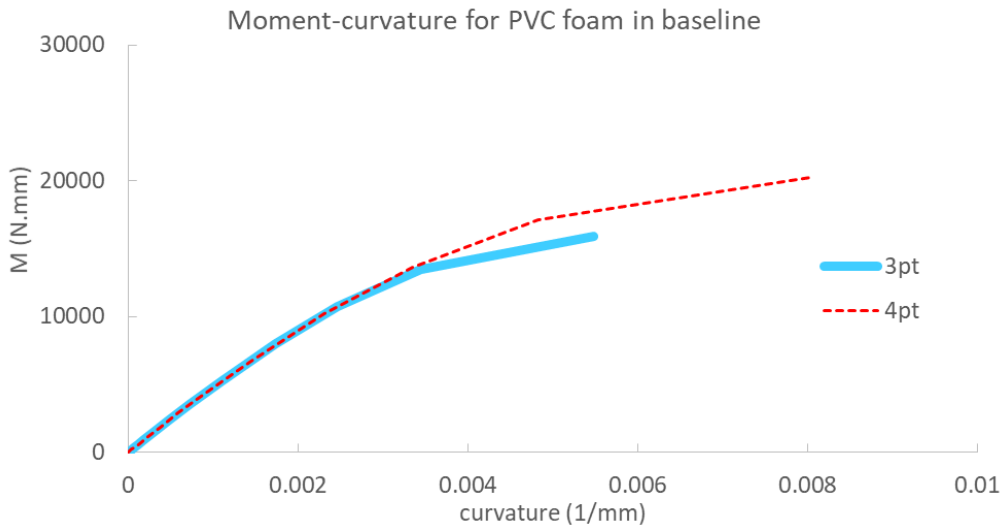

Figure 5-35 : Moment- curvature for PVC foam in baseline condition (3 point and 4 point bending comparison)

Figure 5-36 shows the four point bending test for PVC foam conditioned in sea water at 50°C and the model that is used to get material properties. The material properties that are obtained from this test are E=50MPa and B=6.

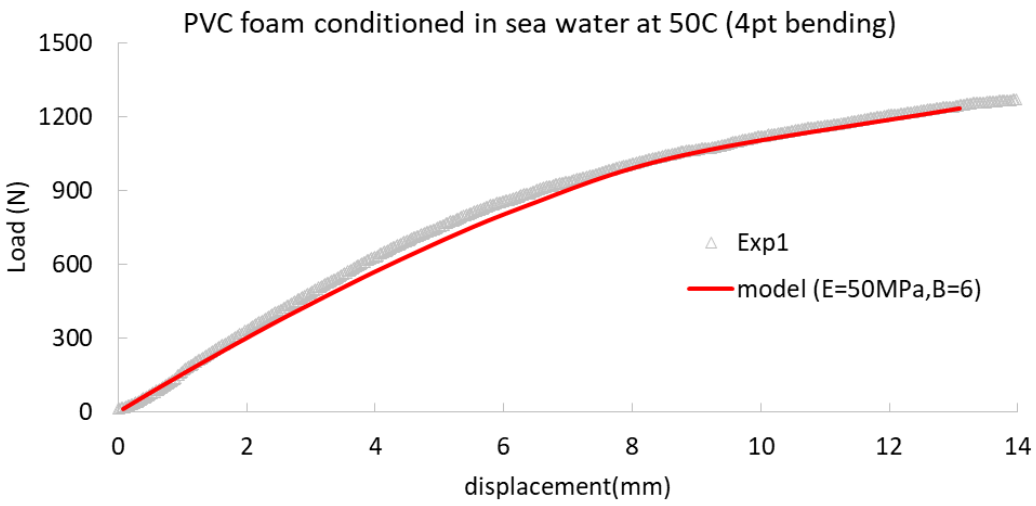

Figure 5-36: Experimental and FE result for 4 point bending in PVC foam at 50°C

The same procedure is done for Polyurethane in four point bending condition. Analytical calculation using Eq. 5-29 and assuming the elastic modulus equal to 26 MPa for Polyurethane foam leads to result in Figure 5-37.

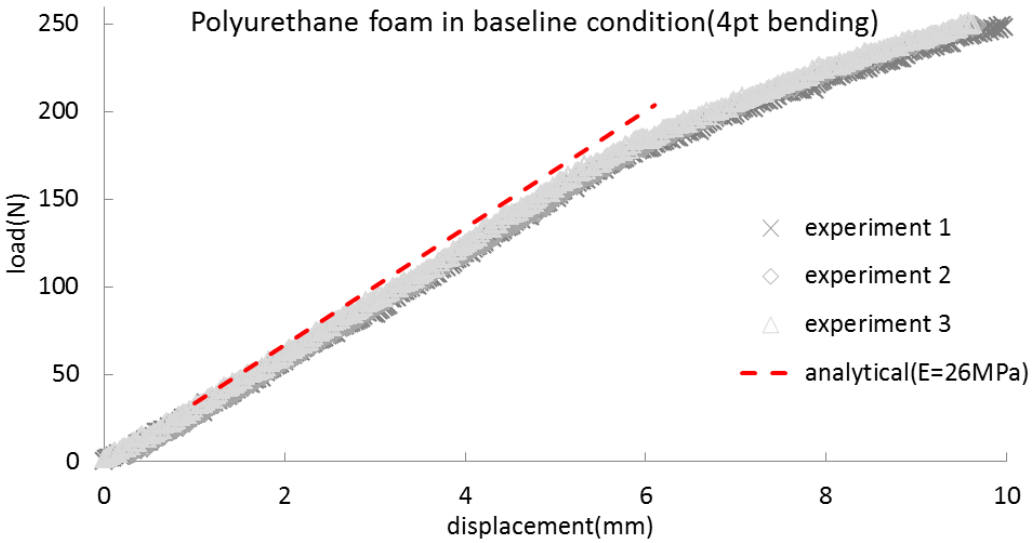

Figure 5-37: Four point bending analytical result for Polyurethane foam in baseline condition and comparison with experiment

The nonlinear model result and comparison with experiment are shown in Figure 5-38. The material properties from calibration are *E=30* MPa and *B= 17*. Comparing the elastic modulus, *E*=30 MPa, from nonlinear model and *E*=26 MPa from the analytical calculation does not show any significant difference. Figure 5-39 shows the comparison between model using properties from 3 point bending with four point bending model in baseline condition and they are relatively close.

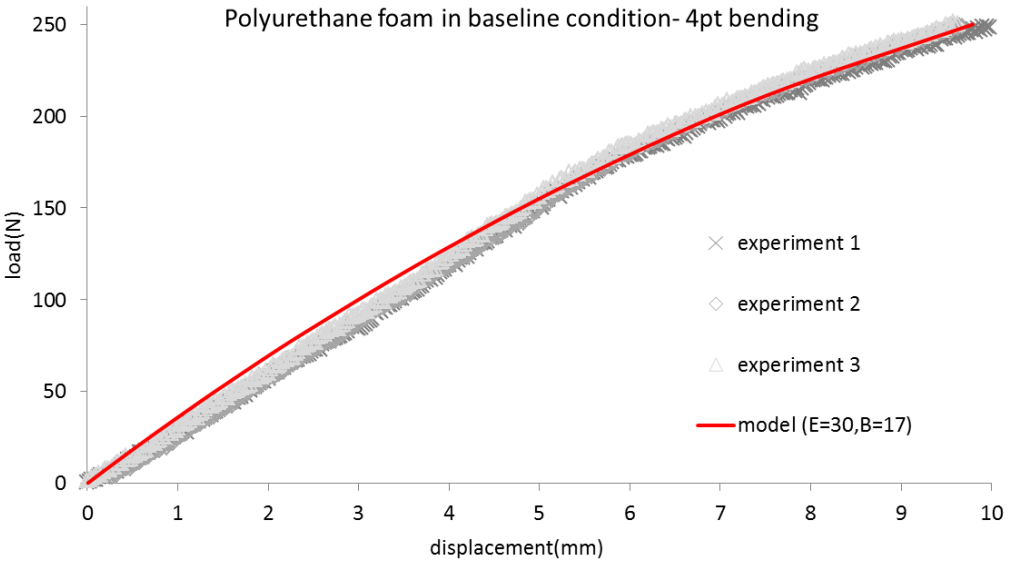

Figure 5-38: Four point bending for Polyurethane foam in baseline condition; model and experiment

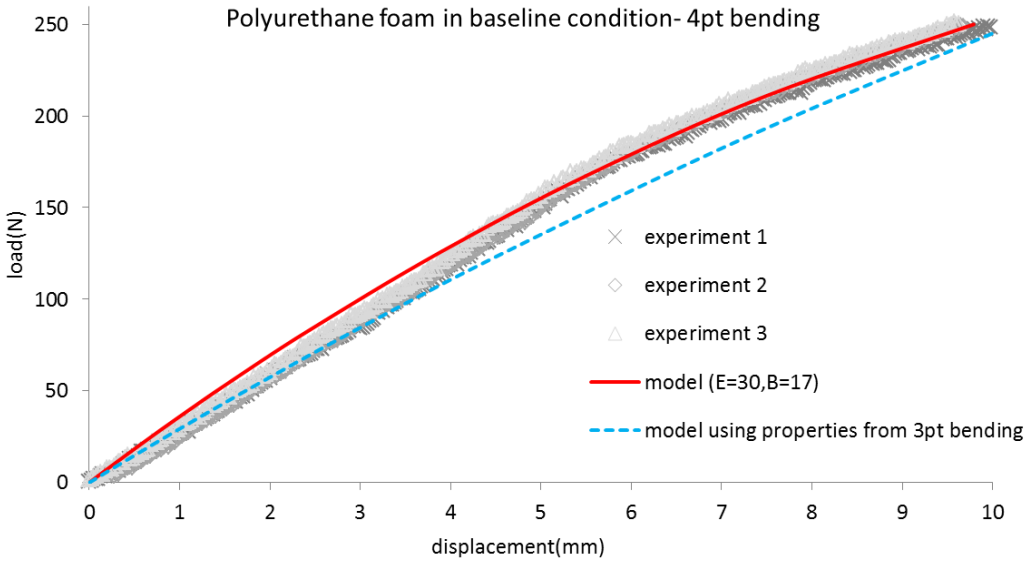

Figure 5-39: Comparison of results from 3 point bending and 4 point bending for Polyurethane foam in baseline condition

5.2.3. Three Point Bending Model for Sandwich Composites

In the previous sections, FE model and mesh were described for CFRP and GFRP skins and foams. In this part the sandwich composite will be simulated. For the sandwich composite we have three point bending and four point bending tests under different loading conditions such as ramp loading, creep and stress relaxation. The specimens are beams consist of PVC foam core and CFRP in CFRP/PVC system and polyurethane foam core and GFRP in GFRP/PU sandwich composite system. Loadings are perpendicular to fiber direction in skins. The tests and modeling are done in two different environmental conditions. The first condition is dry at ambient temperature (baseline condition) and the second condition is after immersion in deionized water at 50°C in GFRP/PU system and immersion in sea water at 50°C in CFRP/PVC system. Figure 5-40 shows the sandwich composites used for three point bending test.

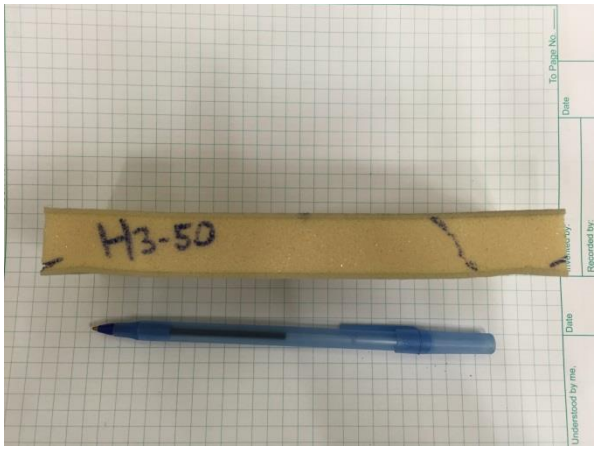

Figure 5-40: Sandwich composite specimen

To simulate the sandwich composite in Abaqus, the foam and skin are modeled separately using partitioning. The nonlinear three dimensional continuum elements (C3D20) are used. A convergence study was first done in order to determine the proper number of elements.

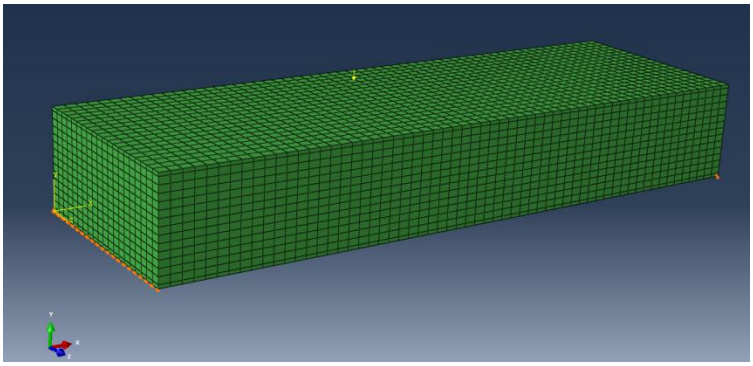

Figure 5-41: ABAQUS model for composite

First, analytical model was considered in determining the overall mechanical response of sandwich composites, considering mainly a linear elastic response. The deflection of the composite beam consists of PVC foam and CFRP skin is analyzed and compared to experimental result. Figure 5-42 shows the core and skins layers. Table 5-12 shows the properties and dimensions of CFRP/PVC sandwich composite at baseline condition:

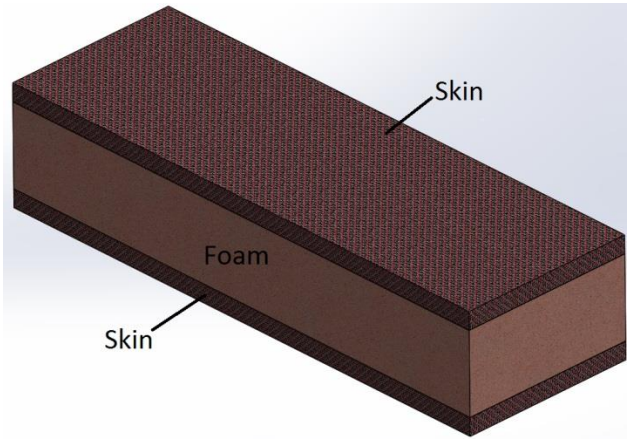

Figure 5-42: Sandwich composite layers

Table 5-12: CFRP/PVC sandwich composite properties and dimensions at baseline

Width (mm)	**E_s (MPa)**	**E_f (MPa)**	**G (MPa)**	**ν**	**t_f (mm)**	**t_s (mm)**
57.3	8000	75	30	0.25	25.16	1.22

For CFRP/PVC Sandwich composite under three point bending loading we have:

$$\overline{EI} = E_f I_f + E_s I_s \qquad (5-4)$$

where the subscript *'f'* shows the properties related to foam and subscript *'s'* shows the skin's properties and E is elastic modulus and I is the second moment of area. G is the shear modulus and A is the cross section area of foam core. So the maximum deflection at the center of the beam is

$$\delta = w\left(\frac{L^3}{48EI} + \frac{1.2L}{4AG}\right) \qquad (5-5)$$

By plotting the analytical calculation and comparing with experimental result we have

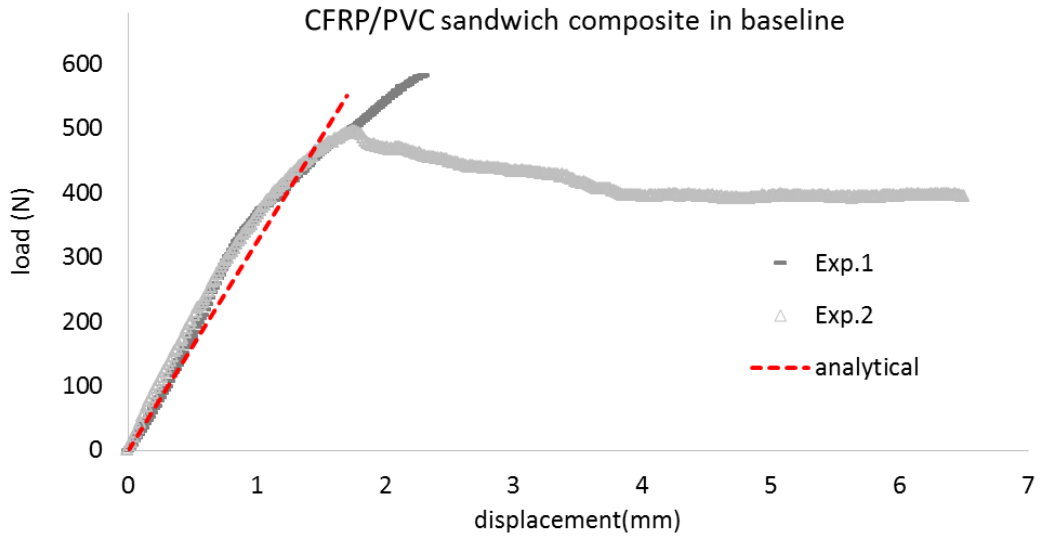

Figure 5-43: Experimental and analytical result for 3 point bending in CFRP/PVC composite in baseline

Assuming the elastic modulus 75 MPa in analytical calculations the analytical plot captures the experiments well as is shown in Figure 5-43 but from the experimental data it is seen that the material behavior is not linear so we need to use the nonlinear model to capture the experimental data accurately. FE analysis was done by considering nonlinear elastic response for both foam and skins. The material parameters for skins and foams are given in Table 5-4 and Table 5-10. The result for the nonlinear model and comparison with the experiment for specimens under baseline condition is shown in Figure 5-44.

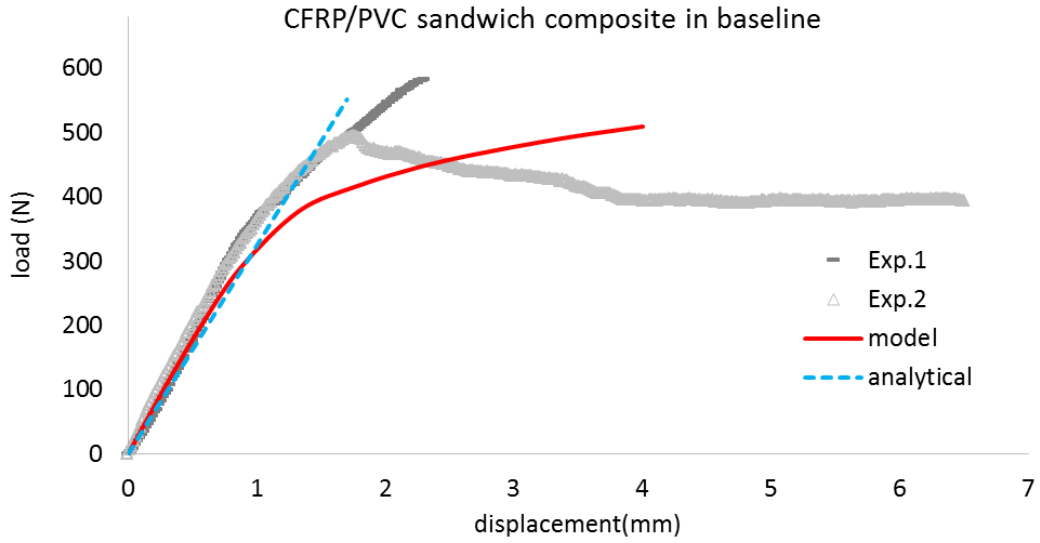

Figure 5-44: CFRP/PVC sandwich composite in baseline; nonlinear model and experiment

To be able to see the stress and strain change in sandwich composites Figure 5-45 to Figure 5-51 show the stress and strain contour in sandwich composite sample, during the quasi static bending tests at different stages of loading. In the FE simulations, the three point bending test induces indentation at the region where the load is prescribed. It is also seen that most of the stresses are carried by the skins, which is expected. Localized strains are seen close to the supports and loading applications, which could lead to damage initiation in these regions.

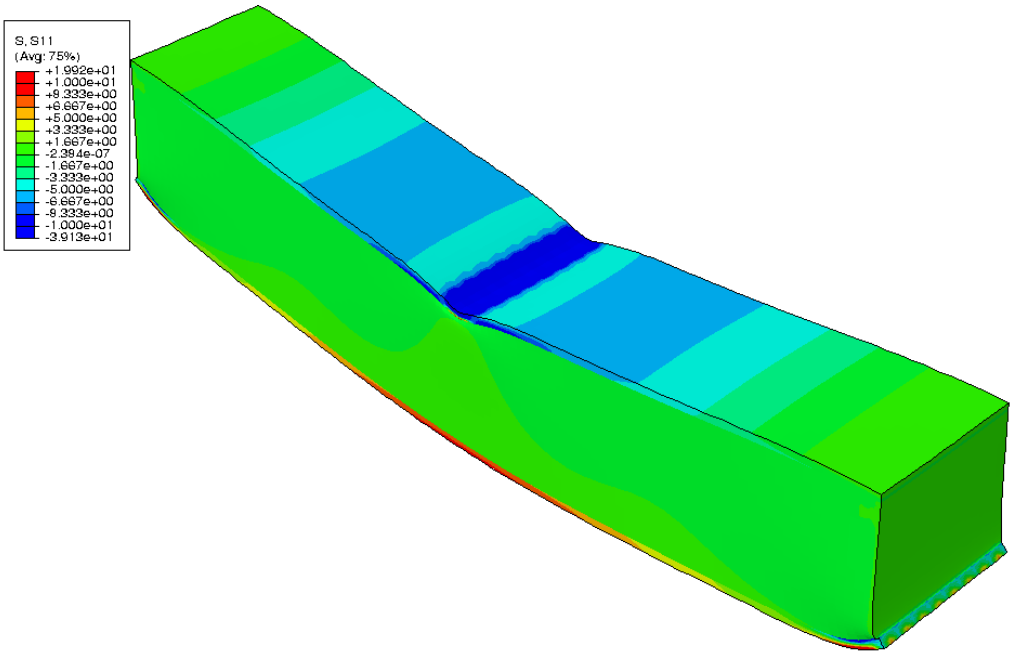

Figure 5-45: Stress (S11) in CFRP/PVC sandwich composite in baseline at 200 N loading

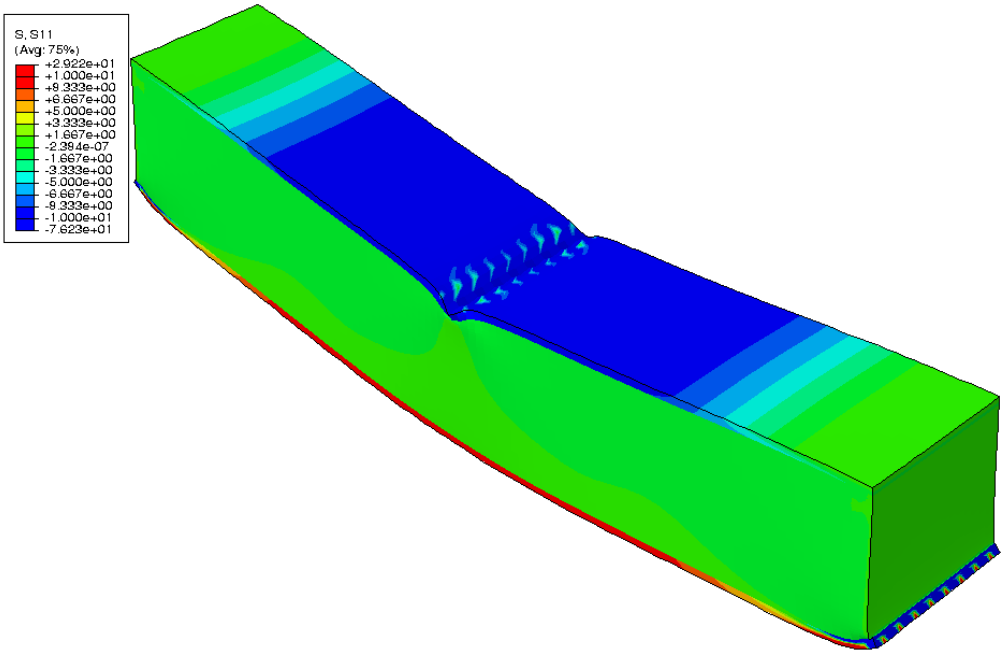

Figure 5-46: Stress (S11) in CFRP/PVC sandwich composite in baseline at 416 N loading

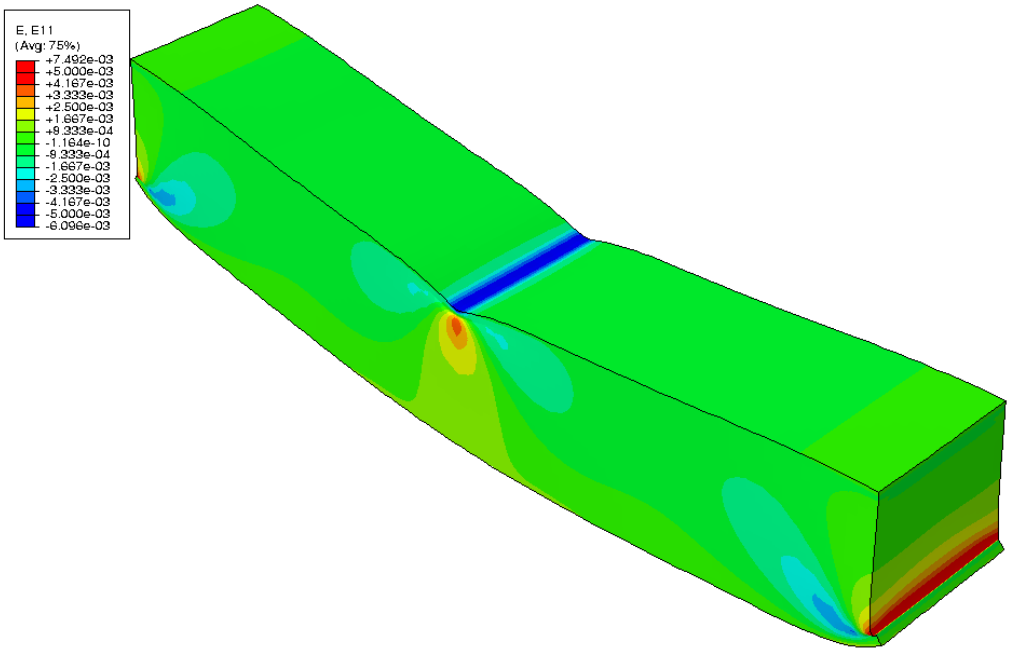

Figure 5-47: Strain (E11) in CFRP/PVC sandwich composite in baseline at 200 N loading

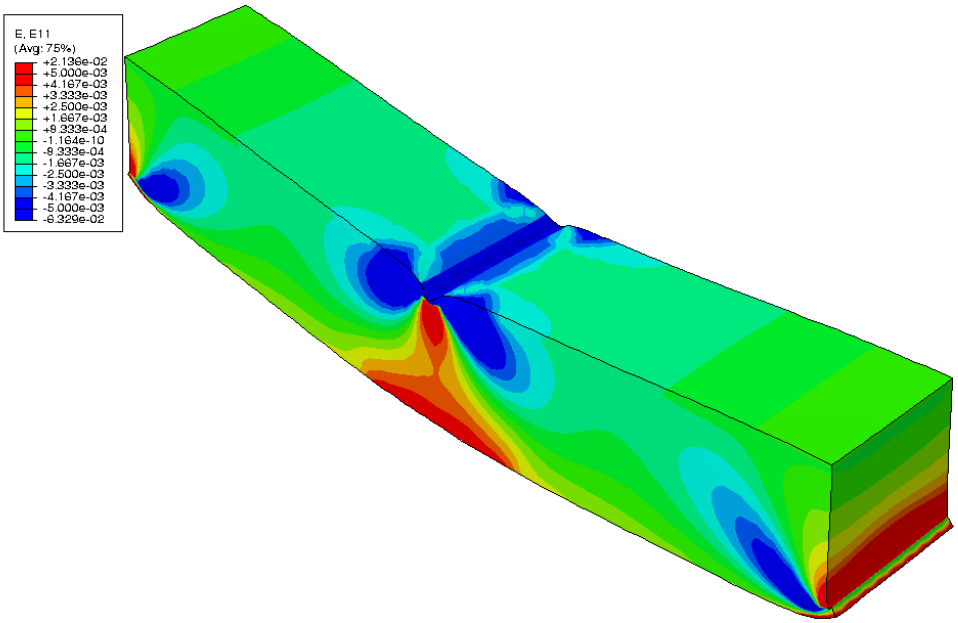

Figure 5-48: Strain (E11) in CFRP/PVC sandwich composite in baseline at 416 N loading

The same tests and calculations were done for the sandwich composite after conditioning in sea water at 50°C. The properties of CFRP/PVC sandwich composite after conditioning in sea water at 50°C, are in the Table 5-13.

Table 5-13: CFRP/PVC sandwich composite properties and dimensions (conditioned at 50°C)

Width (mm)	**E_s (MPa)**	**E_f (MPa)**	**G (MPa)**	**ν**	**t_f (mm)**	**t_s (mm)**
58.6	7000	50	20	0.25	25.8	1

By plotting CFRP/PVC sandwich composite analytical result and comparing with experimental result, we have

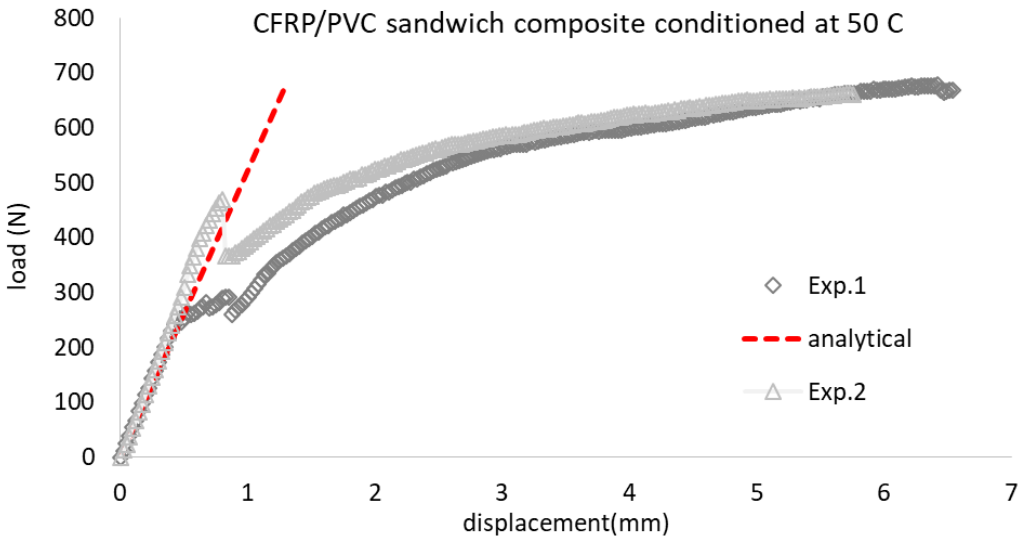

Figure 5-49 : Experimental and analytical result for 3 point bending in conditioned CFRP/PVC composite at 50° C

The experimental result and analytical calculation for linear elastic part are in good agreement. According to Figure 5-49 the sandwich composite behavior is not linear elastic and to be able to capture the experimental data we need to use nonlinear model. The nonlinear model result is shown in Figure 5-50.

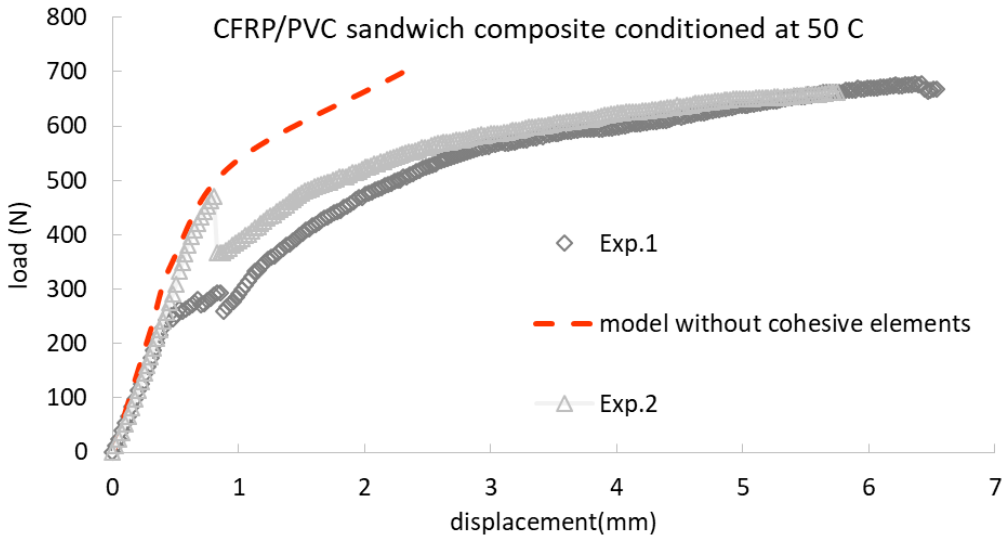

Figure 5-50: CFRP/PVC sandwich composite conditioned at 50° C; nonlinear model and experiment

From Figure 5-50 the model does not capture the experiment completely, which is due to delamination behavior that occurs between foam core and CFRP skin during loading. To be able to capture the experiment after failure, we need to consider delamination in FE model. To consider delamination in sandwich composite, cohesive elements are used. A layer of adhesive is assumed using cohesive elements and the bending leads to debonding in sandwich layers. For modeling the delamination, a thin layer of cohesive elements between the skin and foam were considered. The elastic modulus of cohesive

elements is assumed to be 3000 MPa and the nominal stress at damage initiation assumed to be 0.32 MPa. Linear form of damage evolution based on effective plastic displacement has been used and the effective plastic displacement at the point of failure assumed to be 0.001 mm. By applying excessive load, failure happens in the cohesive elements and it is assumed that when material is fully degraded and the element fails, it will be removed from the mesh and this leads to sliding of skin and foam. The quasi-static bending plot using cohesive elements and considering debonding is shown in Figure 5-51.

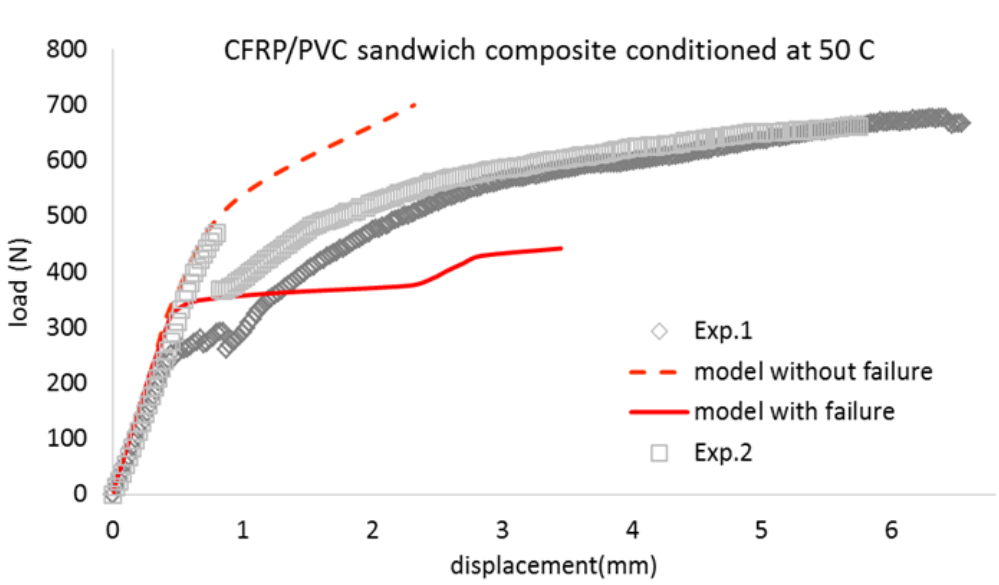

Figure 5-51: CFRP/PVC sandwich composite conditioned at 50° C; nonlinear model with failure and experiment

In Figure 5-51 we can see the debonding occurs when loading is about 350 N and the nonlinear model can predict the sandwich composite behavior accurately before failure

happens but after the delamination we need to consider the cohesive element to better capture the behavior after delamination.

Figure 5-52 to Figure 5-54 show the stress contours in sandwich composite under quasi static bending. From the contours we can see that in loading of about 400N the bottom skin and foam debonds and there is a small sliding between skin and foam. In this stage of loading some parts of the cohesive elements fails due to excessive loading and this causes sliding between the skin and foam.

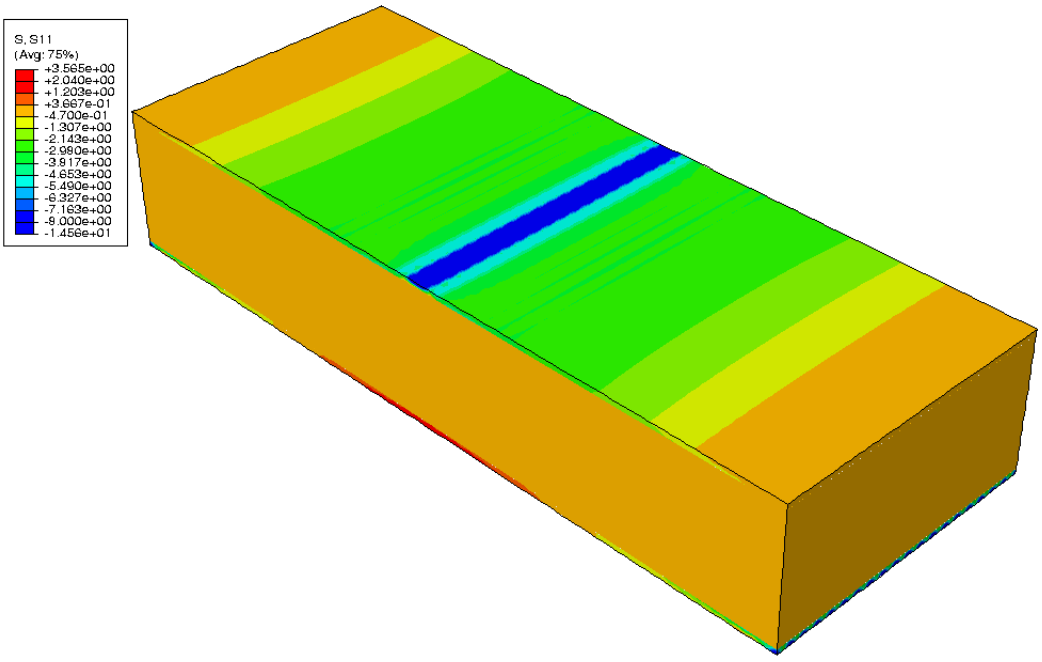

Figure 5-52: Stress (S11) in CFRP/PVC sandwich composite at 50°C with 196 N loading

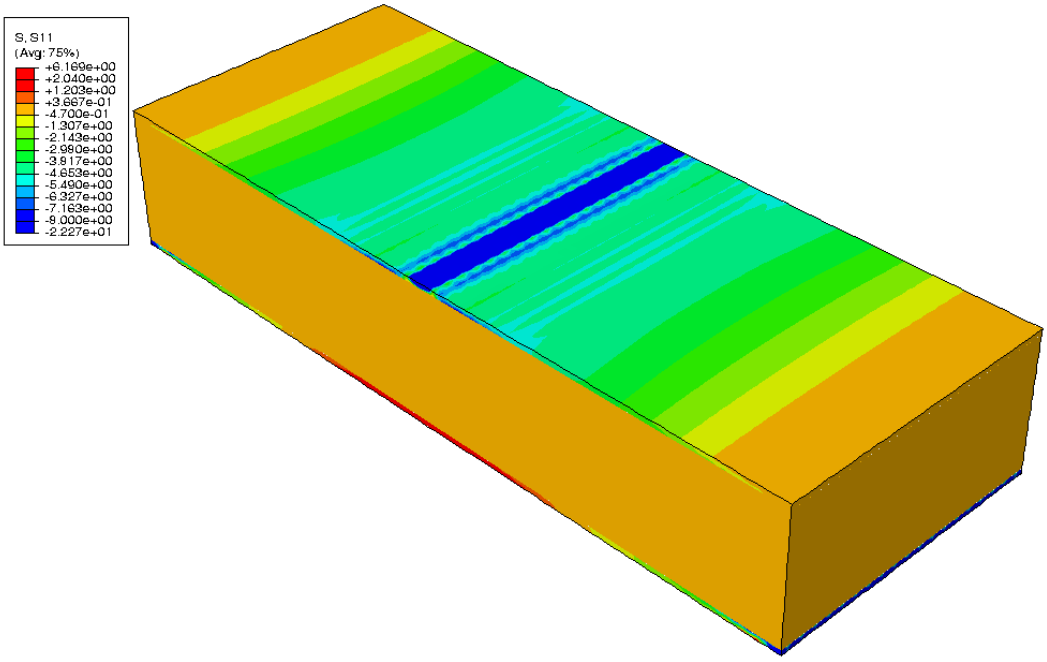

Figure 5-53: Stress (S11) in CFRP/PVC sandwich composite at 50°C with 308 N loading

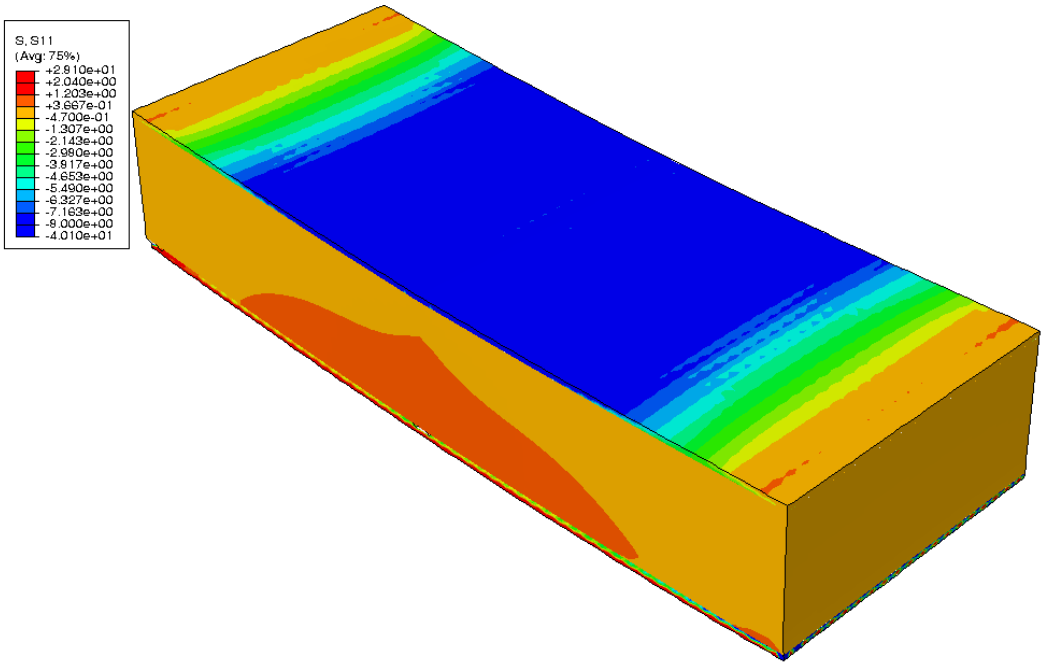

Figure 5-54: Stress (S11) in CFRP/PVC sandwich composite at 50°C with 406 N loading

In the strain contours we use logarithmic strain (LE) in order to illustrate the delamination or crack propagation.

Figure 5-55 and Figure 5-56 show the logarithmic strain at different loadings in sandwich composite under a quasi-static bending test.

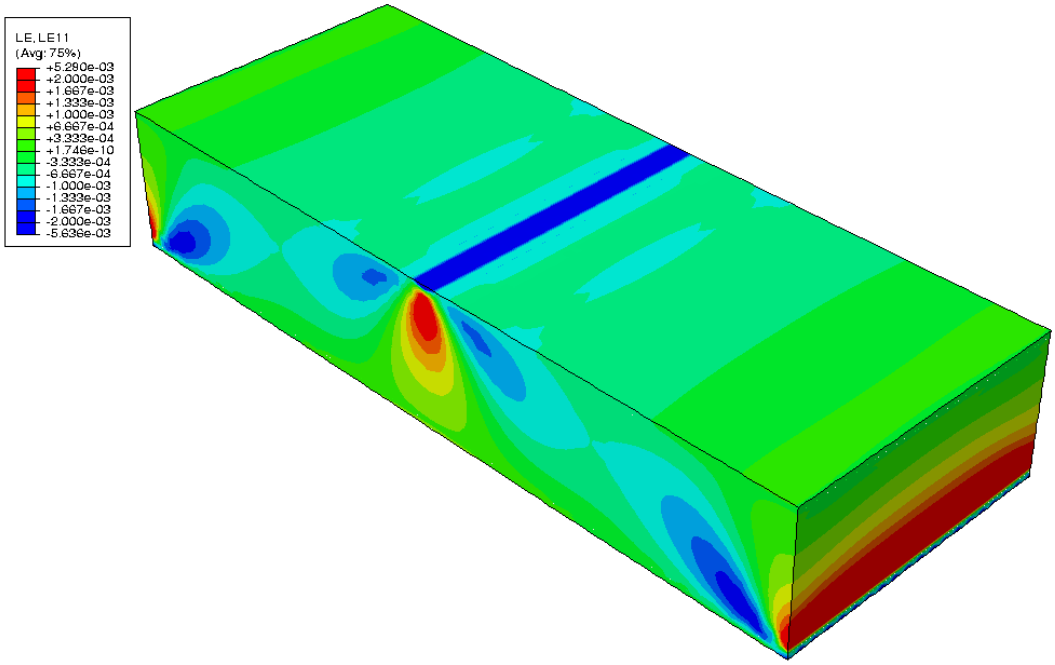

Figure 5-55: Logarithmic strain (LE11) in CFRP/PVC sandwich composite at 50°C with 308 N loading

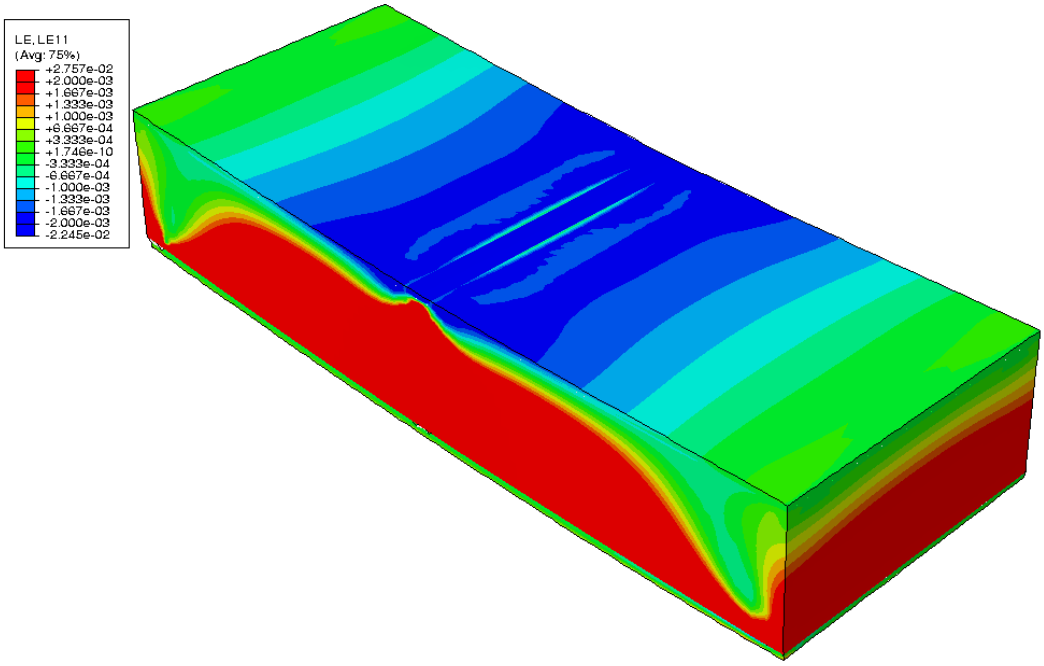

Figure 5-56: Logarithmic strain (LE11) in CFRP/PVC sandwich composite at 50°C with 392 N loading

For the GFRP/PU sandwich composite we did the same tests and modeling for the baseline condition and after conditioning in deionized water at 50°C. For the quasi static bending test at baseline condition, the dimension of the sample is $150 \times 26.04 \times 22.15$ mm and the skin thickness is 1.9 mm. Figure 5-57 shows the analytical calculation assuming E=30MPa captures the experiment. To have the nonlinear behavior of sandwich composite, we used the nonlinear model and the result is shown in Figure 5-58.

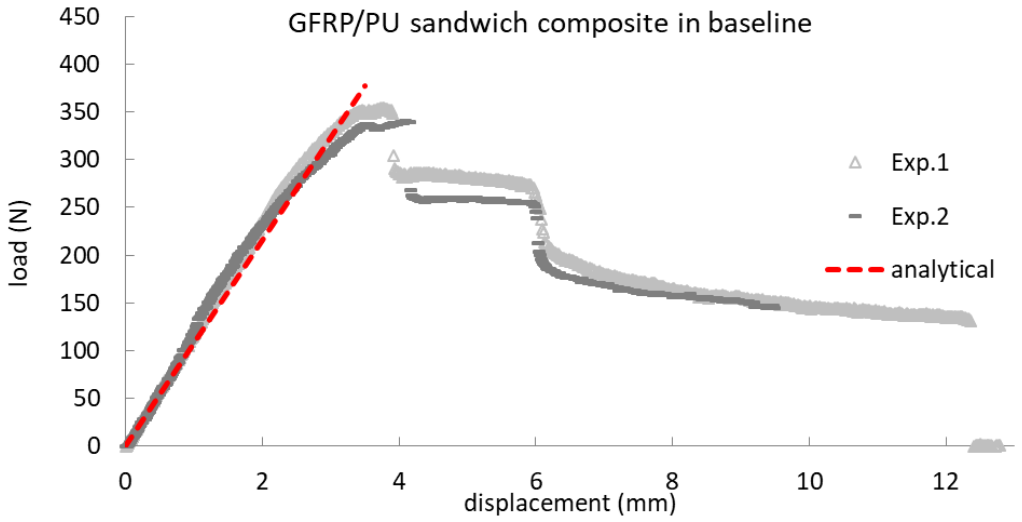

Figure 5-57: GFRP/PU sandwich composite in baseline; analytical calculation and experiment

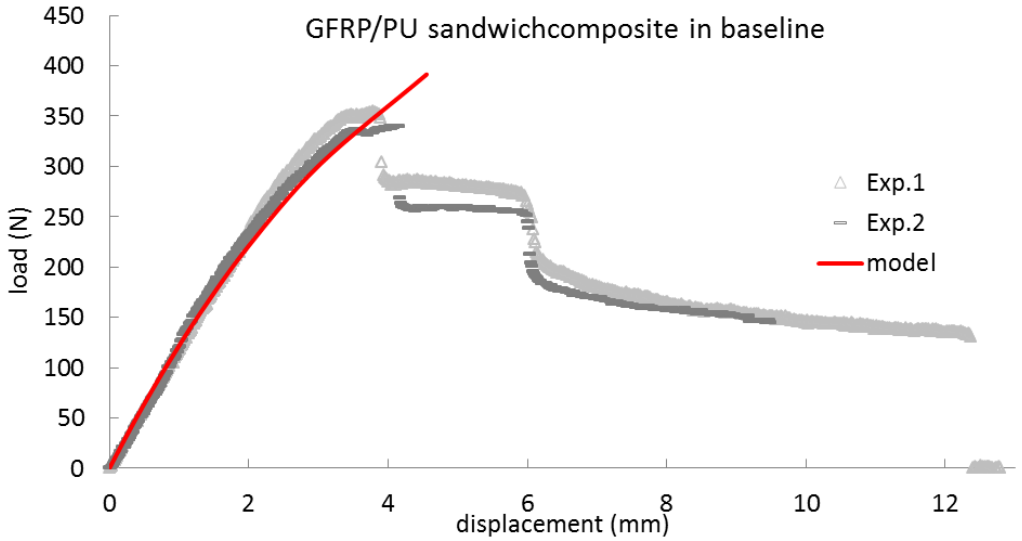

Figure 5-58: GFRP/PU sandwich composite at baseline; nonlinear model and experiment

Figure 5-59 to Figure 5-62 show the stress and strain contour for sandwich composites at different loading.

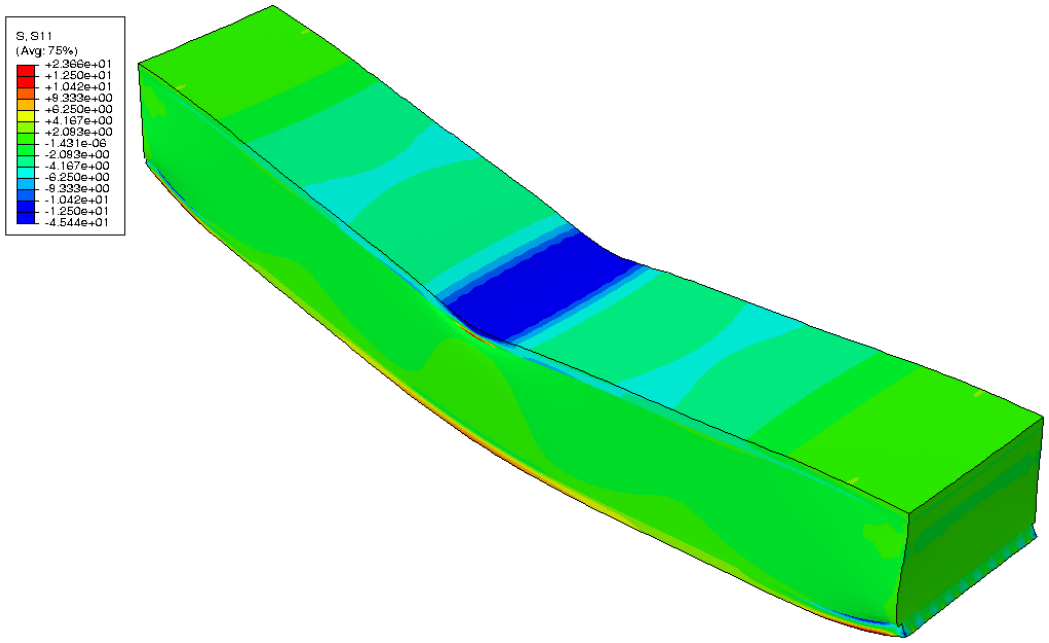

Figure 5-59: Stress (S11) in GFRP/PU sandwich composite in baseline with 157 N loading

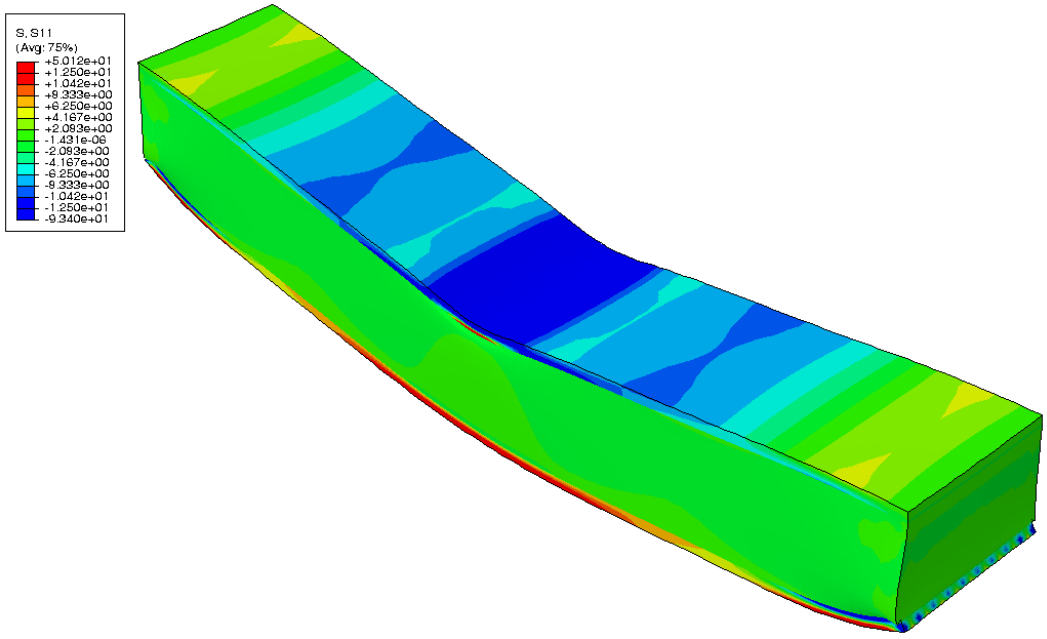

Figure 5-60: Stress (S11) in GFRP/PU sandwich composite in baseline with 313 N loading

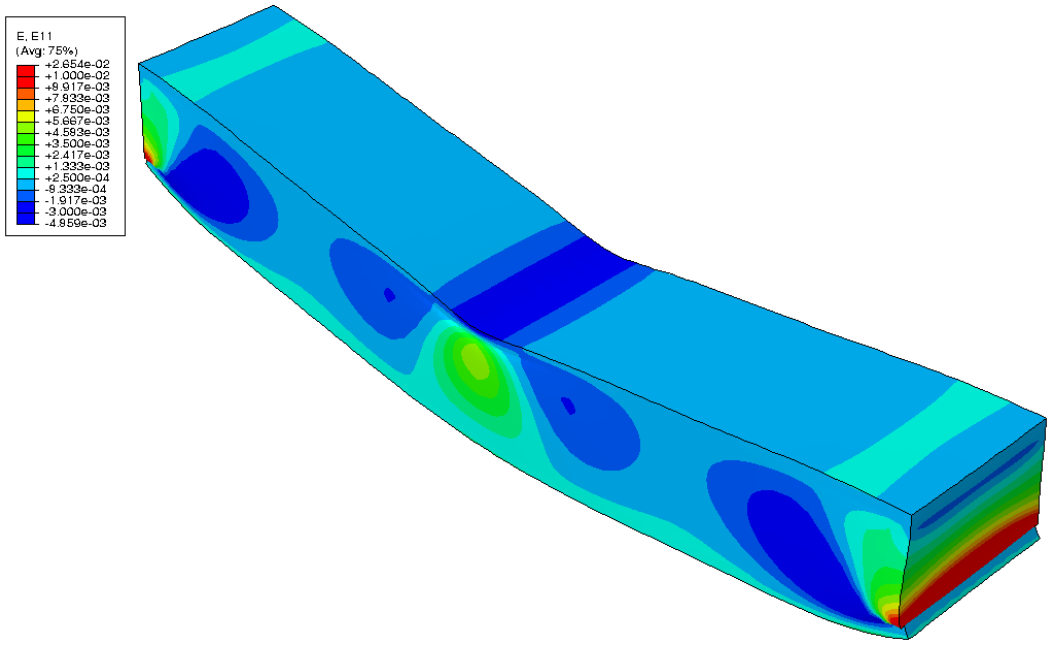

Figure 5-61: Strain (E11) in GFRP/PU sandwich composite in baseline with 157 N loading

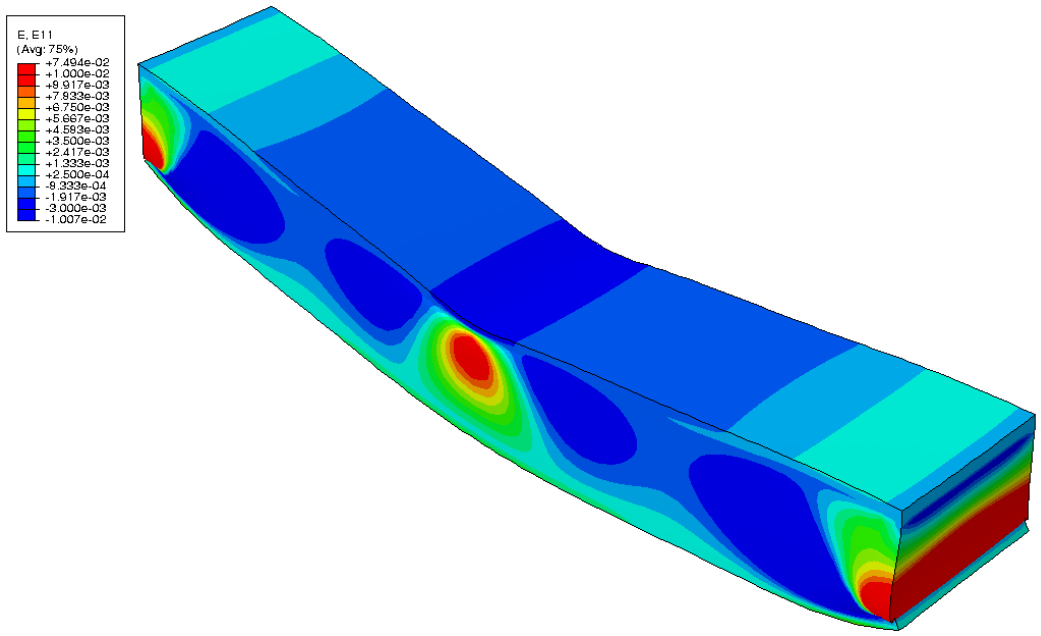

Figure 5-62: Strain (E11) in GFRP/PU sandwich composite in baseline with 313 N loading

Figure 5-63 shows the GFRP/PU sandwich composite nonlinear behavior after immersion in deionized water at 50°C. The dimension of samples is $150 \times 51 \times 22.5\,mm$ and the skin thickness is 1.9 mm. First the simulation is done without assuming any failure in sandwich composite and then assuming crack in sandwich when loading is around 700 N.

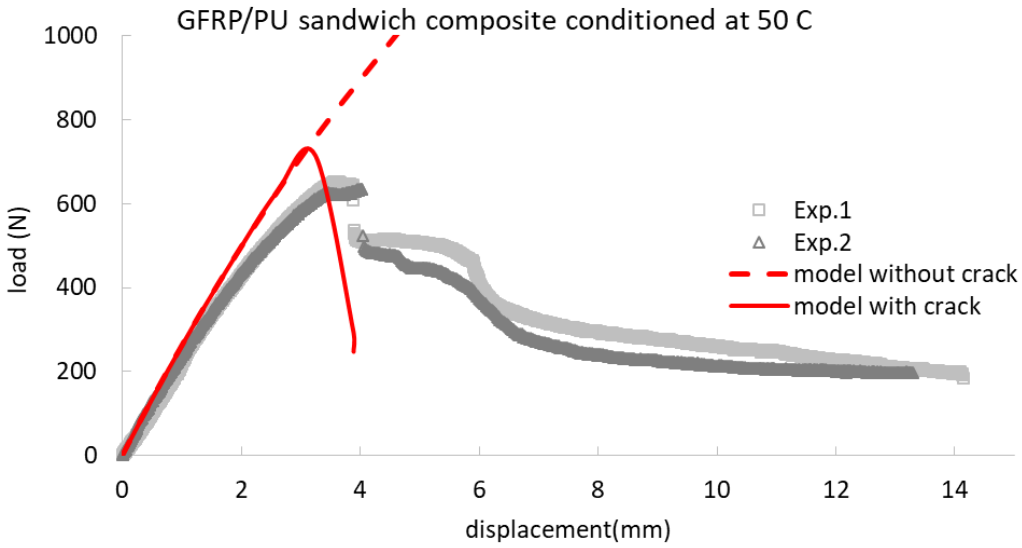

Figure 5-63: NSF sandwich composite conditioned at 50°C in deionized water; nonlinear model and experiment

For modeling the crack initiation and propagation, cohesive elements in crack path are used. The elastic modulus of cohesive elements is assumed to be 5000 MPa and the nominal stress at damage initiation assumed to be 8 MPa. Linear form of damage evolution based on effective plastic displacement has been used and the effective plastic displacement at the point of failure assumed to be 0.09 mm. By applying excessive load, failure happens in the cohesive elements and it is assumed that when material is fully

degraded and the element fails, it will be removed from the mesh and in this way the crack propagates in the material. Figure 5-64 to Figure 5-67 show the stress contour in GFRP/PU sandwich composite after immersion in deionized water at 50°C at different loadings.

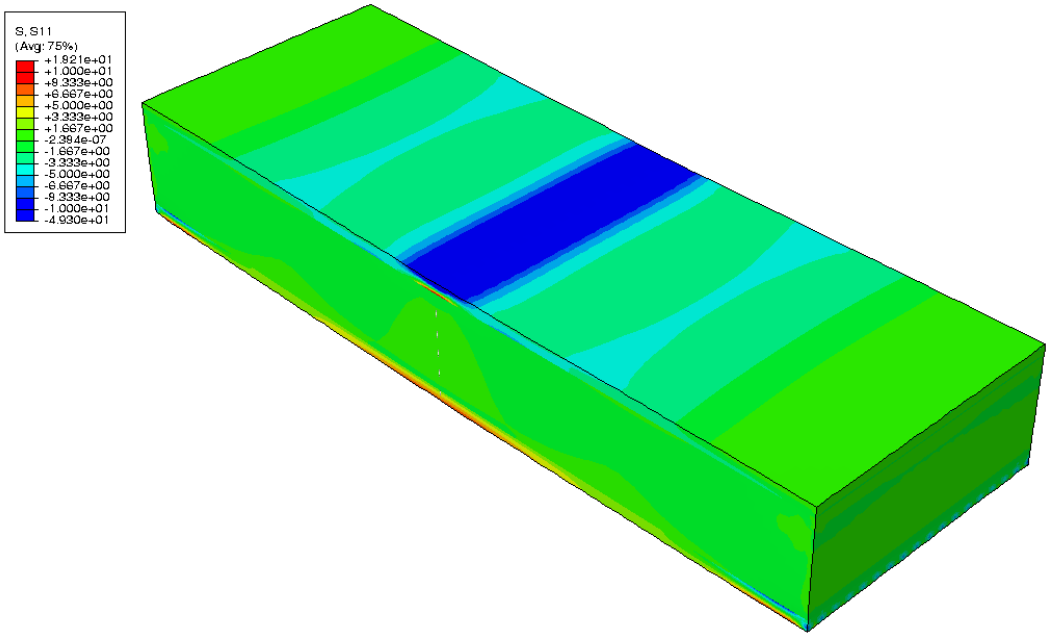

Figure 5-64: Stress (S11) in GFRP/PU sandwich composite at 50°C with 306 N loading

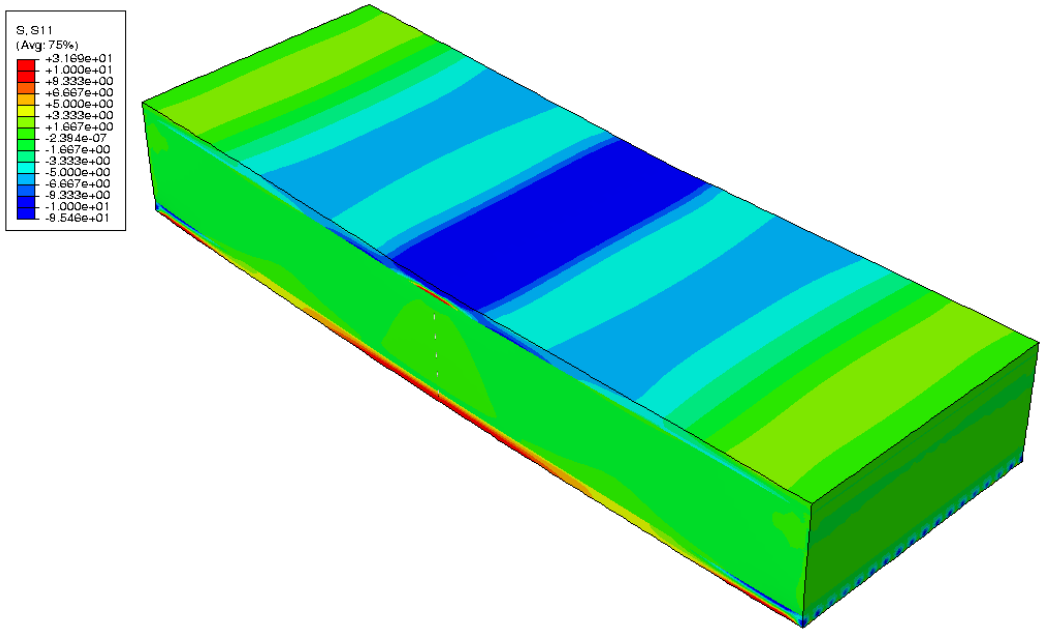

Figure 5-65: Stress (S11) in GFRP/PU sandwich composite at 50°C with 517 N loading

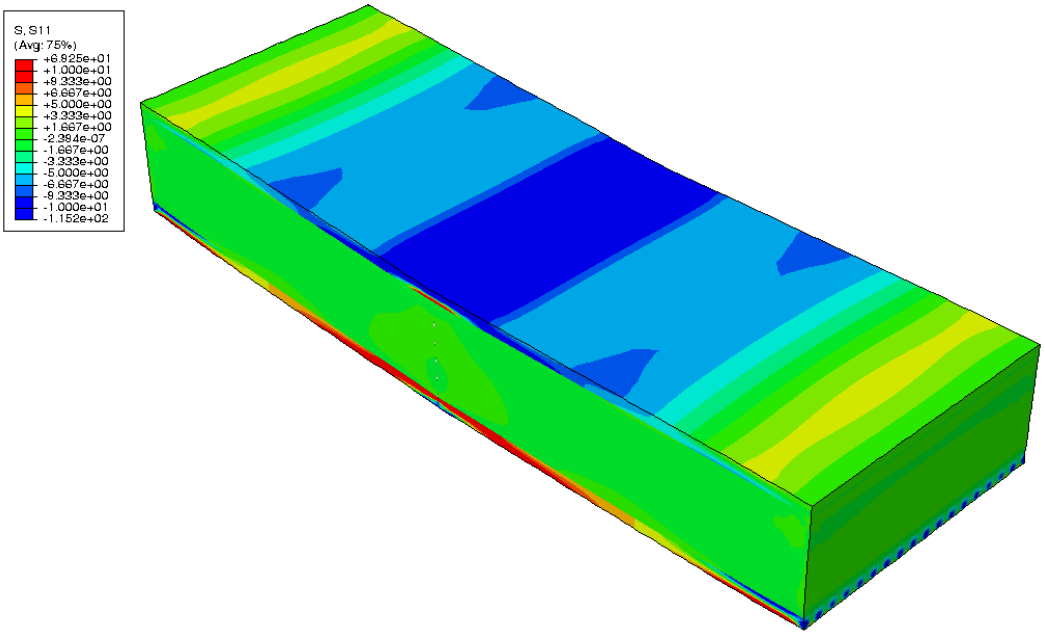

Figure 5-66: Stress (S11) in GFRP/PU sandwich composite at 50°C with 670 N loading

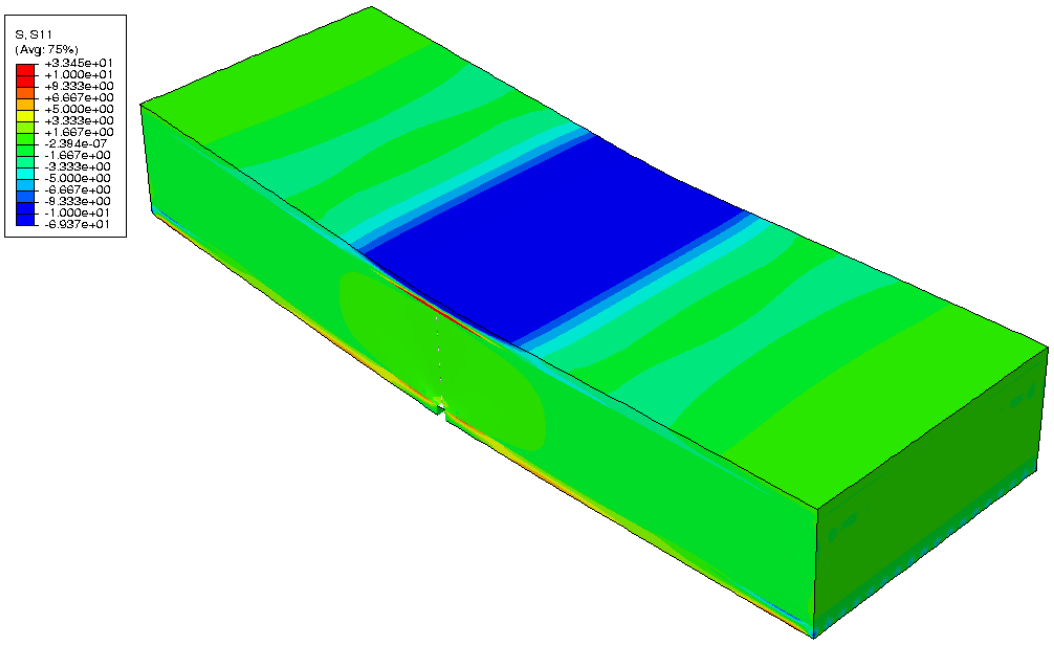

Figure 5-67: Stress (S11) in GFRP/PU sandwich composite at 50°C after crack

In Figure 5-67 the loading is about 300 N after the load drops (as it is shown in Figure 5-63). Figure 5-68 to Figure 5-71 show the logarithmic strain in sandwich composite at different loadings. Also the crack initiation and propagation are shown in these figures.

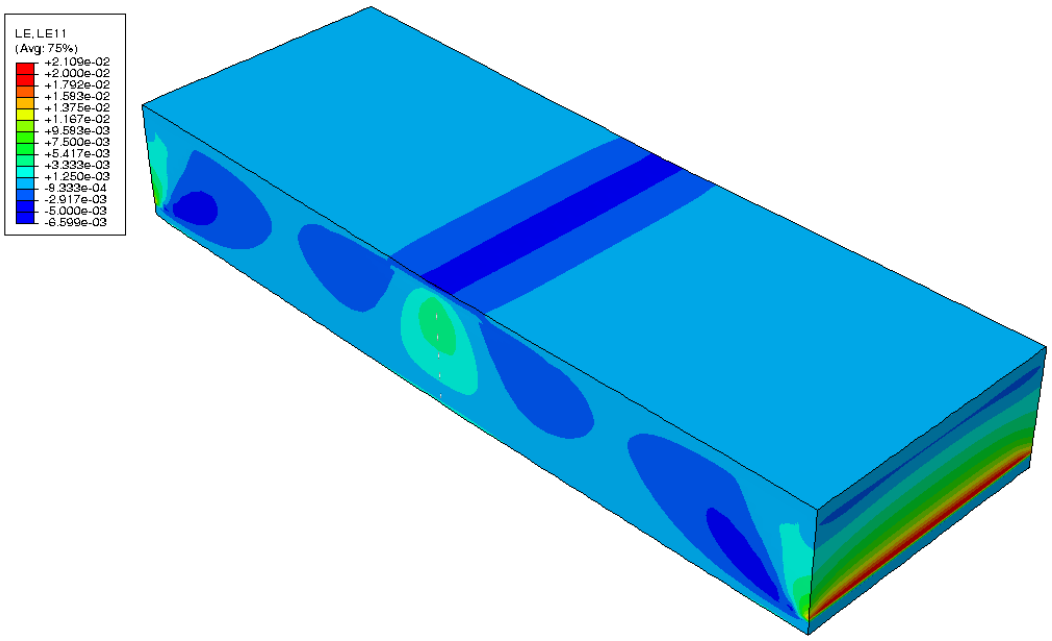

Figure 5-68: Logarithmic strain (LE11) in GFRP/PU sandwich composite at 50°C at 306 N loading

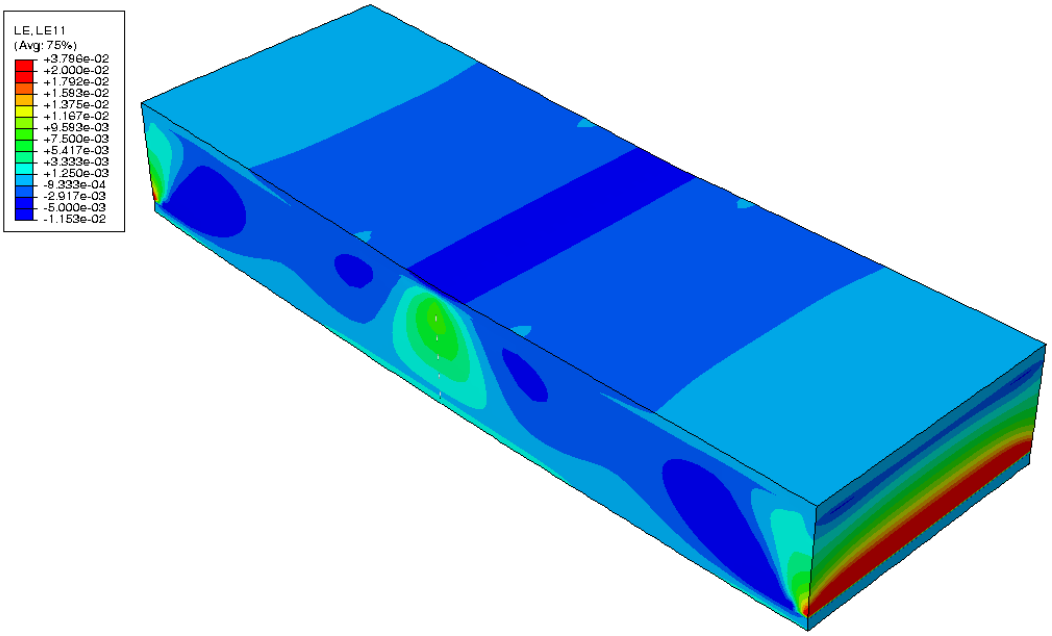

Figure 5-69: Logarithmic strain (LE11) in GFRP/PU sandwich composite at 50°C at 517 N loading

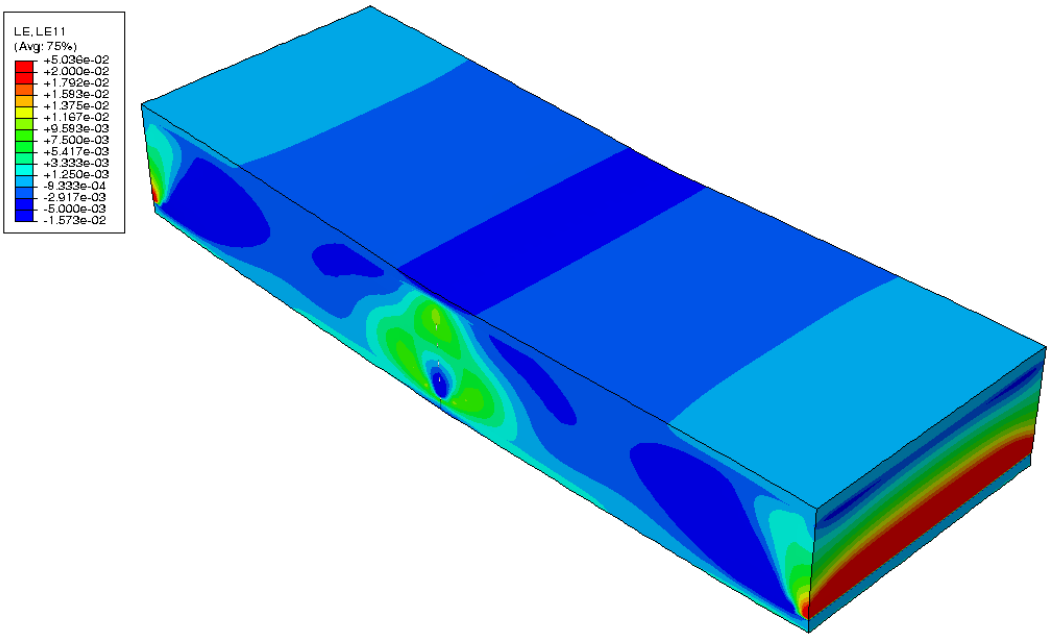

Figure 5-70: Logarithmic strain (LE11) in GFRP/PU sandwich composite at 50°C at 670 N loading

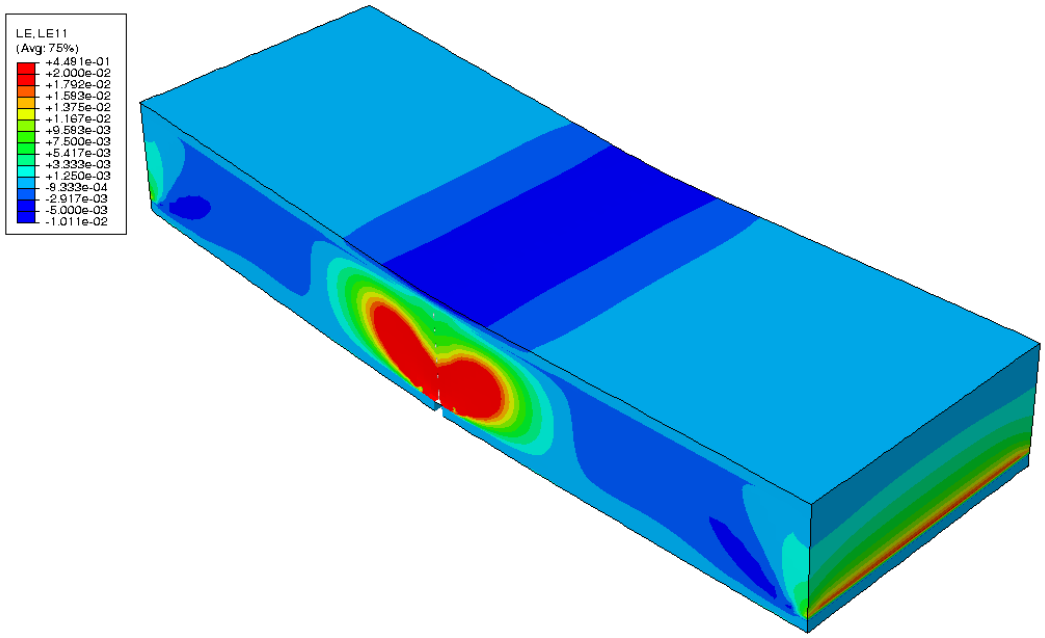

Figure 5-71: Logarithmic strain (LE11) in GFRP/PU sandwich composite at 50°C after crack

5.3. Time-Dependent Response of Foams and Sandwich Composites

Creep and relaxation tests were first conducted for the foam cores under bending. The purpose is to determine the time-dependent properties of the foam core. Later, creep and relaxation tests were also conducted for sandwich composites. The response from the sandwich composites is used to test the constitutive models. FE analyses are used to simulate the creep/relaxation response in sandwich composites. The relaxation modulus needs to be calibrated for the two foams tested (PU and PVC).

5.3.1. Time-Dependent Response of Foams

The time-dependent parameters for PVC foam from the QLV model were calibrated using the creep experiment in Figure 5-72. The Prony series that is used for calibration is

$$\mathrm{E(t)} = \mathrm{E0} + \sum_{\mathrm{n=1}}^{\mathrm{N}} \mathrm{E_n}\left(\mathrm{e}^{-\mathrm{t}/\tau_\mathrm{n}}\right) \qquad (5-6)$$

where E represents the long-term relaxation modulus when the material is fully relaxed and E_n and τ_n represent the relaxation modulus and relaxation time for each Prony term, respectively. The calibrated time-dependent properties are given in Table 5-14.

Table 5-14: FE model time dependent material properties for PVC foam

E	**E_1**	**τ_1**	**E_2**	**τ_2**
64	0.1	250	0.15	15000

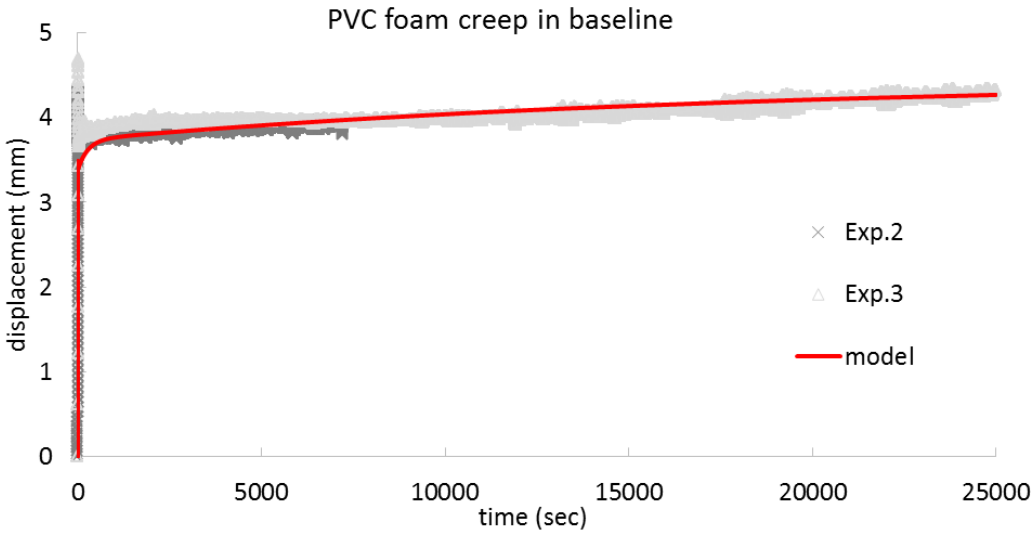

Figure 5-72: PVC foam creep in baseline; model and experiment

Figure 5-72 shows the result for creep under 50% of failure loading under quasi static tests. Creep tests done under 20% of failure loading, are used to validate the time-dependent material parameters within the QLV model. We use the model for creep under 20% of quasi static failure loading. The result is shown in the Figure 5-73. It is seen that QLV model can be used to describe the nonlinear time-dependent response of PVC foam. As it is shown in Figure 5-73, the material properties obtained from creep test under 50% of failure load are used in the model and compared with creep test under 20% of failure load and the result shows there is a good agreement between them.

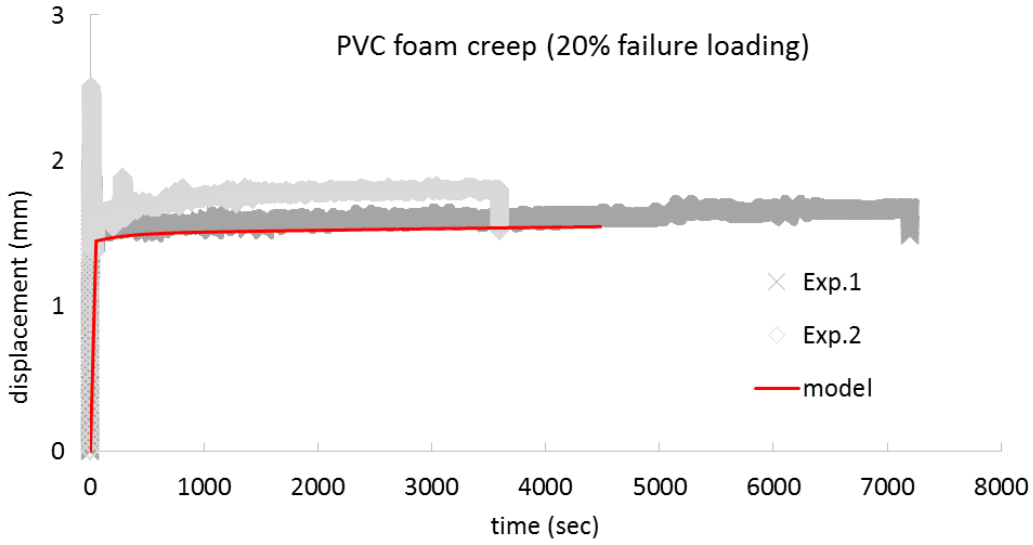

Figure 5-73: PVC foam creep test under 20% failure loading and model prediction

In the next step we use the PVC foam relaxation in four point bending test after immersion the sample in sea water at 50°C to get material properties. The holding displacement is 8.9 mm in this test and the material properties are shown in Table 5-15.

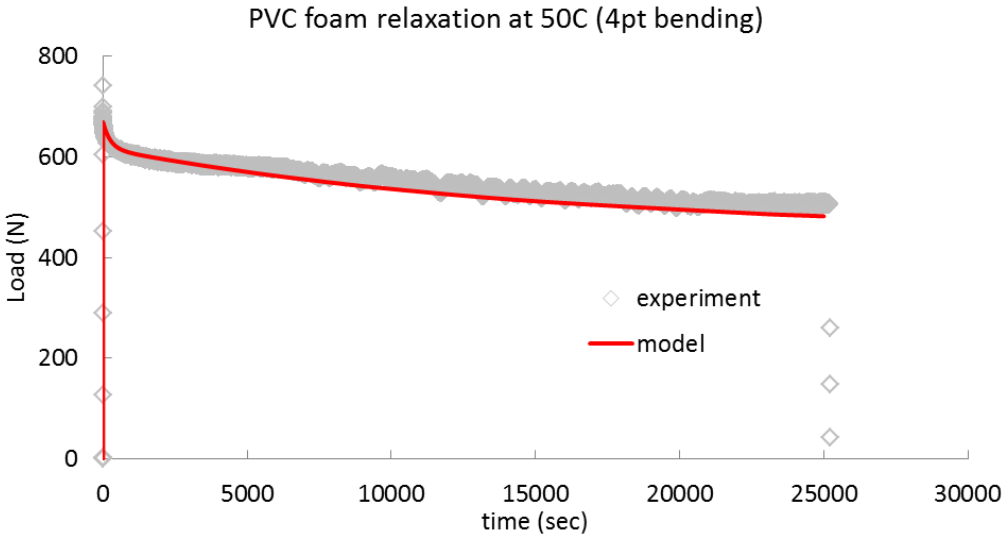

Figure 5-74: PVC foam relaxation at 50°C and comparison with experiment

Table 5-15: FE model time dependent material properties for PVC foam at 50°C

E	**E_1**	**τ_1**	**E_2**	**τ_2**
60	0.12	250	0.38	15000

The value for elastic modulus E, as it is shown in Table 5-14 and Table 5-15 shows a small decreases by conditioning the foam in sea water at 50° C. Also comparison of the time dependent properties shows that by conditioning the PVC foam in sea water at 50°C the relaxation accelerates compared to the one under baseline condition.

For the Polyurethane foam we have the same procedure to obtain the relaxation modulus and time dependent properties. The Figure 5-75 shows that by using the relaxation modulus, *E*, equal to 16 MPa and time dependent properties in Table 5-16, the model captures the experiment well. The load is 65% of failure load in quasi static bending test.

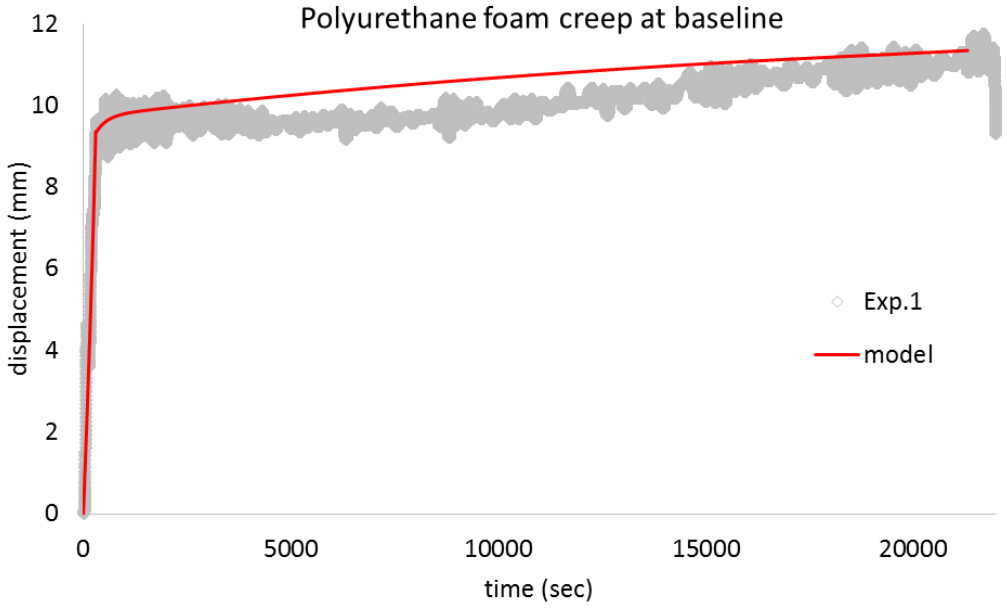

Figure 5-75: Polyurethane foam creep response; model and experiment

Table 5-16: Polyurethane relaxation modulus and time dependent properties at baseline

E	**E_1**	**τ_1**	**E_2**	**τ_2**
16	0.05	250	0.12	15000

In this part we repeated the same test for polyurethane foam after immersion in deionized water at 50° C. The material properties are shown in Table 5-17 and the holding displacement is 6.5 mm for relaxation. Figure 5-76 shows the Polyurethane foam stress relaxation response after immersion in deionized water at 50° C.

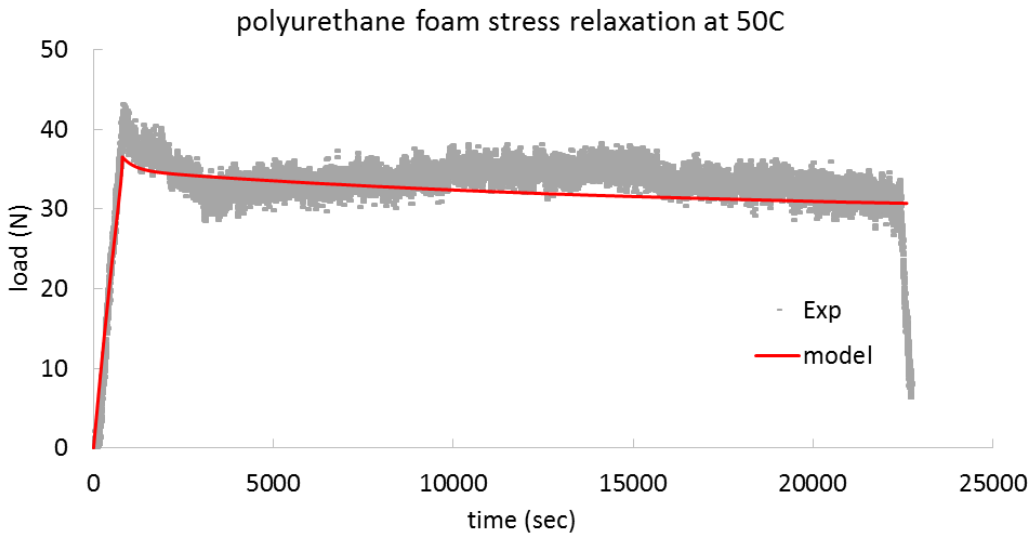

Figure 5-76: Polyurethane foam stress relaxation response after immersion in deionized water at 50° C; model and experiment

Table 5-17: Polyurethane relaxation modulus and time dependent properties at 50° C

E	**E1**	**τ1**	**E2**	**τ2**
14	0.1	350	0.16	15000

The summary of the time dependent material properties for PVC and Polyurethane foams in baseline and after immersion in liquid at 50° C is shown in Table 5-18.

Table 5-18: Time dependent material properties

material	**condition**	**E**	**E_1**	**τ_1**	**E_2**	**τ_2**	**B**
polyurethane	baseline	16	0.05	250	0.12	15000	9
	50°C	14	0.1	350	0.16	15000	7
PVC	baseline	64	0.1	250	0.15	15000	7.2
	50°C	60	0.12	250	0.38	15000	5.7

From the Table 5-18 it can be concluded that by conditioning the foam in liquid at 50°C the elastic modulus slightly decreases. The time dependent material properties also show that conditioning accelerates the creep and stress relaxation.

5.3.2. Time Dependent Behavior of Sandwich Composite

By calibrating the time dependent material properties for the foams in the previous section, we can use them in sandwich composite FE analyses to determine the response of sandwich composites under creep or stress relaxation tests.

The CFRP/PVC system consists of PVC foam core and CFRP skin and the loading is perpendicular to fiber direction. The span width (length of beam) is 150 mm, the width of specimen is 25.6 mm and the sandwich thickness is 27.6. Skin thickness is 1.4 mm. Figure 5-77 shows the CFRP/PVC sandwich composite behavior in baseline condition under stress relaxation with holding displacement of 1.63 mm. Figure 5-77 shows that the sandwich composite model can capture the experimental data very well. In next step, the stress relaxation test is conducted on CFRP/PVC sandwich composite after immersion in sea water at 50°C. The span width (length of beam) is 150 mm, the width is 58.25 mm and the sandwich thickness is 27.8. The skin thickness measured is 1.17 mm. The holding displacement for stress relaxation test is 0.2 mm. Figure 5-78 shows the relaxation test.

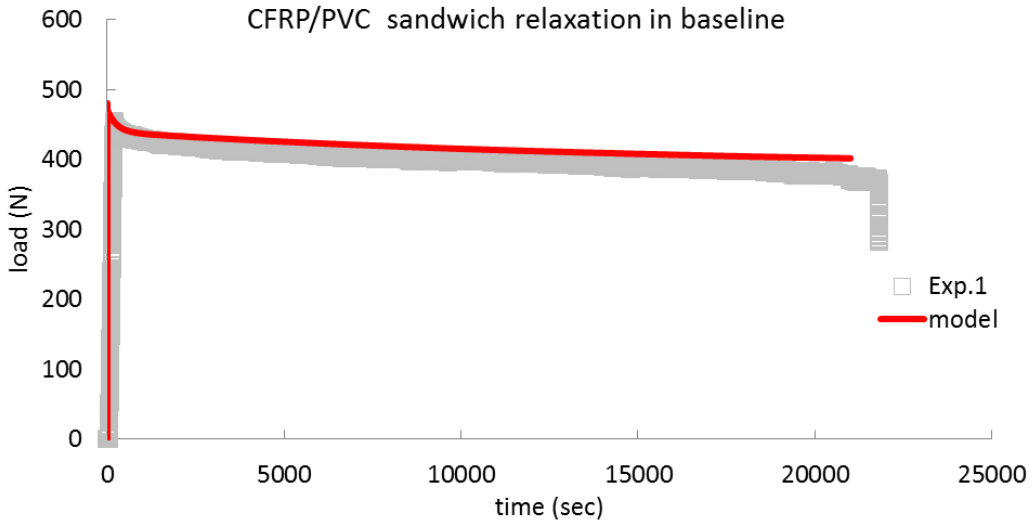

Figure 5-77: CFRP/PVC sandwich composite stress relaxation at baseline condition

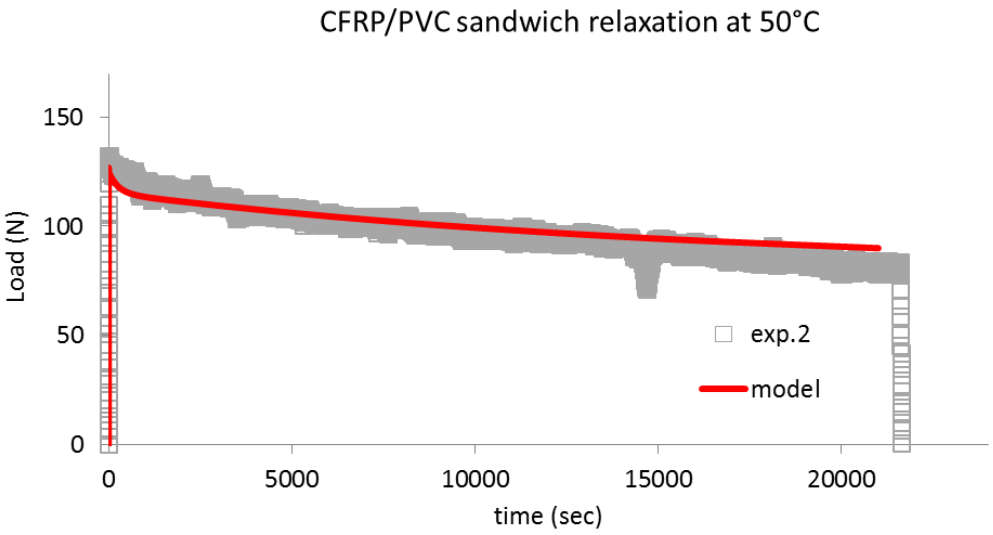

Figure 5-78: CFRP/PVC sandwich composite relaxation at 50°C

To check the accuracy of our model we used that for GFRP/PU sandwich composite to see how it can capture the experimental data. The length of specimen is 150 mm, width is 26 mm and thickness is 22 mm and to do the stress relaxation test, holding

displacement is 1.04 mm. Figure 5-79 shows the GFRP/PU sandwich composite stress relaxation at baseline condition. we can see that the model is in an acceptable agreement with the experimental data.

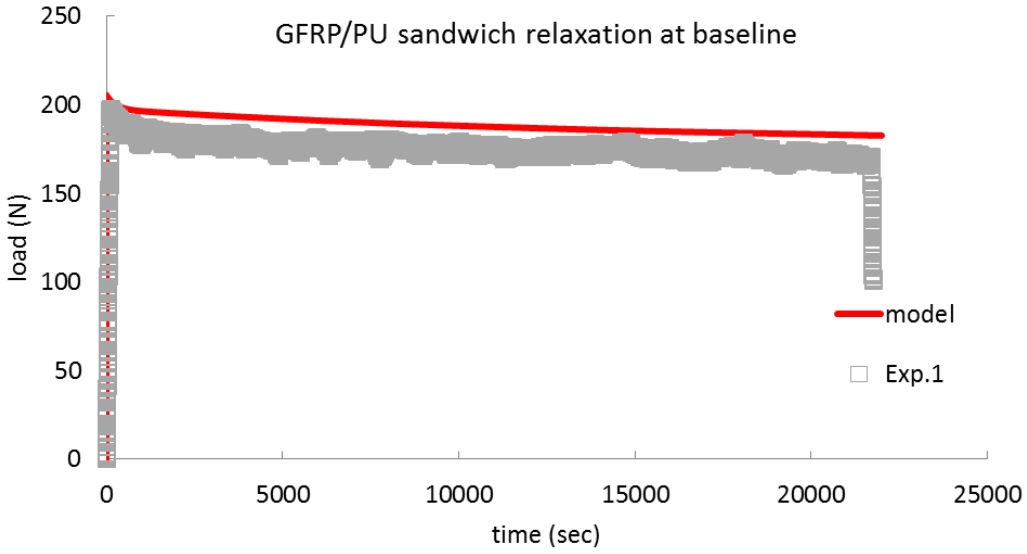

Figure 5-79: GFRP/PU sandwich composite stress relaxation at baseline condition

The next test on GFRP/PU sandwich composite is the stress relaxation test after immersion in deionized water at 50°C. Figure 5-80 shows the result and there is a good agreement between model and experiment.

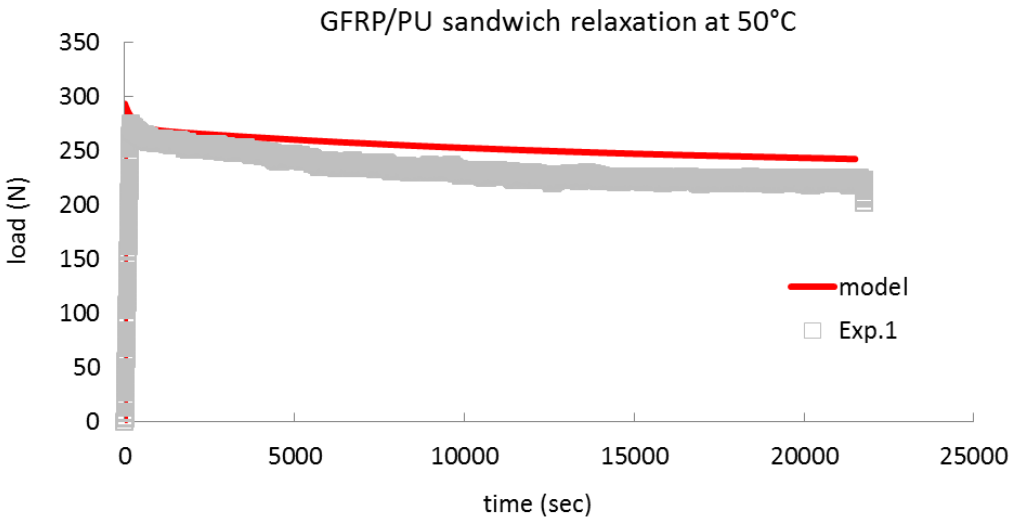

Figure 5-80: GFRP/PU sandwich composite stress relaxation at 50°C

5.4. Time Dependent Response of Foam under Cyclic Loading

In this part we use the material model to investigate the PU foam behavior under cyclic loading. The experiment and FE analysis were conducted for specimens under both dry at 25°C (baseline condition) and after immersion in deionized water at 50°C. The material properties were obtained from the quasi-static and relaxation tests, discussed in previous sections of this study. The displacement in the middle of the beam is fluctuating between 5 and 7 mm with frequency of 1 Hz and the load was measured in about 20000 seconds. The result of FE analysis and experiment for a baseline specimen are shown in Figure 5-81.

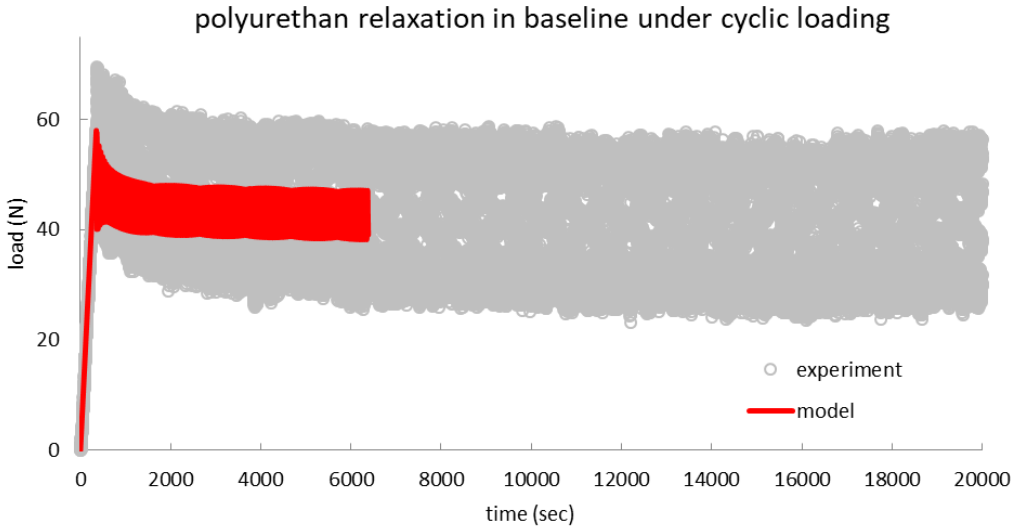

Figure 5-81: Polyurethane foam relaxation in baseline condition under cyclic loading

The qualitative behavior in FE is the same as experiment but there is a difference between maximum and minimum loads during the cyclic test. The experiment shows much higher load range than the load range from the FE simulation. To understand the

reason for this problem the quasi static tests for polyurethane were studied and compared with cyclic FE analysis. It is shown in Figure 5-83. The cyclic FE analysis shows the agreement with quasi static tests and the loads at deflection 5 and 7 mm matches with what we have in cyclic FE result in first cycles. It seems that the much higher load range in the experiment is most likely because of the clamping condition. Lightly clamped specimen would deflect more at the clamp point than a tightly clamped specimen as discussed in [39]. To get a more accurate experimental result we need to repeat the cyclic test several times to obtain the best calming condition that matches with the quasi static tests. In this study because of the limitation in experimental works there is no possibility to have more test result.

The cyclic test also was conducted on polyurethane foam after immersion in deionized water at 50 °C. The result of experiment and FE analysis are shown in Figure 5-82. Again we can see that the model using in FE analysis is capable of prediction of material behavior under cyclic loading and compared to quasi static tests at 5 and 7 mm deflection, in Figure 5-84, there is an agreement between the loads in quasi static tests and load in first cycle in cyclic test. The difference between model and experiment can express as a consequence of clamping or other conditions during the tests.

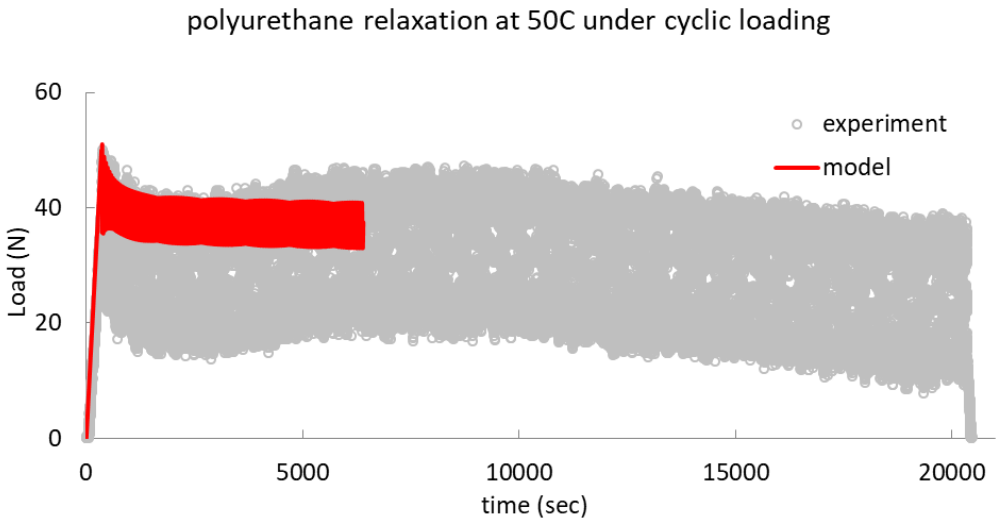

Figure 5-82: Polyurethane foam relaxation at 50°C under cyclic loading

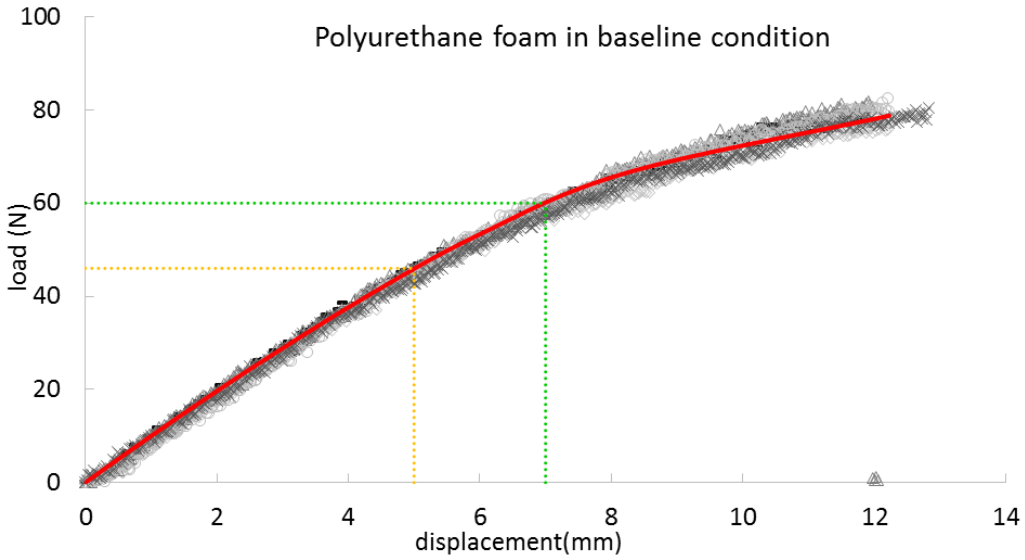

Figure 5-83: Load and displacement check for first cycle in cyclic test on polyurethane foam in baseline condition

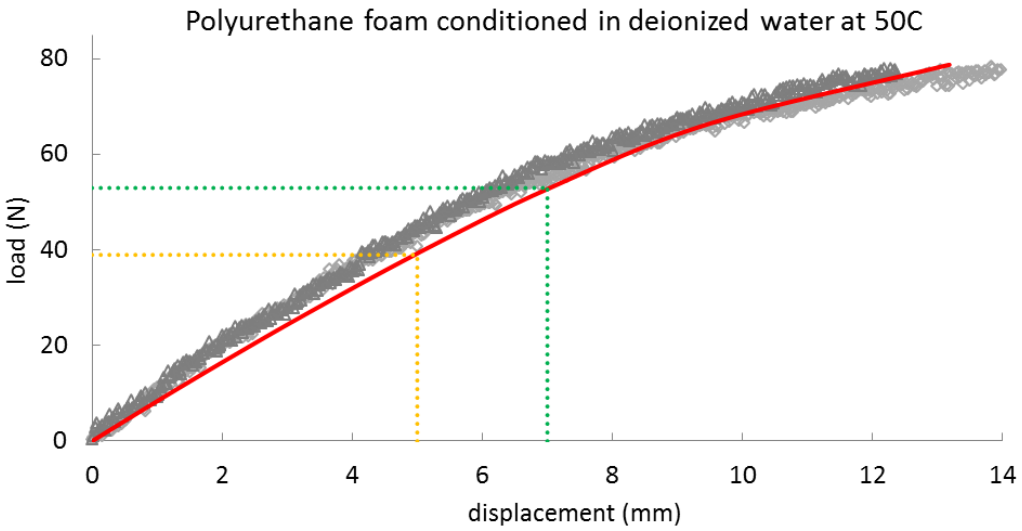

Figure 5-84: Load and displacement check for first cycle in cyclic test on polyurethane foam at 50C

6. CONCLUSIONS

In this study in order to understand the life performance of sandwich composites undergoing combined mechanical loadings and environmental effects, we have presented a multi-scale model for predicting the overall mechanical response of sandwich composites by incorporating different responses of the constituents (skins and foam core). A nonlinear viscoelastic model, following the quasi-linear viscoelastic (QLV) model, is used for the isotropic polymeric constituent (foam core) and an elastic-plastic model is used for the FRP skins. Two systems of sandwich composites, i.e. GFRP skins with PU foam (GFRP/PU) and CFRP skins with PVC foam (CFRP/PVC) are studied. Responses of sandwich composites and their constituents subjected to various histories of mechanical loading (quasi-static, creep/relaxation, and cyclic) under different environmental conditions, such as dry in ambient temperature, immersion in liquid at ambient temperature and immersion in liquid at 50°C are investigated. The GFRP/PU sandwich composites and their constituents were immersed in deionized water, while the CFRP/PVC systems and their constituents were immersed in saline water. After immersion, mechanical tests under different loading histories were conducted.

Using the uniaxial tension tests the fiber reinforced polymers (CFRP and GFRP) properties that are used in skins, are obtained. Then the quasi static and creep/relaxation bending tests were done on PVC and polyurethane foam to get the foam properties in different environmental conditions. Obtaining the properties of fiber reinforced skin and

foam core using the FE analyses and experimental data, we are able to predict the overall mechanical response of sandwich composite under different environmental conditions.

In quasi static bending tests, we loaded the sandwich composites until failure occurred. In CFRP/PVC sandwich composites, delamination occurred between the skin and foam core as a result of excessive loading and we observed sliding of skin and foam on top of each other. The cohesive elements in Abaqus were used to capture the delamination observed in experiment. In GFRP/PU sandwich composite by excessive loading a crack was observed in sandwich composite, and using cohesive elements in Abaqus, the crack propagation in the foam core was simulated.

By investigating the result of the tests and model we can conclude that the time-dependent response in sandwich composites is mainly due to the viscoelastic response of foam and the viscoelastic response of skin is less significant. Also Immersion in fluid can alter the mechanical properties of the constituents in sandwich composites. The polyurethane foam became softer after immersion in 25º C but didn't change by immersion in elevated temperature deionized water and PVC became softer after immersion at 50º C and the effect of immersion in sea water at room temperature wasn't significant.

The mechanical response of sandwich composites at dry condition (baseline) and after immersion in fluid can be quite different. Delamination happens in CFRP/PVC after immersion in 50º C sea water, while it is not seen for the baseline specimen. It is shown

in this study that the proposed multi-scale model together with a nonlinear viscoelastic constitutive model is capable in describing the overall mechanical response of sandwich composites.

REFERENCES

[1] N. Sharma, R. F. Gibson, E. O. Ayorinde,, July, "Fatigue of Foam and Honeycomb Core Composite Sandwich Structures : A Tutorial," *Journal of Sandwich Structures and Materials,* vol. 8, pp. 263-319, July 2006.

[2] D. Gay, Composite materials, design and applications, vol. 1, 2003.

[3] A. P. Mouritz, C. P. Gardiner, "Compression properties of fire-damage polymer sandwich composites," *Composites,* vol. 33, pp. 609-620, 2002.

[4] X. Fan, W. Xiao-qing, "Study on impact properties of through-thickness stitched," *Composite Structures,* vol. 92, p. 412–421, 2009.

[5] R.A.W. MINES; C.M. WORRALLt and A.G. GIBSON, "The static and impact behaviour of polymer composite sandwich beams," *composites,* vol. 25, pp. 95-110, 1994.

[6] C. E. Bakis; L. C. Bank, F.ASCE2; V. L. Brown, M.ASCE; E. Cosenza; J. F. Davalos, A.M.ASCE,J. J. Lesko; A. Machida; S. H. Rizkalla, F.ASCE; and T. C. Triantafillou, M.ASCE, "Fiber-Reinforced Polymer Composites for Construction—State-of-the-Art Review," *JOURNAL OF COMPOSITES FOR CONSTRUCTION,* vol. 2, pp. 73-87, May 2002.

[7] L. Hollaway, "A review of the present and future utilisation of FRP composites in the civil infrastructure with reference to their important in-service properties," *Construction and Building Materials,* vol. 24, pp. 2419-2445, 2010.

[8] A. P. Mouritz, E. Gellert, P. Burchill, K. Challis, "Review of Advanced composite structures for naval ships and submarines," *Composite Structures,* vol. 53, pp. 21-41, 2001.

[9] J. S. Russell, Ed., Perspectives in Civil Engineering, commemorating the 150th anniversary of American scociety of civil engineers, 2003.

[10] J. Cao, J. L. Grenestedt, "Design and testing of joints for composite sandwich/steel hybrid ship hulls," *Composites: Part A,* vol. 35, pp. 1091-1105, 2004.

[11] D.J. HALL and B.L ROBSON, "A review of the design and materials evaluation programme for the GRP/foam sandwich composite hull of the RAN minehunter," *COMPOSITE,* vol. 15, pp. 266-276, 1984.

[12] C. Konga, J. Banga, Y. Sugiyama, "Structural investigation of composite wind turbine blade considering various load cases and fatigue life," *Energy*, vol. 30, p. 2101–2114, 2005.

[13] P. Brøndsted, H. Lilholt, A. Lystrup, "COMPOSITEMATERIALS FORWIND POWER TURBINE BLADES," *Annual Review of Materials Research*, vol. 35, pp. 505-538, 2005.

[14] X. Li, Y. J. Weitsman, "Sea-water effects on foam-cored composite sandwich lay-ups," *Composites, part B*, vol. 35, p. 451–459, 2004.

[15] A. Siriruk, Y. J. Weitsman, D. Penumadu, "Polymeric foams and sandwich composites: Material properties, environmental effects, and shear-lag modeling," *Composites Science and Technology*, vol. 69, p. 814–820, 2009.

[16] A. Siriruk, D. Penumadu, Y. J. Weitsman, "Effect of sea environment on interfacial delamination behavior of polymeric sandwich structures," *Composites Science and Technology*, vol. 69, p. 821–828, 2009.

[17] K. Kolat, G. Neser, C. Ozes, "The effect of sea water exposure on the interfacial fracture of some sandwich systems in marine use," *Composite Structures*, vol. 78, pp. 11-17, 2007.

[18] N. Joshi, A. Muliana, "Deformation in viscoelastic sandwich composites subject to moisture diffusion," *Composite Structures*, vol. 92, p. 254–264, 2010.

[19] Y. Du, N. Yan, M. T. Kortschot, "An experimental study of creep behavior of lightweight natural fiber-reinforced polymer composite/honeycomb core sandwich panels," *Composite Structures* , vol. 106, p. 160–166, 2013.

[20] R. A. Shenoi, H. G. Allen, S. D. Clark, "Cyclic creep and creep–fatigue interaction in sandwich beams," *JOURNAL OF STRAIN ANALYSIS* , vol. 32(1), 1997.

[21] M. Garrido, J. R. Correia, F. A. Branco, T. Keller, "Creep behaviour of sandwich panels with rigid polyurethane foam core and glass-fibre reinforced polymer faces: Experimental tests and analytical modelling," *Journal of Composite Materials*, vol. 48(18), p. 2237–2249, 2014.

[22] Z. Chen, N. Yan, J. Deng, G. Smith, "Flexural creep behavior of sandwich panels containing Kraft paper honeycomb core and wood composite skins," *Materials science and engineering*, vol. A 528, pp. 5621-5626, 2011.

[23] J. S. Kim, L. Arronche, A. Farrugia, A. Muliana, V. La Saponara, "Multi-scale modeling of time-dependent response of smart sandwich constructions,"

Composite Structures, vol. 93, p. 2196–2207, 2011.

[24] R. J. SCUDAMORE, W. J. CANTWELL, "The Effect of Moisture and Loading Rate on the Interfacial Fracture Properties of Sandwich Structures," *POLYMER COMPOSIES,* vol. 23(3), pp. 406-417, 2002.

[25] O. Ishai, C. Hiel, M. Luft, "Long-term hygrothermal effects on damage tolerance of hybrid composite sandwich panels," *COMPOSITES,* vol. 26, pp. 47-55, 1995.

[26] J. Degrieck, W. V. Paepegem, "Fatigue damage modeling of fibre-reinforced composite materials: Review," *Applied Mechanics Reviews,* vol. 54(4), pp. 279-300, 2001.

[27] G. Belingardi , M.P. Cavatorta, R. Duella , "Material characterization of a composite–foam sandwich for the front structure of a high speed train," *Composite Structures,* vol. 61, p. 13–25, 2003.

[28] M. Ramezani, E. Hamed, "Coupled thermo-mechanical creep behavior of sandwich beams_Modeling and analysis," *European Journal of Mechanics A/Solids* , vol. 42, pp. 266-279, 2013.

[29] E. Hamed, M. Ramezani, "Effect of boundary conditions on the creep response of sandwich beams with a viscoelastic soft core," in *from materials to structures: Advancement through innovation*, London, Taylor & Francis Group, 2013, pp. 79-84.

[30] W. N. L. J. O. K. Findley, Creep and Relaxation of Nonlinear Viscoelastic Materials (with an Introduction to Linear Viscoelasticity), Amsterdam: North Holland Publishing Company, 1976.

[31] Y. B. M. V. O. S. I. Frostig, "High-order theory for sandwich beam behavior with transversely flexible core," *Journal of Engineering Mechanics,* vol. 118(5), pp. 1026-1043, 1992.

[32] E. Figueroa, B. Shafiq, I. de la Paz, "Creep to failure and cyclic creep of foam core sandwich composites in sea water," *Journal of Sandwich Structures and Materials,* vol. 0(00), p. 1–14, 2013.

[33] J. Jeon , A. Farrugia , A. Muliana, V. La Saponara , "Understanding Time-dependent Performance of Smart Polymeric Sandwich Composites under Coupled Mechanical and Thermal Stimuli," in *The 9th International Conference on the Mechanics of Time Dependent Materials*.

[34] J. Kim, L. Arronche, A. Farrugia, A. Muliana, V. La Saponara, "Time dependent response of smart sandwich composites," in *16th International Conference on*

Composite Structures, Porto, 2011.

[35] A. Muliana, K.R. Rajagopal, "Modeling the response of nonlinear viscoelastic biodegradable polymeric stents," *International Journal of Solids and Structures*, vol. 49, p. 989–1000, 2012.

[36] Y. C. Fung, Biomechanics, Mechanical properties of living tissues, New York: Springer,, 1981. .

[37] "Abaqus Theory Manual 4.2.1, Plasticity models: general discussion," [Online]. Available: https://www.sharcnet.ca/Software/Abaqus610/Documentation/docs/v6.10/books/stm/default.htm.

[38] D. Mohr, "Three Dimensional Rate-independent Plasticity," 2015. [Online]. Available: https://www.ethz.ch/

[39] B.R.K. Blackman, A.J. Kinloch & M. Paraschi, "The determination of the mode II adhesive fracture resistance, GIIC, of structural adhesive joints: An effective crack length approach," *Engineering Fracture Mechanics*, vol. 72, pp. 877-897, 2005.

APPENDIX I

NUMERICAL ALGORITHM

In this work the numerical algorithm for the 3D quasi-linear viscoelastic model is used for polymer undergoing degradation and integrate it with a finite element (FE) formulation to define the viscoelastic polymer deformation. This numerical algorithm solves 3D quasi-linear viscoelastic model which is compatible with a displacement based FE code. The mechanical properties of the materials are assumed to change with the degradation. Degradation is assumed to be dependent on strain and concentration of water and the diffusion process is assumed independent of the deformation and degradation of the materials and governed by Fick's law. Solving the equation that governs the diffusion of water, allows us to determine the deformation that depends on degradation in the viscoelastic polymeric material.

The numerical algorithm is implemented at each Gaussian material point within elements in the Finite Element analyses. The rate of degradation at a fixed time t is approximated as:

$$\frac{\partial d}{\partial t}(t) \approx \frac{d(t) - d(t - \Delta t)}{\Delta t} = \frac{d^t - d^{t-\Delta t}}{\Delta t} \tag{1}$$

Deformation and concentration of water lead to degradation that using backward difference, is written as:

$$d^t \approx d^{t-\Delta t} + \frac{\Delta t}{\tau_D}(1-d^t) f(\varepsilon^{t-\Delta t}) g(C^t) h(Tt) \tag{2}$$

The time-dependent stress in Eq. (5-26) is approximated as

$$\begin{aligned}\sigma_{ij} = {} & 2C_1 K_\infty \int_{0^-}^{t} E_0(d) e^{B\bar{\varepsilon}} \frac{d\varepsilon_{ij}}{ds} ds \\ & + 2C_1 \sum_{n=1}^{N} K_n \int_{0^-}^{t} e^{-\frac{\varphi^t - \varphi^s}{\tau_{Rn}}} E_0(d) e^{B\bar{\varepsilon}} \frac{d\varepsilon_{ij}}{ds} ds \\ & + \delta_{ij} C_2 K_\infty \int_{0^-}^{t} E_0(d) e^{B\bar{\varepsilon}} \frac{d\varepsilon_{kk}}{ds} ds \\ & + \delta_{ij} C_2 \sum_{n=1}^{N} K_n \int_{0^-}^{t} e^{-\frac{\varphi^t - \varphi^s}{\tau_{Rn}}} E_0(d) e^{B\bar{\varepsilon}} \frac{d\varepsilon_{kk}}{ds} ds\end{aligned} \tag{3}$$

$$\begin{aligned}\sigma_{ij} = {} & 2C_1 K_\infty {P^t}_{ij} + 2C_1 \sum_{n=1}^{N} {q^t}_{ij(n)} + \delta_{ij} C_2 K_\infty {P^t}_{kk} \\ & + \delta_{ij} C_2 \sum_{n=1}^{N} {q^t}_{kk(n)}\end{aligned} \tag{4}$$

By assuming

$$\Delta\varphi^t \equiv \varphi^t - \varphi^{t-\Delta t} \approx \frac{\Delta t}{a(d^t)} \tag{5}$$

The history variables can be written as:

$$q_{ij(n)}^{t} =$$

$$e^{-\frac{\Delta\varphi^t}{\tau_{Rn}}} q_{ij(n)}^{t-\Delta t} + \frac{\Delta t}{2} K_n \left[E_0(d) e^{B\bar{\varepsilon}} \frac{\Delta\varepsilon_{ij}}{\Delta t} \Big|_t + e^{-\frac{\Delta\varphi^t}{\tau_{Rn}}} E_0(d) e^{B\bar{\varepsilon}} \frac{\Delta\varepsilon_{ij}}{\Delta t} \Big|_{t-\Delta t} \right] \tag{6}$$

$$q_{kk(n)}^{t} =$$

$$e^{-\frac{\Delta\varphi^t}{\tau_{Rn}}} q_{kk(n)}^{t-\Delta t} + \frac{\Delta t}{2} K_n \left[E_0(d) e^{B\bar{\varepsilon}} \frac{\Delta\varepsilon_{kk}}{\Delta t} \Big|_t + e^{-\frac{\Delta\varphi^t}{\tau_{Rn}}} E_0(d) e^{B\bar{\varepsilon}} \frac{\Delta\varepsilon_{kk}}{\Delta t} \Big|_{t-\Delta t} \right] \tag{7}$$

By solving the time dependent stress incrementally we have

$$\sigma_{ij}^{t} = \sigma_{ij}^{t-\Delta t} + \Delta\sigma_{ij}^{t} \tag{8}$$

and the incremental stress is:

$$\Delta\sigma_{ij}^{t} = K_\infty \left(E_0(d) e^{B\bar{\varepsilon}} \Big|_t + E_0(d) e^{B\bar{\varepsilon}} \Big|_{t-\Delta t} \right) \left\{ 2C_1 \frac{\Delta\varepsilon_{ij}{}^{t}}{2} + \delta_{ij} C_2 \frac{\Delta\varepsilon_{kk}{}^{t}}{2} \right\} \tag{9}$$

$$+2C_1 \sum_{n=1}^{N} \left[q_{ij(n)}^{t-\Delta t} \left(e^{-\frac{\Delta\varphi^t}{\tau_{Rn}}} - 1 \right) + \frac{1}{2a(d^t)} K_n \left[E_0(d) e^{B\bar{\varepsilon}} \Delta\varepsilon_{ij} \Big|_t + e^{-\frac{\Delta\varphi^t}{\tau_{Rn}}} E_0(d) e^{B\bar{\varepsilon}} \Delta\varepsilon_{ij} \Big|_{t-\Delta t} \right] \right]$$

$$+\delta_{ij} C_2 \sum_{n=1}^{N} \left[q_{kk(n)}^{t-\Delta t} \left(e^{-\frac{\Delta\varphi^t}{\tau_{Rn}}} - 1 \right) + \frac{1}{2a(d^t)} K_n \left[E_0(d) e^{B\bar{\varepsilon}} \Delta\varepsilon_{kk} \Big|_t + e^{-\frac{\Delta\varphi^t}{\tau_{Rn}}} E_0(d) e^{B\bar{\varepsilon}} \Delta\varepsilon_{kk} \Big|_{t-\Delta t} \right] \right]$$

h^t is defined as :

$$h^t \equiv E_0(d)e^{B\bar{\varepsilon}}\Big|_t \tag{10}$$

It is needed to determine stiffness matrix at each material point at each instant of time to be able to provide trial strains or displacement for the next step.

The consistent tangent stiffness matrix is:

$$C_{ijkl} = \frac{\partial \Delta\sigma_{ij}^t}{\partial \Delta\varepsilon_{kl}^t} = K_\infty \frac{\partial \Delta h^t}{\partial \Delta\varepsilon_{kl}^t}\left\{2C_1\frac{\Delta\varepsilon_{ij}^t}{2} + \delta_{ij}C_2\frac{\Delta\varepsilon_{kk}^t}{2}\right\} \tag{11}$$

$$+K_\infty(h^t + h^{t-\Delta t})\left\{C_1\delta_{ik}\delta_{jl} + \frac{C_2}{2}\delta_{ij}\delta_{kl}\right\}$$

$$+2C_1\sum_{n=1}^{N}\left[\frac{1}{2a(d^t)}K_n\left(\frac{\partial h^t}{\partial \Delta\varepsilon_{kl}^t}\Delta\varepsilon_{ij}^t + h^t\delta_{ik}\delta_{jl}\right)\right]$$

$$+\delta_{ij}C_2\sum_{n=1}^{N}\left[\frac{1}{2a(d^t)}K_n\left(\frac{\partial h^t}{\partial \Delta\varepsilon_{kl}^t}\Delta\varepsilon_{mm}^t + h^t\delta_{kl}\right)\right]$$